Optimization of Direct Methanol Fuel Cells:

An Experimental Approach

A Thesis Presented by Nathaniel Metzger

Submitted to the Graduate School of Engineering at

the University of Kansas in partial fulfillment of the requirements for the degree of MASTER OF SCIENCE IN MECHANICAL ENGINEERING

X

Chair:
Dr. Xianglin Li

X

Dr. Chris Depcik

X

Dr. Gibum Kwon

Date Defended: 05/12/2022

The thesis committee for Nathaniel Metzger certifies that this is the approved version of the following thesis:

Optimization of Direct Methanol Fuel Cells: An Experimental Approach

X

Chair:
Dr. Xianglin Li

X

Dr. Chris Depcik

X

Dr. Gibum Kwon

Date Approved: 05/27/2022

ABSTRACT

Recently, fuel cells have gained significant attention for their capability of producing power with different fuels at reduced levels of carbon dioxide emissions. Of the many options of fuel cells, direct methanol fuel cells (DMFCs) are considered promising candidates for stationary and small portable power applications. However, there are numerous technical barriers preventing more widespread use of DMFCs, primarily the crossing over of unreacted fuel through the membrane and the slow reaction kinetics on the anode. This work provides a comprehensive experimental approach to optimizing the cell as a whole. First, various methods of reducing fuel crossover are considered. Then, various anode catalysts are evaluated for performance characteristics. The cathode is also considered through the use of platinum metal group (PGM) free catalysts. Finally, the fabrication of the membrane electrode assembly (MEA) is optimized by examining various methods of catalyst ink deposition on the substrate. By taking a comprehensive approach, this work provides a pathway for the fabrication of DMFCs capable of enhanced power densities and reduced fuel crossover by using a variety of techniques.

ACKNOWLEDGMENTS

There are many that played an active role in the development of this work, and on my journey through graduate school. First, I would like to thank my advisor Dr. Xianglin Li for his support and encouragement both in entering the graduate program and having a positive experience throughout my time here. Without his help, I would not have been able to have achieved my goals in research and academic development. I would also like to thank my committee members, Dr. Depcik and Dr. Kwon, for their time and effort in reviewing and considering my thesis. Both have also contributed significantly to my academic career both in the classroom and laboratory settings. Additionally, I would like to thank all of the collaborating organizations we have had the pleasure of working with over the last few years including Kansas State University, Carnegie Melon University, University of Buffalo, General Graphene Corporation, Giner Incorporated, and many others who have contributed to this work. I also want to express my appreciation to the Department of Energy' Office of Energy Efficiency and Renewable Energy (EERE) whose grant helped to fund our research under the Fuel Cell Technologies Office award number DE-0008440. The American Society of Mechanical Engineering (ASME) also made this work possible by allowing the use of work recently published in the Journal of Electrochemical Energy Conversion and Storage which is deeply appreciated. Finally, I would like to thank my family and close friends that have supported me throughout this journey. I know it has been difficult, but the love and support of them allowed me to stay focused on my goals and enjoy my work along the way.

TABLE OF CONTENTS

Page

LIST OF TABLES

LIST OF FIGURES

Nomenclature

Acronym	Definition
ACS	American Chemical Society
AIChE	American Institute of Chemical Engineers
CC	Carbon cloth
CL	Catalyst layer
CNFs	Carbon nanofibers
CNTs	Carbon nanotubes
CP	Carbon paper
DI	Deionized
DMFC	Direct methanol fuel cell
DoE	Department of Energy
EIA	Energy Information Administration
ESCA	Electrochemical surface area
FML	Fuel management layer
GDL	Gas diffusion layer
GGC	General Graphene Corporation
HET	High electron transfer
IPA	Isopropyl alcohol
JEECS	Journal of Electrochemical Energy Conversion and Storage

JM	Johnson Matthey
KSU	Kansas State University
KU	University of Kansas
MEA	Membrane electrode assembly
MOR	Methanol oxidation reaction
MPL	Microporous layer
MWCNTs	Multi-walled carbon nanotubes
NCNTs	Nitrogen doped carbon nanotubes
NREL	National Renewable Energy Laboratory
ORR	Oxygen reduction reaction
PEM	Proton exchange membrane
PEMFC	Proton exchange membrane fuel cell
PGM	Platinum Group Metals
PSD	Pore size distribution
PTFE	Polytetrafluoroethylene
RH	Relative humidity
SEM	Scanned electron microscopy
TKK	Tanaka Precious Metals
UB	University of Buffalo
WML	Water management layer

CHAPTER 1

INTRODUCTION

1.1 Background

As concerns about the sustainability and environmental effects associated with traditional fossil fuels continue to grow, alternative means of producing power are gaining more traction. The United States Energy Information Administration (EIA) predicts that in 2022 46% of the electric generating capacity additions to the grid will come from solar power, 17% from wind, and 11% storage from batteries, while natural gas only represents 21% of planned additions [1]. Advances in technologies have reduced emissions from many industries, however, others still account for large portions of carbon dioxide (CO_2)emissions. For example, the electric power industry was producing an average of 60 kg_{CO2}/MMBtu since 1975, however, the addition of renewables, nuclear, and natural gas along with a shift away from coal fired plants resulted in the average carbon dioxide emissions to drop to 48 kg_{CO2}/MMBtu in 2016. On the other hand, the transportation industry has averaged a carbon intensity of approximately 70 kg_{CO2}/MMBtu for decades [2]. This represents both a need for the continued advancement of more sustainable means of power production as well as a significant market gap that fuel cells can help to fill. Direct methanol fuel cells are promising candidates for small and portable electronics, stationary applications, and material handling applications due to their low operating temperature and inexpensive fuel. However, the current designs of DMFCs require higher catalyst loading than similar fuel cells resulting in higher installation costs. Additionally, there is a myriad of technical limitations preventing wider applications of DMFCs such as use in cell phones and laptops. [3]

This thesis will attempt to expand upon many of the common barriers that DMFCs encounter and provide a road map to optimization of the overall cell based upon research done over the last two years.

1.2 Basic Operations of DMFCs

Direct methanol fuel cells are a subset of a larger group of fuel cells called proton exchange membrane fuel cells (PEMFCs). In both cases, fuel is supplied to the anode and air is supplied to the cathode. Both kinds of cells use platinum on the anode and cathode on carbon supports, and DMFCs use a platinum ruthenium alloy on the anode to help reduce catalyst poisoning. PEMFCs require catalyst loading of less than 1 mg/cm^2 and are capable of higher power densities of approximately 250-300 mW/cm^2, based on the author's experiments, making them the cheaper choice with current technologies [4]. Currently, PEMFCs cost 1,868 $/kW whereas DMFCs cost 3,772 $/kW [5]. The primary difference is that PEMFCs use hydrogen as a fuel. DMFCs differ because they derive the hydrogen ions from methanol fuel as opposed to pure hydrogen gas. This occurs via a methanol oxidation reaction (MOR) on the anode as shown in Eq. 1. It is important to note that water is required for the MOR to occur, therefore, a dilute methanol-water solution must be used. To use pure methanol water would have to be passively supplied via back diffusion from humidified air in the cathode, or an externally pumped water supply. This will be detailed further in Chapters 3 and 5.

$$\mathrm{CH_3OH} + \mathrm{H_2O} \rightarrow 6\mathrm{H^+} + 6\mathrm{e^-} + \mathrm{CO_2} \quad (1)$$

Once the hydrogen ions reach the cathode where air is being supplied, an oxygen reduction reaction (ORR) occurs as detailed in Eq. 2. The overall reaction that occurs can be seen in Eq. 3.

$$\frac{3}{2}\,O_2 + 6H^+ + 6e^- \rightarrow 3H_2O \qquad (2)$$

$$CH_3OH + \frac{3}{2}\,O_2 \rightarrow\ 2H_2O + CO_2 \qquad (3)$$

As the hydrogen ions transfer across the proton exchange membrane (PEM), electrons are transferred through an external circuit allowing for power to be provided to connected systems. This process is detailed visually in figure 1.1 (a), with the anode and MOR shown in red, and the cathode and ORR shown in blue. The air supplied to the cathode is typically humidified to a relative humidity (RH) of 100%. The typical structure of a membrane electrode assembly (MEA) consists of a 3

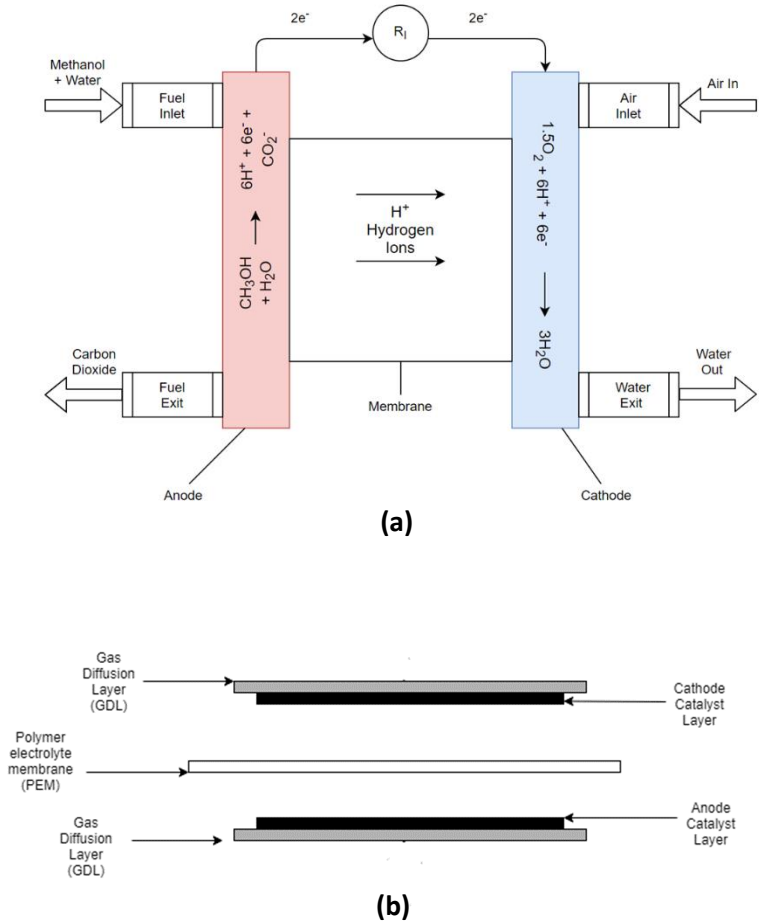

Figure 1.1: A direct methanol fuel cell under ideal fuel consumption conditions (a); MEA structure (b)

gas diffusion layer (GDL) on the anode with an applied catalyst, a PEM, and the structure mirrored on the cathode side as seen in figure 1.1 (b). In order to make the MEA, catalyst solutions are fabricated using a variety of components. These solutions are then applied to the GDLs by a variety of methods. These processes will also be detailed further in later Chapter 6.

1.3 Benefits of DMFCs as an alternative power source

There are numerous potential benefits to DMFCs over other energy sources. The benefit most focused on is the reduction of CO_2 emissions. Eq. 3 shows that DMFCs do produce CO_2 as a product of the reaction, however, methanol is a biofuel and produced in a variety of ways. While it is flammable and slightly toxic, it is easy to store, refuel, and handle. On the other hand, pure hydrogen gas is volatile posing risks of explosions, and requires specialized personnel to store, and transport [6]. This results in increased infrastructure costs related to the use of hydrogen as a fuel. For example, the National Renewable Energy Laboratory states that for one material handling fleet the related infrastructure costs for a hydrogen fuel cell operated fleet is 17,000 $/month whereas a battery operated fleet costs approximately 75 $/forklift/month [7]. Furthermore, the process of producing hydrogen is cost intensive both in personnel, and in practice with current Department of Energy target costs between $3.10/kg and $3.70/kg not accounting for compressions, storage, and dispension costs [8]. In a liquid state, methanol has a high volumetric energy density when compared to other fuels like hydrogen, which generally needs to be compressed to high pressures for use. For example, methanol's energy density is 8.3 times higher than hydrogen compressed at 200 bar, and approximately 2.6 times higher than Lithium-ion batteries [9]. Additionally, all PEMFCs, including DMFCs, operate at relatively low

temperatures between 30 °C and 130 °C with a typical operating temperature of 80 °C. These cells are also quick to reach full operating capacity and operate quietly. This makes DMFCs ideal for small and portable power applications requiring lower power input [6]. DMFCs can also be ideal for material handling applications such as the deployment of DMFC powered forklifts for warehouses. This is discussed in detail in the economic benefits chapter of this thesis. Finally, the theoretical efficiency of DMFCs is 97%. However, with current technologies it is typical to see efficiencies similar to an internal combustion engine (ICE) that are between 30%-40% [10].

1.4 Current Limitations of DMFCs

While methanol boasts many advantages as a fuel, several limitations that currently prevent DMFCs from meeting similar performance standards to hydrogen-fueled PEMFCs. The two main technical limitations of wider use of DMFCs have been identified as the slow reaction kinetics of the MOR on the anode, and the crossing over of unreacted methanol fuel through the PEM [11]. These two limitations, and their mitigation through a variety of methods, will be the primary focus of this thesis, though other limitations will be briefly addressed. In fact, many of the other drawbacks of DMFCs stem from these two fundamental problems. For example, the slow MOR on the anode causes a lower catalyst utilization than that of PEMFCs that results in peak power densities of between 100-140 mW/cm^2 [6]. As a result, DMFCs require much higher platinum metal group (PGM) loadings with the typical anode catalyst loading being 4.5 mg_{PtRu}/cm^2, and the cathode loading at approximately 1.5 mg_{Pt}/cm^2.Additionally, the crossing over of concentrated fuel from the anode to the cathode results in an unstable stack voltage reducing cell potential. Furthermore, the slow MOR and low catalyst utilization on the anode limits the overall power

density capable from the cell. It is important to note at this point that power density refers to the amount of power generated per unit area of the MEA and is the most common quantification of performance. These factors combined result in high installation costs for applications where significant power generation is needed since the active surface area of the cell is directly proportional to the power production capability of the cell. In fact, the catalyst loading on the anode and cathode account for 56% of the cost of the cell [12]. While DMFCs cost 3,772 $/kW to operate, this price is heavily dominated by the installation of the cell with pure methanol costing approximately 0.43 $/GGE [5]. On the lower end, the Department of Energy (DoE) defines a target power of a PEMFC as 100 kW and 250 kW on the higher end. Using the current associated costs this would result in a DMFC costing $377,200/$943,000 whereas a hydrogen PEMFC costs $186,800/$467,000 to manufacture on the low/high target end, respectively [13]. The current costs are one of the reasons DMFCs are unattractive to many markets with the most recent technology.

1.5 Experimental Goals and Theoretical Limits

The research presented in this work is funded by the DoE's Office of Fuel Cell Technology Office award number DE-0008440. In 2020, the DoE defined an experimental goal for DMFCs of reaching a peak power density of 250 mW/cm^2 using 4 mg/cm^2_{PGM} or less [5]. This goal was increased to 300 mW/cm^2 using 3 mg/cm^2_{PGM} in 2021 [5]. Furthermore, this project defines the goal of maintaining this power density using "highly concentrated" methanol, though the concentration is not explicity defined [5]. However, based on Eq. 1 it can be seen that for every mole of methanol, one mole of water is required for the MOR to occur. Therefore, it can be

assumed that the optimal molar concentration will be 50% methanol. It will be shown in Chapter 3 and 5 that performance at even higher concentrations is possible if water generated from the cathode can be utilized via back diffusion through the membrane. Current simulations show that maximum theoretical energy efficiency of approximately 97% occurs at much lower concentrations of 2.5M and operating temperatures of 30 °C [14]. At these operating conditions recent literature shows that a maximum power density of between 10-20 mW/cm^2 is possible using commercial components, which is far from the target power density defined by the DoE [15]. It will be shown in Chapter 3 of this work that higher peak power densities can be achieved under these operating conditions using modified PEMs.

At standard operating temperatures of 80 °C, higher power densities are possible. Recent literature indicates a peak power density achievable is approximately 100 mW/cm^2 using 3.2 mg/cm^2_{PGM} [16]. Similarly, Manthiram et al. shows that the maximum peak power density at 1M concentrations using commercial components is 110 mW/cm^2 [17]. However, most published work report peak power densities below this value at similar operating conditions. For example, Albani et al. shows a power density of 50 mW/cm^2 at 1M methanol and 70 °C [18]. Santiago et al. achieved a peak power of 45 mW/cm^2 under the same conditions [19]. Theoretical values presented in recent models show a moderate improvement in this, and report power densities of 124 mW/cm^2 and 140 mW/cm^2 at 80 °C and 100 °C, respectively [20]. Using modified materials and increased operating conditions has been shown to further improve the peak power density. Bagli et al. report that the use of TiO_2 modified PEMs and operating temperatures of 145 °C yields a maximum power density of 210 mW/cm^2 using air, however, this operating temperature falls outside of the parameters of 80 °C defined by the DoE for this project [21]. A model constructed

by Miao et al. came to similar conclusions indicating a power density of 120 mW/cm^2 using current technology. They concluded that even if the anode and cathode catalytic activity was increased by 10 times, the maximum achievable power density was 254 mW/cm^2 [22]. This highlights the challenge associated with meeting the goals defined by the DoE in this project, as even model results do not meet the target power densities.

This work will show that a power density of 100-140 mW/cm^2 is regularly achievable using commercial components and standard operating conditions of 80 °C, 0.1 L/min air, and 50 kPa backpressure. Furthermore, power densities of >250 mW/cm^2 can be reached using PGM-free cathode catalysts and elevated operating conditions of 1 L/min air and 200 kPa backpressure [5]. In addition to improved peak power densities, it will be demonstrated that power density can be maintained using PGM-free cathode catalysts and pure methanol. Furthermore, the use of fuel management layers (FMLs) and modified PEMs allow the preservation of peak power density using 15M, or approximately 50% by weight, methanol solution. While these results still fall outside the goals defined by the DoE in this project, significant progress towards the achievement of these goals are shown through the use of modified anode components, PEMs, and catalysts.

CHAPTER 2

GAS TRANSFER IN DMFCs

2.1 Understanding Carbon Dioxide Transfer in DMFCs using a Pore-Scale Model

The following section will detail the transfer of carbon dioxide within DMFC using a pore-scale model. This will primarily be described using the recently published journal article *Understanding Carbon Dioxide Transfer in Direct Methanol Fuel Cells Using a Pore-Scale Model* (JEECS-20-1825) which was published in the ASME Journal of Electrochemical Energy Conversion and Storage in 2021. The authors of this work are Nathaniel Metzger, Archana Sekar, Dr. Jun Li, and Dr. Xianglin Li. ASME is the original publisher of this work and permission to use it in its entirety as a part of this thesis was generously granted by ASME. In this work, a liquid-vapor two-phase model is used to examine how carbon dioxide moves from the catalyst layer through the porous components of the fuel cell such as the GDL, catalyst layer (CL), and PEM. A typical MEA is designed using a GDL coated with a catalyst layer on both the anode and cathode, separated by a PEM. These GDLs can have hydrophilic, hydrophobic, or no microporous layers (MPLs) designed to effectively provide water and fuel to the cell without flooding the anode. This work provides insight into how to design these components by controlling the pore size distribution and wettability of the porous layers in the cell in a favorable way for liquid management and allows the DMFC to run at higher concentrations of fuel. This is useful because using concentrated fuel increases the energy density of the fuel. Furthermore, using concentrated fuel instead of dilute methanol solution reduces the overall volume and weight required to have onsite or in

possession of the user. This is especially useful in applications where large and bulky fuel reserves are not ideal, such as in portable power applications.

The model is constructed by examining the capillary pressures experienced within the porous layers of the cell and then using probability distribution functions to estimate the size of the pores and whether they will be filled with fuel or water at a given time. Traditionally, hydrophobic MPLs have been used on anodes to keep water from flooding active catalyst sites. However, this work shows that by making the anode MPL hydrophilic, or by introducing a layer of large pores in varied locations on the anode side as a fuel management layer (FML), the pores would then naturally be filled by water thus increasing the capillary pressure that unreacted fuel must overcome to cross over to the cathode before it fully reacts [23]. Three design suggestions on the anode portion of the MEA were given to reduce the fuel crossover seen in typical DMFCs. First, it is suggested to add a hydrophilic layer between the GDL and the hydrophobic MPL on the anode. Model results indicate an increase of greater than $1.5x10^5$ Pa in capillary pressure through this layer of the MEA. Alternatively, one can add a layer of large pores between the hydrophobic microporous layer and the CL on the anode resulting in a capillary pressure increase of $5.1x10^2$ Pa. Finally, it was suggested to make the anode MPL hydrophilic as opposed to hydrophobic which results in the same pressure increase of $1.5x10^5$ Pa in the MPL itself [23]. The individual contributions of each author are as follows. See Appendix A-4 for the full permissions and work.

Nathaniel Metzger; Xianglin Li: Experimental validation and model construction

Archana Sekar; Jun Li: Electrode (anode and cathode) fabrication

Chapter 3

Fuel Crossover as a Major Limiting Factor

3.1 Baseline Tests and Experimental Setup

Before discussing the modification of fuel cell components, it is necessary to define the experimental setup and baseline tests. A Scribner 890e Fuel Cell Tester was connected to a 5 cm^2 MEA cell to test all MEAs. However, it is possible to increase the size of the cell to 25 cm^2 as desired but this is only done in the case of final designs to save costs on high catalyst loadings. Figure 3.1 (a-b) shows the experimental setup with labels on each major component.

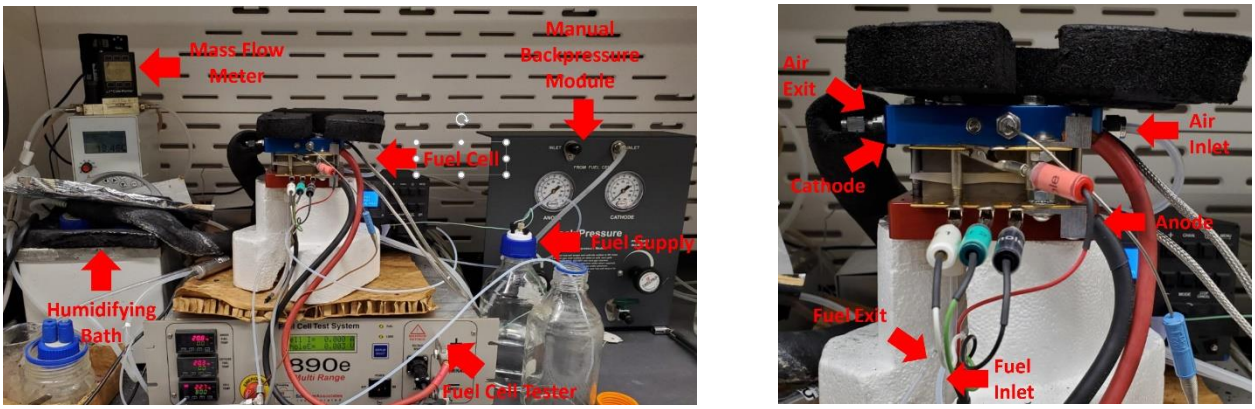

(a) **(b)**

Figure 3.1: Complete fuel cell experimental setup (a); and fuel cell structure (b)

The standard fabrication procedure is as follows. Catalyst solution for the anode is fabricated by mixing appropriate amounts of deionized (DI) water, isopropyl alcohol (IPA), anode catalyst, and Nafion® 10% ionomer so that the ionomer to PtRu ratio is 0.4. The solution is then sonicated for two hours in a Branson 1800 sonicator to adequately disperse the solution. 1-2 mL of solution is then dripped into an Iwata Ninja Jet airbrush and spray coated onto the GDL to

achieve the desired catalyst loading. The substrate is then dried for one hour at 74 °C in a Magic Mill food dehydrator. The anode is then allowed to dry overnight. The cathode is fabricated in the same manner except for that the ionomer to Pt ratio is 0.2. For baseline tests, Sigracet 29BC (with a hydrophobic MPL) and Toray Carbon Paper (CP) (without a MPL) is used for the anode and cathode, respectively. The anode is then placed in a PTFE gasget with a Nafion® membrane and the cathode placed on top. The gasket is then closed within a piece of aluminum foil and hot pressed using a Dulytek DE10K at 135 °C and 345 kPa for five minutes. See Appendix A-1 for a detailed standard MEA fabrication procedure.

Prior to testing it is necessary to activate a MEA. The standard activation procedure is as follows. The MEA is inserted into the Scribner 890e fuel cell test system and heated to 80 °C and supplied with 0.1 L/min of air to the cathode heated so that the relative humidity (RH) is 100%, and with 0.25M methanol to the anode at 0.5 mL/min. Once heated, the MEA was allowed to rest at the open circuit voltage (OCV) for three minutes. The OCV for each MEA varies, but is typically between 0.55 V and 0.7 V for MEAs fabricated with commercial components. A polarization scan was then performed after which the MEA was held at a constant 0.4 V for one hour. This process was repeated for approximately four hours until the performance and resistance appeared to be stable.

In standard tests, air is supplied to the cathode at a rate of 0.1 L/min fully humidified to 100% RH. Fuel is supplied to the anode at a rate of 1 mL/min using 1M methanol and held at stoichiometric ratios as concentrations increase. For example, 3M methanol solution would yield a fuel flow rate of 0.33 mL/min. The cathode is pressurized to 50 kPa backpressure using a

Scribner manual backpressure regulating module. This setup also allows for anode and cathode supply lines to be changed to desired materials such as N_2, H_2, or vapor depending upon the desired testing parameters. For standard methanol tests, the cell is allowed to rest at the OCV for three minutes. A polarization scan is then performed by scanning from the OCV to 0.2V. This process is repeated three times for each concentration to ensure performance is stable. Most commonly, this is done at 1M, 3M, and 7.5M methanol solutions. This will be referred to as the standard testing procedure for the remainder of this work and any changes to this procedure will be detailed as needed. Figure 3.2 details the results of a baseline test using MEA 54. The power density, represented by the solid points, increases with current density. The current density "i", shown in empty points, increases as the voltage decreases. This is due to the way tests are done. The voltage is scanned from the OCV down to 0.2V and the fuel cell device records the current density that is generated as this occurs. It should be noted that in all figures containing performance results, power density will be represented by solid points and current density will be represented by empty points with only the colored border. Detailed standard fuel cell set up, activation, and testing procedures can be found in Appendix A-2.

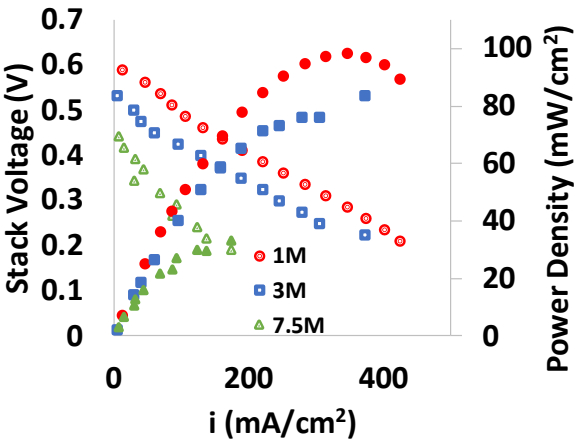

Figure 3.2: A baseline test conducted on MEA 54 at 80 °C and 50 kPa backpressure

The Scribner 890 fuel cell tester functions by holding each data point for 30 seconds to allow for the reading to stabilize and minimize error. However, with all experimental data there

is an error in the results. The error associated with the reported data in this work will be according to product specifications obtained from Scribner and are as follows [24]. The current collected has a reported error of +/- 0.3% of the observed current density. Similarly, the recorded voltage has an accuracy of 3 mV with an error of +/- 0.3% of the reading [24]. Therefore, the error in power density can be taken as the simple average of the error in voltage and current. Power is obtained by multiplying the voltage and the current, as seen in Eq. 4. The error in power density can then be obtained using the simple average calculation shown in Eq. 5

$$\mathrm{P} = \mathrm{V} * \mathrm{I} \tag{4}$$

$$\mathrm{P}_{err} = (V * I)(\frac{0.3\%}{V} + \frac{0.3\%}{I}) \tag{5}$$

For example, the results presented in figure 3.2 would have the following associated errors. At a peak current density and minimum voltage the error is 400 mA/cm^2 (+/- 1.2 mA/cm^2) and 0.2 V (+/- 0.0006 V). This results power density error of 1.2%, or approximately 1 mW/cm^2, at these operating conditions. Since the error associated with each data point is relatively low, and due to the large number of data points, error bars will not be included in the figures of this work. Repeatability is also addressed by performing each polarization scan three times using the Scribner Fuel Cell software. After repeating the scans, and ensuring no outliers are present, the most stable polarization scan is reported. This is common practice within the fuel cell community and recommended by recent work published in the Journal of Power Sources [25].

3.2 Fuel Management Layer Design

As mentioned in Chapter 2, one effective means of reducing fuel crossover is introducing a fuel management layer on the anode. While the designs and locations of these layers may vary, their function is similar. Each FML acts by altering the mass transport properties on the anode by diffusing the methanol prior to reaching the catalyst layer. Based on conclusions from the work presented in the previous chapter it can be seen that the primary design principle in reducing fuel crossover is to limit the liquid interaction between the catalyst layer and serpentine fuel channels of the cell as seen in figure 3.3 (a). Furthermore, the model concludes that the most effective way to do this is by controlling the pore size and distribution as the thickness does not play as large of a role since the capillary pressure is much greater than the liquid flow resistance by at least two orders of magnitude [23]. The first design proposed in this section is adding a layer of large pores between the liquid fuel channels and GDL on the anode side of the MEA. This was done by inserting a 3mm thick layer of AvCarb G300A graphite felt purchased from the fuel cell store (Product number: 1595053). It is important to note here that

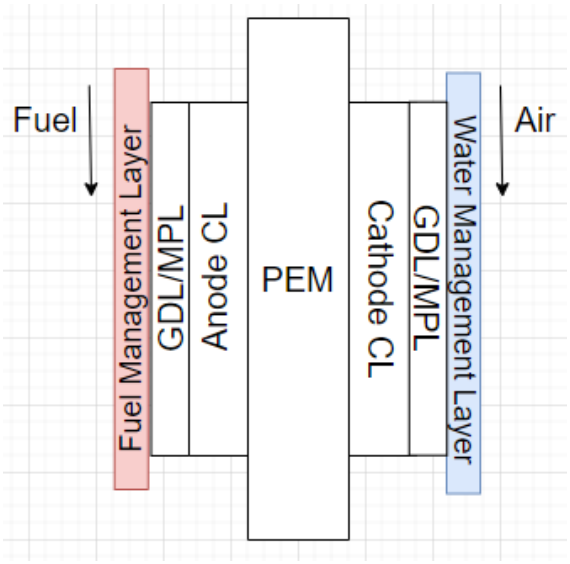

(a)

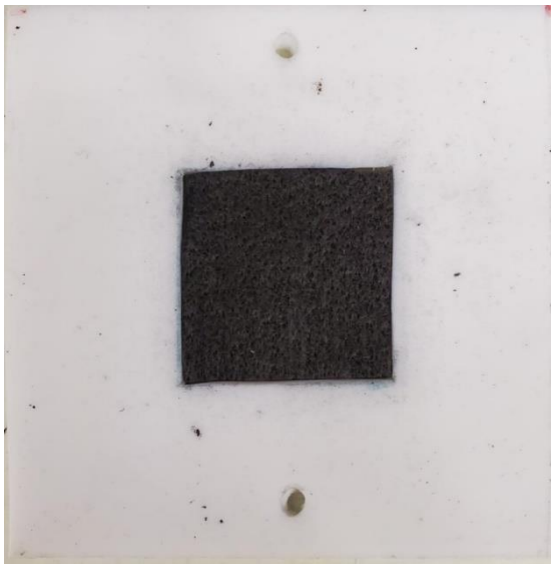

(b)

Figure 3.3: Schematic of experimental design (a); a 3mm thick carbon felt FML gasketed

FMLs must remain conductive in order to be effective. A gasket of equal thickness should also be used to avoid unnecessary pressure differentials on the MEA. A layer of PTFE gasket purchased from the fuel cell store (Product number: 592863) was added to mitigate this effect. Figure 3.3 (b) shows the gasketed fuel management layer used in these experiments. Table 3.1 details the MEA used in the experiments where this FML was tested.

Table 3.1: MEAs tested with and without a felt FML

	Cathode	PEM	Anode	FML
MEA 37	JM Pt/C 60% 1.5 mg/cm^2 (HiSPEC 9100)	Nafion® 212	TKK PtRu 77% 4.51 mg/cm^2 (TEC86E86)	AvCarb G300A graphite felt

MEA 37 was fabricated in the following way. The anode catalyst solution was made according to the standard fabrication procedure with appropriate amounts of TKK 77% PtRu catalyst (TEC86E86). The solution was then spray coated onto Sigracet 29AA carbon paper (without an MPL) using a Iwata Ninja Jet spray coater. The cathode solution was mixed using a similar procedure so that the ionomer to Pt ratio was 0.2. The solution was then spray coated onto Toray 060 carbon paper (without an MPL). Figure 3.4 details the performance of MEA 37, which was fabricated using commercial components and used as a baseline comparison for the MEAs in this study. It should be noted that MEA 37 was one of the highest performing MEAs

tested in this lab as shown in section 3.1. Figure 3.4 (a) shows that without the FML the MEA experiences performance losses of 40% when concentration is increased from 1M to 3M and 68% when increased to 7.5M. Figure 3.4 (b) shows the benefits of the FML with minimal losses in performance when concentration is increased. In fact, the performance at 15M is comparable to the peak power seen at 7.5M without an FML. However, the overall peak power density with this FML is limited. Figure 3.4 (c) shows that this is primarily because of the increased ohmic

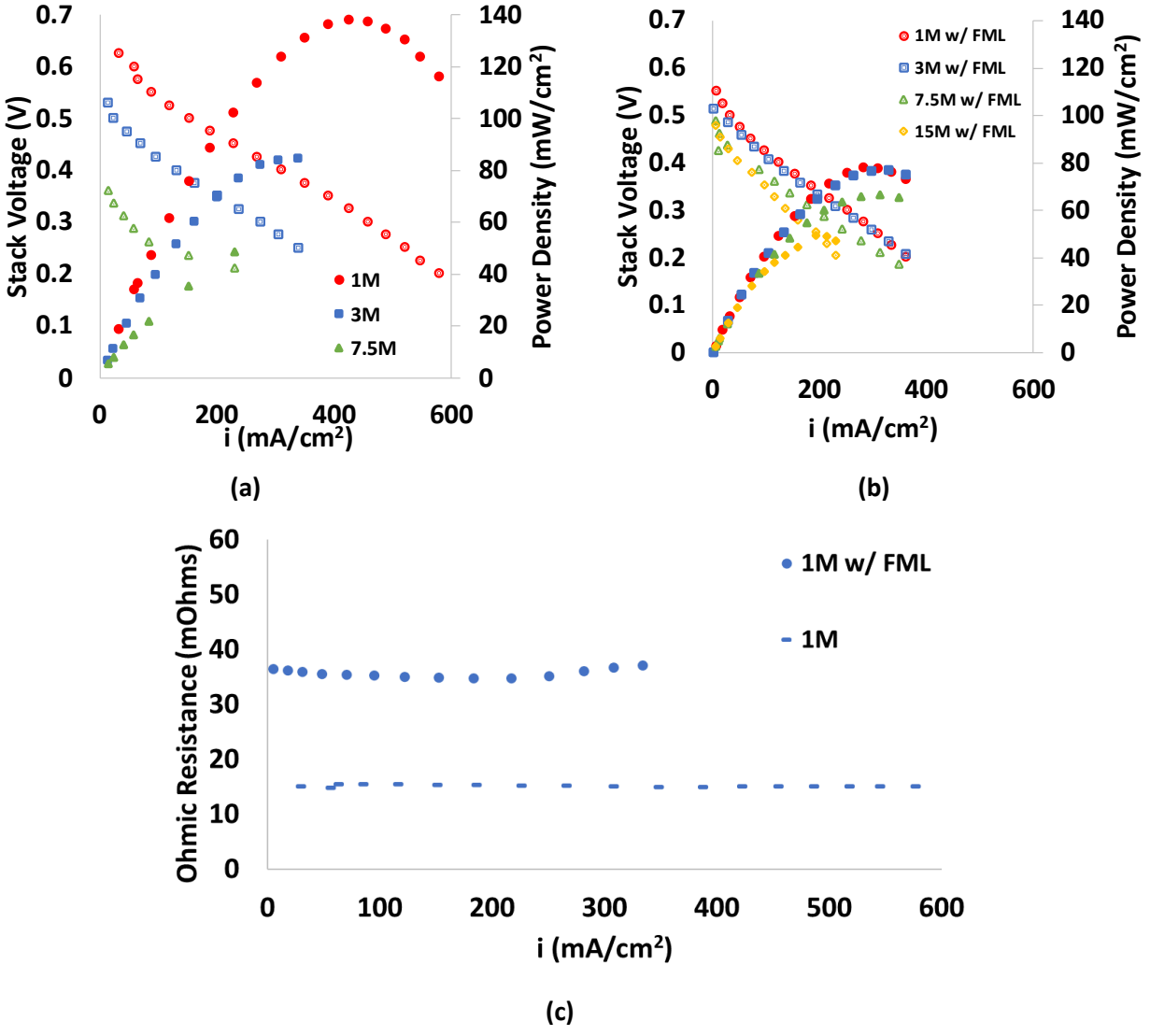

Figure 3.4: Performance of MEA 37 without an FML (a), with an FML (b), Resistance comparison at 1M (c); All tests run at 80 °C and 50 kPa backpressure

resistance due to the thickness of the FML. Therefore, it is recommended to design FMLs to minimize the electric resistance while still allowing for diffusion of methanol prior to reaching the CL.

3.3 Design of Microporous Layers

The role of MPLs on either the anode or the cathode has been consistently identified as a leading contributing factor to the crossing over of fuel from the anode to cathode, and water from the cathode to anode. This component has received significant attention in the research community. For example, a study by Liu et al. found that cathode flooding is a primary cause of decreases in performance due to the increased water presence blocking the inflow of air to the cathode [26]. Based on that, the authors concluded that the cathode should be hydrophobic on the MPL to push water back through the membrane to the cathode. Furthermore, they concluded that the reversed electro-osmotic drag had the potential to reduce fuel crossover from the anode due to the increased resistance [26]. On the anode side, it is typical to also use a hydrophobic MPL with a significant thickness to reduce methanol crossover. However, Li et al. found that hydrophilic MPLs on the anode provide superior performance in passive DMFCs under constant discharge conditions. The authors concluded that at the medium to high current density ranges the performance of hydrophobic MPLs on the anode was better suited due to the decreased accumulation of water in the cathode [27]. Based on these works, as well as the work presented in Chapter 2, it was decided to test the effect of hydrophilic MPLs on active DMFC systems. In order to do this, two MEAs with hydrophilic MPLs were fabricated which are listed in Table 3.2. These MEAs are compared to MEA 14 which was fabricated with a hydrophobic MPL to examine

the differences. It should be noted that MEA 14 was fabricated using TKK 50% PtRu catalyst (TEC66E50), which had a lower-performing power density in baseline tests than MEA 37. Additionally, the effect of post-fabrication treatment on the MPL was examined and is also detailed in Table 3.2.

The hydrophilic solutions were fabricated in the following way. One gram of DI water was placed into a glass bottle and 500 mg of Vulcan XC-72R activated carbon support was added. Next, 4 grams of Nafion® 10%, or 400 mg of Nafion® total, was added to the mixture so that the ionomer to carbon ratio was 0.8. The solution was then sonicated using the Branson 1800 sonicator for 2.5 hours. The slightly longer sonication time was due to the high dry mass content of the mixture and to ensure that adequate dispersion was reached. It was decided to use only DI water as the solvent since the faster evaporation of IPA may have caused increased cracking in the MPL. The sonicated solution was then dropped into the Iwata Ninja Jet air brush 1-2 mL at a time and spray-coated onto two separate 2.5 cm x 2.5 cm pieces of Toray 060 carbon paper (without a MPL) so that the loading was approximately 1 mg/cm^2 of hydrophilic MPL. One anode substrate was allowed to dry under atmospheric conditions for 24 hours. The other was placed into a Magic Mill food dehydrator and dried for one hour at 74 °C. It was suspected that this would improve the pore size distribution of the MPL, which was identified as a critical factor in the performance of the GDL in the previous section. After drying, an anode solution was fabricated using TKK 50% PtRu catalyst (TEC66E50) and the fabrication procedure detailed in the previous section of this thesis so that the ionomer to PtRu ratio was 0.4. The catalyst solution was then spray coated onto the two hydrophilic anode substrates so that the PtRu loading was approximately 4.5 mg/cm^2. The cathodes were fabricated in a similar manner by collaborators at

Kansas State University (KSU) so that the loading was approximately 1.5 mg/cm^2. The MEAs were then hot pressed at 135 °C for five minutes at 345 kPa. Both the anode and cathode for MEA 14 was fabricated by KSU and hot pressed at the University of Kansas (KU). Each MEA was activated according to the standard activation procedure detailed in section 3.2. After activation, the same series of tests were performed on each MEA. Using 1M methanol solution supplied at a rate of 1 mL-min and air supplied at a rate of 0.1 L/min with an applied back pressure of 50 kPa at 80 °C, polarization curves were performed by allowing the MEA to rest at OCV for three minutes. A polarization scan was then performed by scanning the MEA from OCV to 0.2V, and recording the current density, power density, and ohmic resistance during the scan. The scans were repeated at 3M, and 7.5M solutions keeping a stoichiometric ratio of fuel flow rates, and the same air flow, temperature, and backpressure. Figure 3.5 shows the peak power densities recording during these tests.

Table 3.2: MEAs tested with hydrophilic MPLs

	Cathode	**PEM**	**Anode**	**MPL**
MEA 14	JM Pt/C 60% Approximately 1.5 mg/cm^2 (HiSPEC 9100)	Nafion® 212	TKK PtRu 50% Approximately 4.5 mg/cm^2 (TEC66E50)	Sigracet 29BC Hydrophobic MPL
MEA 25				Hydrophilic MPL 1.28 mg/cm^2 on Toray CP; Air

		dried for 24 hours
MEA 32		Hydrophilic MPL 1.28 mg/cm^2 on Toray CP; Dehydrated at 74 °C for one hour

It can be seen from the results in figure 3.5 that the hydrophilic MPLs did indeed have an impact on the performance using 3M methanol solution regardless of the post-fabrication treatment of the GDL. Both MEA 25 and 32 achieved comparable peak power densities of 68.1 and 70.1 mW/cm^2 at 3M concentration, respectively. The MEA 14 experienced its peak power density of 71.4 mW/cm^2 using 1M solution. However, under 3M fuel conditions, MEA 14 was only able to achieve 21.7 mW/cm^2. This large performance drop from 1M to 3M fuel solutions is quite typical with MEAs fabricated with commercial components

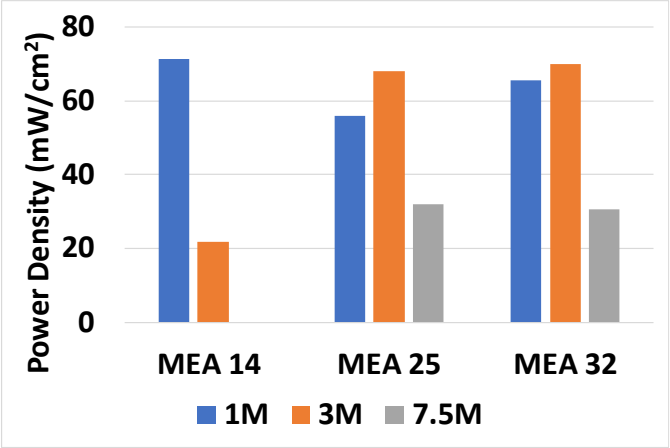

Figure 3.5: Peak power density comparison of MEAs 14, 25, and 32 and varied concentrations

and hydrophobic MPLs on the anode. The benefit of the hydrophilic MPL seems to be diminished at 7.5M, or 25% by weight, concentrations as shown in figure 3.5 by more than 50%.

A few conclusions can be drawn from these results. First, the hydrophilic MPLs do act to enhance performance at slightly increased concentrations. However, it is believed that the recommended MPL loading of approximately 1 mg/cm^2 proposed by Li et al. may result in an increased pore size distribution (PSD), whereas the more recent work Metzger, Li et al. suggests that a decreased PSD and pore size would enhance the reduction of crossover [23] [27]. Second, the performance between MEA 25 and MEA 32 indicated that there is not a large difference between air drying and dehydrating for post-fabrication treatment of the MPL. It is believed that this is because the relatively low temperature and drying time of the dehydrating process did not likely have an effect on the PSD. Due to this, it was decided to hot press further hydrophilic GDLs to determine if this was the case. However, there was difficulty in the carbon support surviving this process without damage. Therefore, these MPLs could not be tested under full cell conditions. However, SEM images were able to be taken and confirmed that the PSD was indeed improved after hot pressing as shown in figure 3.6.

The three MPLs seen in figure 3.6 were fabricated in the same manner as the MPLs on MEA 25 and 32, however, these were spray coated as one MPL, then cut separately for post-fabrication treatment. This allowed the MPL loading to be consistent between the three GDLs so that the thickness and PSD changes due to post-fabrication treatment could be more accurately measured. It can be seen from figure 3.6 (a)-(c) that each subsequent post-fabrication process does improve the PSD. Therefore, it is recommended to explore varied gasket thickness according

to the thickness of the MPL to reduce damage to carbon backing. Table 3.3 details the average thickness of each MPL as measured by SEM imaging using a Hitachi H-8100 Scanning Electron Microscope with the help of the KU Microscopic and Analytical Imaging Lab.

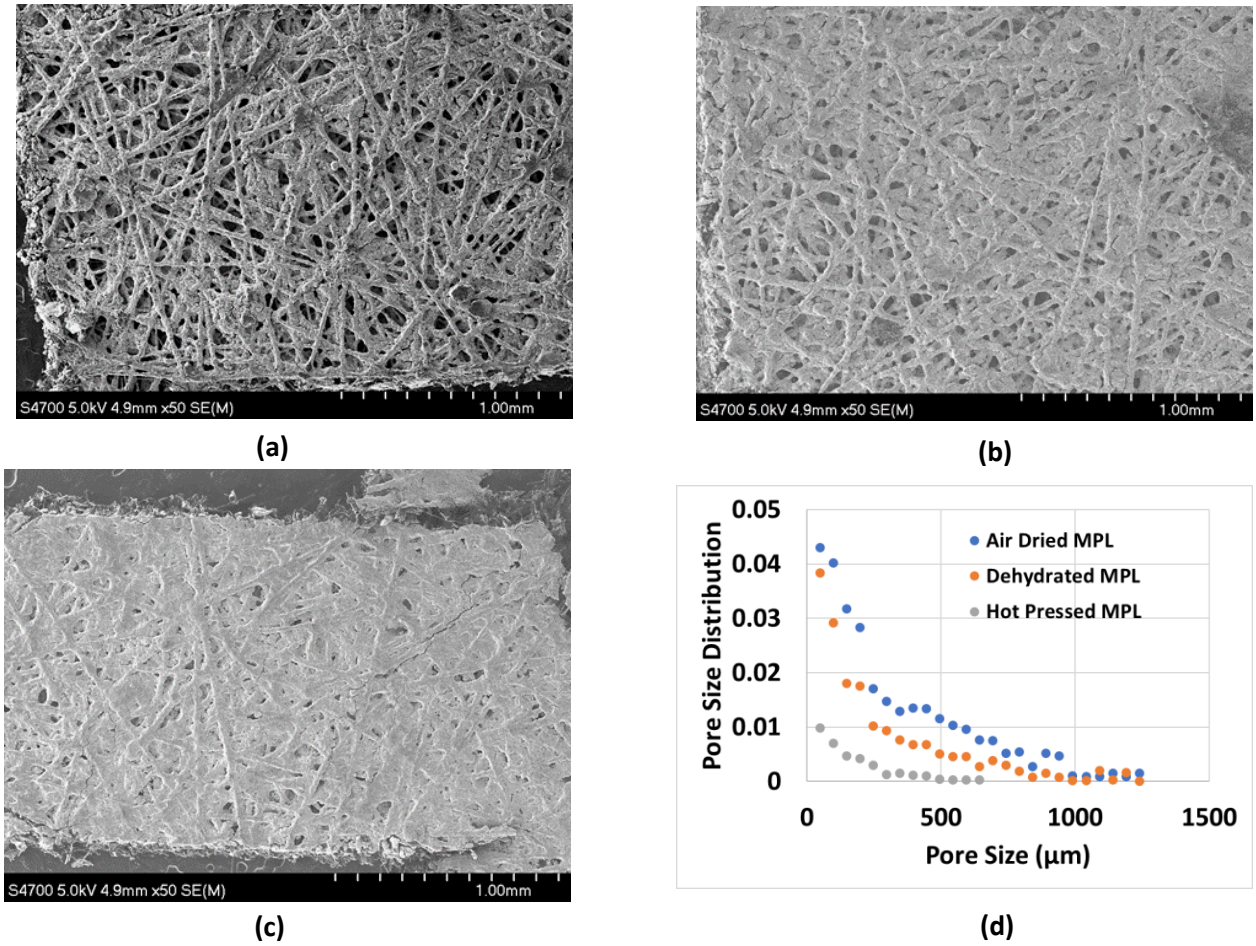

Figure 3.6: SEM images of air dried (a), dehydrated (b), hot pressed (c) MPLs; and pore size distribution (d)

Table 3.3: Microporous Layers Fabricated and Imaged

	MPL Loading	**Mean MPL Thickness (µm)**
Air Dried	1.52 mg/cm^2	170.3

Dehydrated at 74 °C for one hour	186.5
Hot Pressed at 345 kPa and 135 °C for one minute	140.4

The third and final conclusion that can be taken from this study is that while hydrophilic anode MPLs do seem to slightly reduce the crossover and allow the cell to operate optimally at 3M fuel concentrations, the in order for DMFCs to be effective in portable power applications the use of pure methanol will become necessary to maximize the energy density in fuel packs. Therefore, it is recommended to further improve upon this design and not consider it an ultimate solution to the problem of crossover. Rather these hydrophilic gas diffusion layers can be considered a promising component in an overall approach to reducing fuel crossover in the DMFC.

3.4 Polymer Electrolyte Membrane Modification

Another approach that has been investigated in recent years is the modification of the PEM by graphene, zwitterionic polymers, and other novel materials [28]. The aim to reduce the fuel crossover either by providing a barrier that larger methanol particles cannot pass through, such as in graphene, or by limiting the crossover due to ion-dipole interaction differences as with the zwitterionic polymers. This section will investigate both of these approaches as well as their effectiveness in allowing the DMFC to operate at elevated concentrations.

3.4.1 Graphene Coated PEMs

Graphene has been a material with extensive research done in recent years and has the potential for many applications in the electrochemical sector. This is due to a variety of properties that lend well to this application such as a large theoretical surface area of 2630 m^2 g^{-1}, high charge mobility, mechanical durability, and high chemical stability [29]. Additionally, it is known for its thermal conductivity and high electron transfer (HET) properties [29]. It will be shown later in this section that the high thermal conductivity of graphene limits the current application of these layers in the PEM when typical operating temperatures of 80 °C is approached. Very recently, Su et al. published a comprehensive analysis of recent findings on various graphene components and their derivatives where it relates to fuel cell applications. They found that graphene had applications beyond modification of the PEM, such as in the current collectors and even as potential cathode catalysts due to their desirable chemical properties [29]. This work will only focus on the graphene-enhanced PEMs so to focus on applicable data completed by the authors in laboratory experiments. However, many other potentials of graphene should be further investigated as recent studies show high promise in fuel cell applications.

To study the effect of graphene coated PEMs, the authors collaborated with General Graphene Corporation (GGC) which is well known for the mass production of a variety of graphene products. Due to the limited fabrication ability of the lab at KU, all fabrication of modified PEMs were performed at GGC by onsite staff. Thus, the fabrication of the PEMs will not be detailed in this work. The anodes and cathodes paired with these membranes were fabricated according to the standard fabrication procedure detailed in previous sections. The anode catalyst used in this study was TKK 50% PtRu, and the ionomer to PtRu ratio was held at 0.4 as in previous studies. The cathode catalyst remained the same using JM 60% Pt/C (HiSPEC 9100) with an

ionomer to Pt ratio of 0.2. Anode catalyst loadings were held at approximately 4.5 mg/cm$^2_{PtRu}$ and cathode loadings were held at 1.5 mg/cm$^2_{Pt}$. Anode GDLs utilized Sigracet 29BC carbon paper (with a hydrophobic MPL), and the cathodes used Toray CP (with no MPL) to remain consistent with previous studies. This study analyzed four different Nafion® membranes modified with various forms of graphene and were compared with MEA 14, which utilized a Nafion® 212 membrane and commercial components fabricated with the TKK 50% catalyst (TEC66E50). These MEAs and their respective components are detailed in Table 3.4.

Table 3.4: MEAs utilized in the study of various graphene enhanced Nafion® membranes

	Cathode	**Anode**	**PEM**
MEA 14	JM Pt/C Appx 1.5 mg/cm^2 (HiSPEC 9100)	TKK 50% Appx 4.5 mg/cm^2 (TEC66E50)	Nafion® 212
MEA 18			CVD Graphene on Nafion® 212
MEA 21			CVD Graphene on Nafion® 115
MEA 22			Nafion® 211 – Graphene – Nafion® 211
MEA 27			Nafion® HP – Graphene – Nafion® HP

MEAs 18 and 21 utilized graphene applied by chemical vapor deposition (CVD) whereas MEAs 22 and 27 had a sandwiched graphene approach in which membranes of varied thickness were used to sandwich the graphene. As mentioned before, the methodology behind each MEA is to prevent methanol crossover by filtering out methanol particles according to their larger size. Figure 3.7 (a-b) details the results at 80 °C and figure 3.8 (a-c) details the results at 30 °C. MEA 18 was activated according to the standard procedure detailed in previous sections using 0.25M methanol at 80 °C. It was then speculated and later confirmed by GGC that the long duration and high temperature of activation delaminated the graphene layer from the PEM. Therefore, we decided to reduce the activation temperature to 30 °C for MEA 21, 22, and 27.

Figure 3.7 (a) shows that MEA 22 exhibited the highest peak power density at 1M, with MEAs 18 and 21 exhibiting reduced peak power density in comparison to MEA 14. Figure 3.7 (b) indicates the enhanced tolerance to 3M methanol solution of each MEAs 18, 21, and 22 in comparison to MEA 14 which showed drastic peak power losses in comparison to the treated

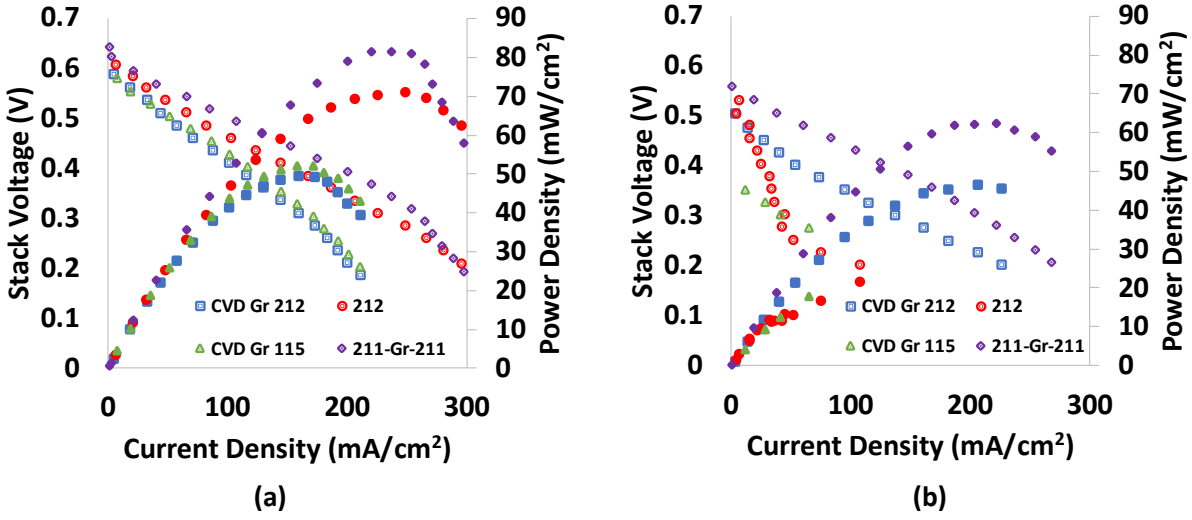

Figure 3.7: Performance results of MEAs 14, 18, 21, and 22 at 1M (a), 3M (b); 80 °C, 1 ml/min fuel (1M), 0.1 l/min air, 50 kPa backpressure.

membranes. While the performance loss was not as pronounced with the graphene membranes, there was still a reduction in peak power density. However, since it was advised by GGC that high temperatures cause delamination of the graphene layers it was decided to test MEAs 22 and 27 at 30 °C.

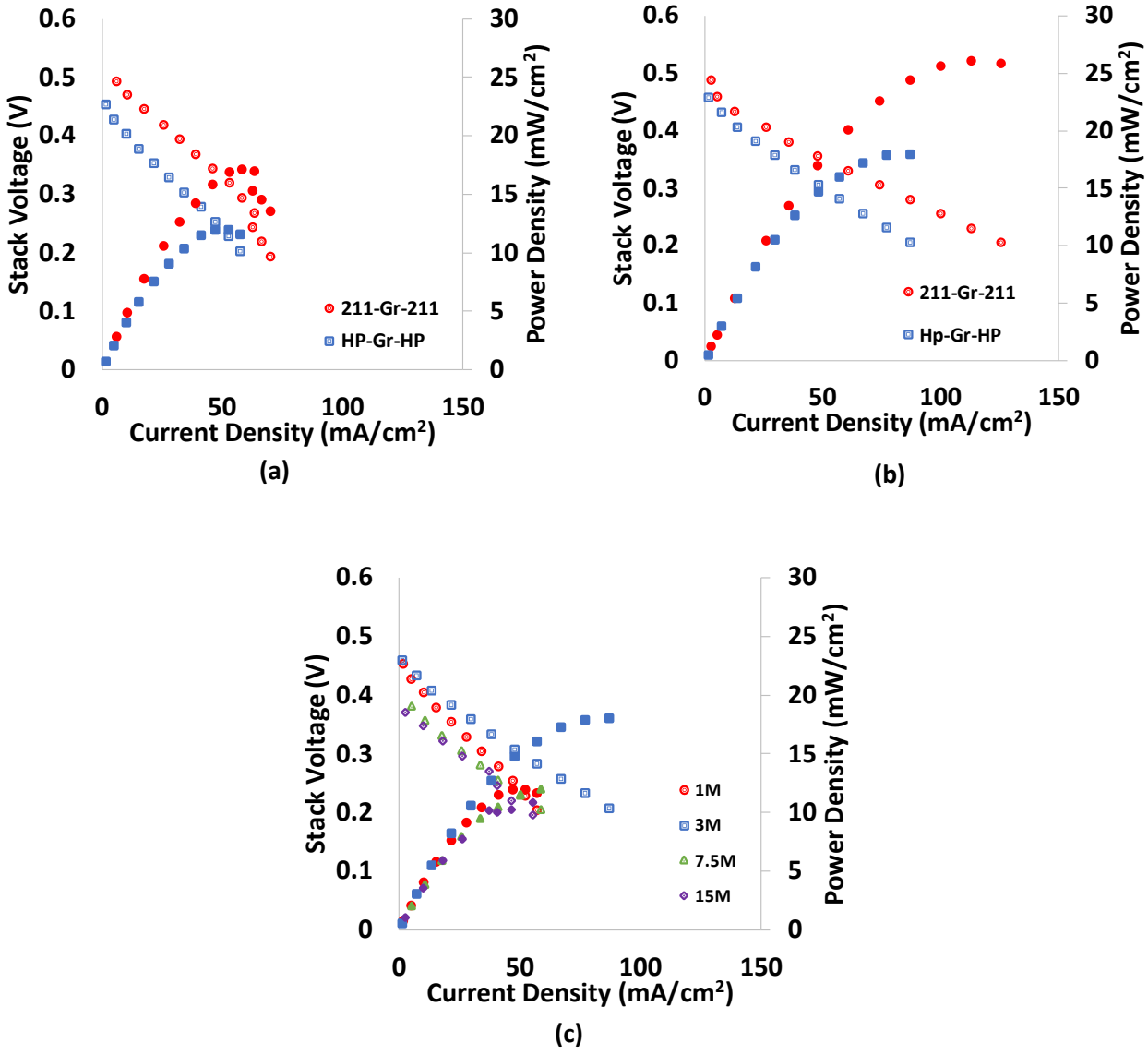

Figure 3.8: Performance results of MEAs 22, and 27 at 1M (a), 3M (b), and MEA 27 at varied concentrations (c); 30 °C, 1 ml/min fuel (1M), 0.1 l/min air, 50 kPa backpressure.

Figure 3.8 (a) shows the results of standard testing of MEA 22 and 27 at 1M and 30 °C. It is clear the peak power density was lower than typical; however, this was expected due to the low temperature. Figure 3.8 (b) highlights the benefits of using graphene enhanced membranes not only exhibiting tolerance to increased methanol concentration but showing an increase in peak power density. Furthermore, MEA 27 showed a high tolerance to increased concentration exhibiting peak performance at 3M, and preserving peak power density up to 15M, or approximately 50% by weight, as seen in figure 3.8 (c). After testing MEA 27 at 30 °C it was decided to test at an intermediate temperature of 65 °C. It is well known that the vapor point of methanol is approximately 65 °C so this provides useful information as to the impact of the phase state of methanol when using graphene-based membranes. Figure 3.9 shows the results of these tests. It can be seen that while an improved peak power density of approximately 55 mW/cm^2 is achieved, the tolerance to increased methanol concentration is lost by 55%.

A sample was cut from the membrane of MEA 27 before and after testing for SEM imaging. Figure 3.10 (a) shows the membrane before it was tested, and figure 3.10 (b) shows the membrane after testing at 65 °C. The delamination of the layers in the membrane can be clearly seen in these images. This shows that even at intermediate temperatures delamination still occurs and the effectiveness of crossover reduction is diminished.

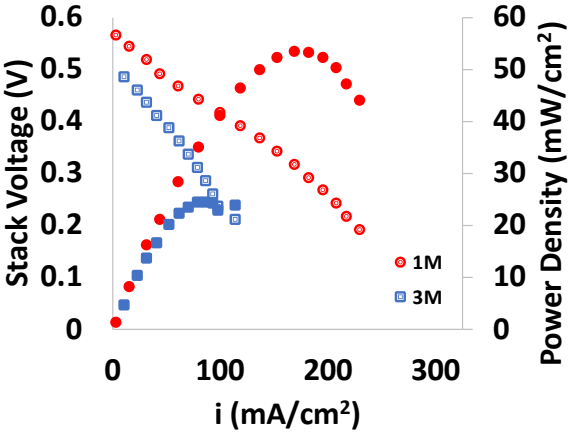

Figure 3.9: Performance results of MEA 27 at varied concentrations; 65 °C, 1 mL/min fuel (1M), 0.1 L/min air, 50 kPa backpressure.

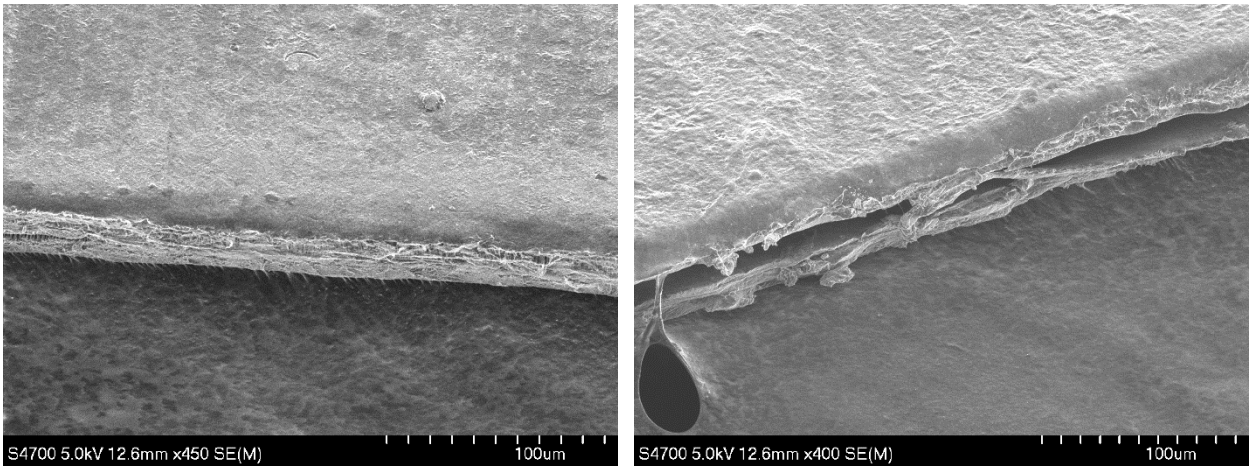

(a) **(b)**

Figure 3.10: SEM Images of MEA 27 before testing (a), and after testing (b) showing delamination of graphene layers.

There are many implications in the results of these tests. First, graphene has promise in fuel cell applications, specifically in the reducing fuel crossover. However, the current technologies limit the application of graphene-coated PEMs due to the high thermal conductivity of graphene. Furthermore, the graphene layers are very thin on the order of nanometers. While the material itself possesses mechanical durability as detailed by Su et al., such thin layers are fragile by nature. This is especially true when the graphene is applied to the outer layers of the membrane such as with MEAs 18 and 22. The second is that the delamination of these layers is primarily due to the swelling of the Nafion® membrane under hot methanol solution conditions. Rao et al. found that Nafion® can be swelled up to 25% of its volume due to its polymer nature under typical operating conditions [30]. A variety of treatments can mitigate this as Rao details in their work [30]. Therefore, it is recommended to further investigate ways to strengthen the durability of Nafion® prior to the application of graphene to mitigate this effect. It is also

important to consider the liquid-vapor state of methanol under the varied operating conditions. Methanol evaporates between 60 °C and 70 °C depending on pressure, and exactly at 64.9 °C with no applied pressure. This provides useful information as to the reason of reduced effectiveness at elevated temperatures. It is well known that when any material vaporizes, the particle size decreases. Since the function of the graphene sorts out methanol based upon the larger liquid particles, it makes sense that the vapor particles can more easily pass through the layer at high temperatures. This is further exacerbated by the expansion of the graphene layer due to Nafion® swelling. Furthermore, the exact vaporization point of methanol explains why this effect is diminished at precisely 65 °C. Therefore, the following recommendations are made. Graphene-based fuel cell components show high promise but are not yet applicable for high performance PEMs within the cell. Further study should be done on reinforcement of the of the membrane in order for the cell to run at operating temperatures of 80 °C. Rao et al. shows that ultraviolet (UV) irradiation of the membrane can reduce the swelling to 20%, however, this should be further reduced not to not damage the graphene layers [30]. It is also recommended to investigate the application of graphene within other parts of the cell as recommended by Su et al. earlier in this section. This is particularly interesting in applications as a cathode catalyst since the reduction of PGM content in the overall cell greatly reduces installation costs which dominate the price of DMFCs [29]. Finally, it is recommended that a mechanically enhanced graphene layer be investigated. Su et al. also mentions the application of 3-D graphene [29] which may prove more robust when swelling occurs.

3.4.2 Modifications of PEMs via a zwitterionic polymer

Over the last decade the study of zwitterionic polymers has received attention in the fuel cell community, especially in its ability to reduce methanol permeability by differences in ion-dipole interactions. This is due to their ability to reasonably preserve proton conductivity while simultaneously reducing methanol flux throughout the membrane. A study conducted by Tripathi et al. compared the performance of three different weight percentages of a customized zwitterionic polymer. Their work found that these polymers can achieve this, especially at low temperatures while maintaining a proton conductivity similar to that of Nafion® 117 [31]. However, they also mention that water uptake and parasitic free-radical attacks are particularly high at operating temperatures are at 80 °C which is optimum for cell power production. To mitigate this, they suggest using a crosslinked structure to make the hydrophilic pore size smaller making it harder for the free-radical groups to penetrate the membrane [31].

To further examine the possibilities of zwitterionic polymers in DMFCs the authors of this work collaborated with the surface science laboratory at KU, led by Dr. Gibum Kwon. This study focused on using three separate zwitterionic polymer coated Nafion® HP. The first membrane used a baseline zwitterionic coating, the second used a zwitterionic coating with twice the crosslink density, and the third membrane was coated with the zwitterionic polymer to twice the thickness of the first membrane. Dr. Kwon and his graduate students performed the fabrication of these membranes. Since the coating was under development by the lab, detailed fabrication or chemical makeup was not shared. The thickness of the coating was also very thin, on the order of nanometers, but not directly measured. Fabrication of the anode, cathode, and overall, MEA was performed by the authors according to standard fabrication procedures detailed in earlier sections of this paper. As with the graphene study, TKK 50% PtRu (TEC66E50) was used as the

anode catalyst and JM 60% Pt/C (HiSPEC 9100) was used for the cathode. Each GDE was fabricated according to the standard procedure previously detailed. Dr. Kwon and his lab noted that the maximum temperature sensitivity of these membranes was approximately 65 °C so activation was done at 30 °C as well as initial polarization testing. After tests near room temperature were complete, each MEA was tested at 65 °C to determine if the coating was effective near its thermal limit. Table 3.5 details the construction of each MEA. All activation and testing was done according to the standard procedures defined at this work at the temperatures referenced.

Table 3.5: MEAs utilized in the study of various zwitterionic Nafion® membranes

	Cathode	**Anode**	**PEM**
MEA 29			Zwitterionic polymer on Nafion® HP
MEA 30	JM 60% Pt/C Appx 1.5 mg/cm^2 (HiSPEC 9100)	TKK 50% PtRu Appx 4.5 mg/cm^2 (TEC66E50)	Zwitterionic polymer on Nafion® HP with 2x crosslinks
MEA 31			Zwitterionic polymer on

	Nafion® HP with 2x thickness

Figure 3.11 (a-b) shows the results of testing on each MEA at 30 °C at 1M (a) and 3M (b). It can be seen from the results that MEA 29 with the plain ionic coating on HP had the most positive effect on crossover reduction increasing from 13 mW/cm^2 to 20 mW/cm^2 when increased from 1M to 3M. MEA 30 and 31 both exhibited reduced peak power density at 1M as seen in figure 3.11 (a). The peak power density only increased marginally (>2 mW/cm^2) when the concentration was increased to 3M as shown in figure 3.11 (b). Furthermore, MEA 30 and 31 had nearly identical performance indicating that increasing the crosslink density or the thickness of the coating had a similar effect.

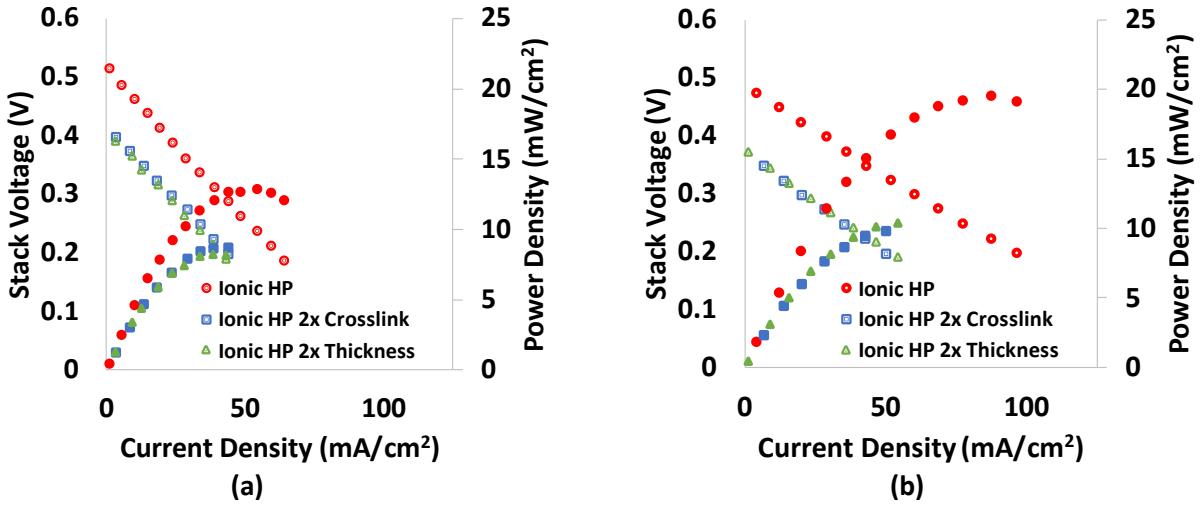

Figure 3.11: MEAs 29, 30, and 31 results at 1M (a), and 3M (b) 30 °C, 1 ml/min fuel (1M), 0.1 l/min air, 50 kPa backpressure

Figure 3.12 (a-b) shows the performance of each MEA when the temperature was increased to the sensitivity limit of 65 °C. It can be seen in figure 3.12 (a) that increasing the temperature improved the peak power density of each MEA reaching a maximum of 40 mW/cm^2 with MEA 29. The peak power densities of MEAs 30 and 31 remained reduced at 19 mW/cm^2 and 21 mW/cm^2, respectively. The results seen in figure 3.12 (b) are particularly interesting. MEA 29 experienced a reduced peak power density of approximately 24 mW/cm^2; however, MEA 31's peak power density increased slightly to approximately 25 mW/cm^2, or by about 23%. MEA 30 did not experience this and the peak power remained the same. This indicates that increasing the thickness improves the temperature tolerance more than increasing the crosslink density, which is useful for further research.

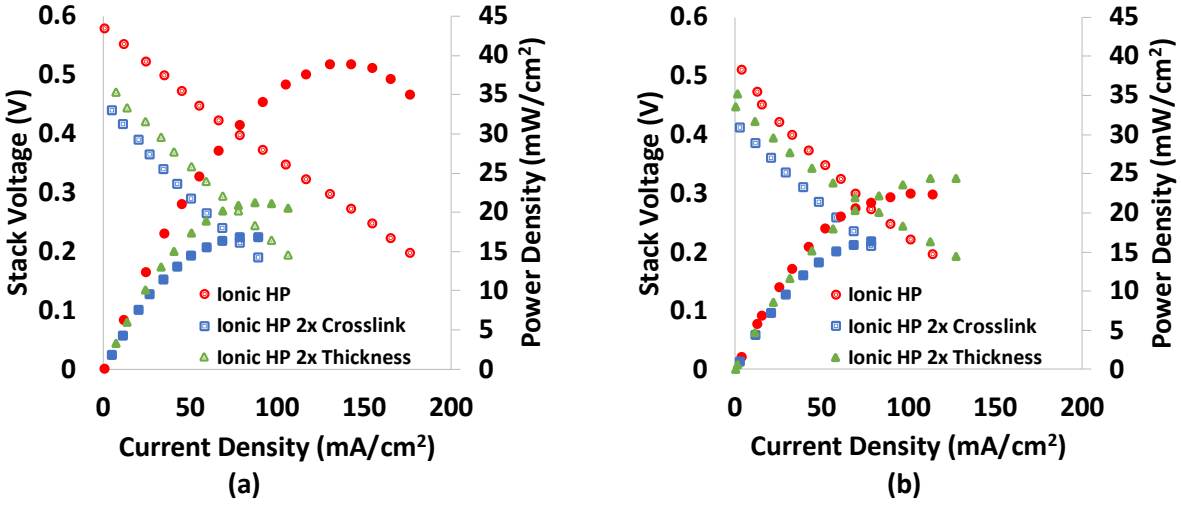

Figure 3.12: MEAs 29, 30, and 31 results at 1M (a), and 3M (b) 65 °C, 1 mL/min fuel (1M), 0.1 L/min air, 50 kPa backpressure

While the zwitterionic polymer did not perform as well as Tripathi et al. predicted in their analysis, there was some success at lower temperatures, particularly with the plain zwitterionic polymer. This may provide useful information as to whether the thickness of the coating or the

crosslink density plays a more important role in the effectiveness of crossover reduction at elevated temperatures. Based on the data presented, the thickness of the coating provides a slightly more robust membrane at higher temperatures. In contrast, a coating with the same thickness, but twice the crosslink density suffers more from layer expansion near its thermal limit.

The results and studies presented in this section have led to the following conclusions and recommendations. First, the zwitterionic polymer has attracted much attention in recent years and clearly has the potential for crossover reduction. However, based on experimental data obtained by the author and conclusions made by those in recent works, the current state of the zwitterionic coating does not allow it to achieve optimum performance at elevated temperatures, particularly at operating temperatures of 80 °C. One of Tripathi et al.'s conclusions may lend useful information in this aspect. Their work tested three different weight percentages of a Nafion® membrane coated with the zwitterionic polymer. It should be noted here that the chemical build of their coating may differ from that of the one at KU, however, the electrochemical functionality is very similar. Based on their results, the methanol-water uptake of the Nafion® membrane increases with the weight and density of the coating [31]. While the coatings are mechanically stable, it can be assumed that such a thin coating as tested in this study would fracture under heavy Nafion® swelling conditions just as observed in the graphene-coated membrane study in section 3.4.1. This would explain why the increased crossover was observed at elevated temperatures. Therefore, it is recommended that either the mechanical stability of the membrane or coating itself needs to be improved so it can be utilized at higher temperatures. Next, it is recommended to investigate the membrane after testing by SEM imaging to determine the loss of the coating and whether it was due to membrane swelling or the chemical

decomposition of the coating itself. This information would prove useful in focusing further research. Finally, testing a sandwich structure with the coating on the inside of two Nafion® membranes is recommended. This could be performed using Nafion® HP membranes as were tested in this study. This may allow for the swelling damage to the coating to be reduced without adding significant resistance that would contribute to performance loss since two Nafion® HP membranes are still thinner than a 212 membrane which is most often used in these studies. The reason for this recommendation is that swelling of the membrane is primarily along the in-plane. The physical construction of the fuel cell, and the fact that it is clamped between 27 and 41 Nm of torque by a series of bolts, heavily restrict the swelling in the through-direction. It may also be investigated to perform the coating on an already swelled membrane to mitigate this effect, though this has proved difficult both with zwitterionic and graphene coatings primarily because the fabrication process is difficult on a wet and swelled membrane.

Chapter 4

ANODE CATALYST OPTIMIZATION

4.1 Variations in Commercial Catalysts

The slow reaction kinetics on the anode side of DMFCs has been repeatedly identified as a leading barrier to more widespread use of the cells. Additionally, it contributes to fuel crossover heavily as the longer reaction time allows more unreacted methanol to pass through the cell. Furthermore, the long reaction time and carbon dioxide (CO_2) generation contributes to catalyst poisoning [32] which damages the performance of the anode over long term use. Catalyst poisoning is a phenomenon that occurs when CO_2 is generated within the CL as a part of the MOR and blocks active Pt sites making them unavailable for methanol oxidation. Due to these reasons, many commercial companies have attempted to create high performance anode catalyst with varying success. While many catalysts have been developed focused on PGM including Nickel, Cobalt, and other materials, the focus of this work will remain on PtRu based catalysts primarily on carbon supports. The primary difference in these catalysts is the kind of support material used, the PGM content of the catalyst, and ratio of Pt:Ru. Each factor plays an important role in the electrochemical performance of the anode. For example, in order to achieve high performance, it is necessary to have a high electrochemical surface area (ECSA). Advanced carbon support provides this due to its large ESCA, and Vulcan XC-72R is commonly used as a support. Furthermore, improved carbon supports have been investigated by many such as carbon nanotubes (CNTs), multiwalled carbon nanotubes (MWCNTs), and graphene enhanced carbon support [33]. The PGM content also plays a large role in performance as the amount of available

Pt sites is crucial for high power output. The ratio of platinum to ruthenium is important in the durability of the cell as ruthenium is utilized to scrub the CO_2 off of active Pt sites [32] to allow for longer life of the MEA.

Due to the difficulty in producing an effective anode catalyst, few companies remain in the market consistently as available for research and development uses. This work will focus on the study of three anode catalysts, two of which have been discontinued after testing. Johnson Matthey PtRu (75%) (HiSPEC 12100), TKK 50% PtRu (TEC66E50), and TKK 77% PtRu (TEC86E86) was studied to examine the differences in performance of each commercial catalyst. Detailed design specifications for each catalyst can be found in Appendix A-3 of this work. Three anodes were fabricated according to the standard fabrication procedure, each on Sigracet 29BC (with a hydrophobic MPL) so that the PtRu loading was approximately 4.5 mg/cm^2_{PtRu} and the ionomer to PtRu ratio was 0.4. Similarly, three cathodes were fabricated using JM 60% Pt (HiSPEC 9100) so that the Pt loading was approximately 1.5 mg/cm^2_{Pt} and the ionomer to Pt ratio was 0.2. Each MEA utilized a Nafion® 212 membrane as a PEM. Table 4.1 details the construction of each of these MEAs. The anodes and cathodes for MEA 12 and 14 were fabricated by KSU and the anode and cathode for MEA 54 was fabricated by KU using the same procedure. Each anode catalyst utilized a high surface area carbon support. The molar ratios varied with each catalyst and are also detailed in table 4.1.

Table 4.1: MEAs tested comparing three different commercial anode catalysts

	Cathode	Anode	PEM	Molar Ratio (Pt:Ru)
MEA 12	JM Pt/C Appx 1.5 mg/cm^2 (HiSPEC 9100)	JM PtRu 75% Appx 4.5 mg/cm^2 (HiSPEC 12100)	Nafion® 212	1:1
MEA 14		TKK PtRu 50% Appx 4.5 mg/cm^2 (TEC66E50)		2:1
MEA 54		TKK PtRu 77% Appx 4.5 mg/cm^2 (TEC86E86)		2:1

Each MEA was activated and tested according to the standard procedures detailed in section 3.1. Figure 4.1 (a-b) details the results of these tests. When compared with performance of similar MEAs reported in recent publications, the results are quite encouraging. Figure 4.1 (c) shows the resistance of each MEA during testing at 1M. It can be seen from the results that the resistance is closely related to the performance of each MEA and are inversely proportional. For example, MEA 12 had the highest peak power density and the lowest ohmic resistance and MEA 14 showed the lowest peak power with the highest resistance. It should be noted here that the ohmic resistance measured by the Scribner 890e is a combination of all resistances experienced by the MEA, therefore it is difficult to tell which resistance is limiting the MEA. However, from a

structural view, it can be assumed that the increased thickness of the CL will result in a higher mass transfer resistance. This explains why MEA 14, which required a much thicker CL due to the lower PGM content, experienced a higher resistance. Both MEA 12 and 14 had similar thickness and thus comparable ohmic resistances. Thus, the molar ratio may explain the differences between MEA 12 and 54. MEA 12 had a 1:1 Pt to Ru ratio and MEA 54 had a 2:1 ratio as seen in

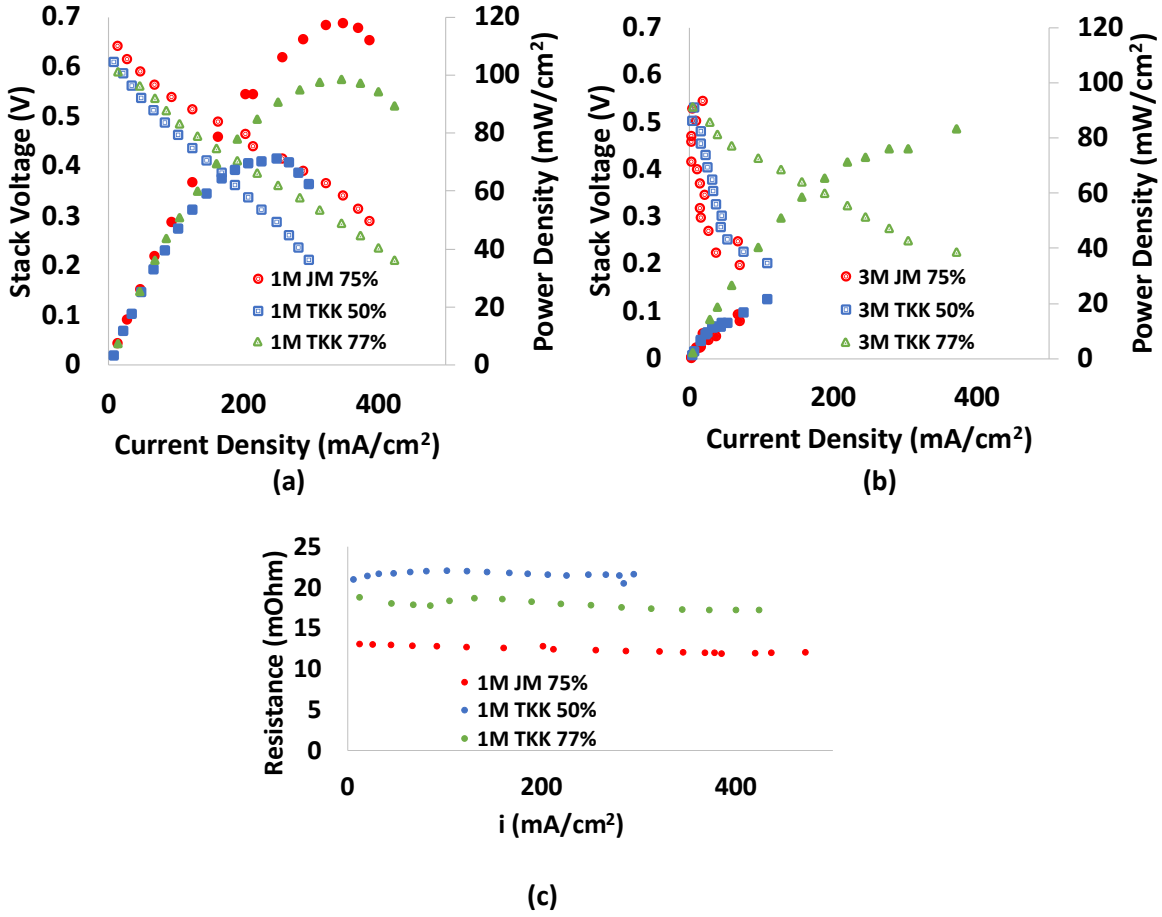

Figure 4.1: Performance results of MEA 12, 14, and 54 using 1M methanol (a); and 3M methanol (b); Ohmic resistance comparison of each MEA during testing (c); All tests run at 80 °C and 50 kPa backpressure according to the standard testing procedure using 1 mL/min fuel (1M), 0.1 L/min air

table 4.1 so MEA 54 had a higher Pt content and a lower Ru content. This suggests that MEA 54 is not as effective at removing CO_2 from active Pt sites resulting in less available catalyst reactions.

MEA 12 on the other hand had the same molar amount of Ru so this MEA was more effective at scrubbing CO_2 thus resulting in more catalyst activity on the anode.

These tests are important in providing a baseline for other MEAs. It can clearly be concluded that the JM 75% (HiSPEC 12100) is the best anode catalyst for the standard tests defined in this work. However, results seen in Chapter 3 show that by altering other components of the MEA, such as the GDL, the performance of the TKK 77% (TEC86E86) can be improved beyond the results seen with MEA 12. However, the true difficulty comes in securing a catalyst for R&D purposes. Of the three anode catalysts presented in this section, only the TKK 50% (TEC66E50) is still available for purchase. Therefore, the following recommendations are made. The PGM content of the catalyst must first be considered. The anode in DMFCs require a much higher catalyst loading than that of the cathode resulting in a much thicker layer and increased mass transfer resistance. Therefore, a higher PGM content is suggested for the anode catalyst. The molar ratio also must be considered. While results can be obtained using both 1:1 and 2:1 ratios that are comparable with what is typically seen with commercial catalysts, DMFC components will need to be optimized to account for fuel and water management within the cell. Finally, it is important to perform baseline tests and optimization for each anode catalyst purchased. This lab has found an ionomer to PtRu ratio 0f 0.4 in the anode is optimum for tests performed, however, this is expected to vary between catalyst with large PGM and molar ratio differences. The GDL also must be optimized based upon the catalyst to provide the best mass transport qualities. Additionally, variations in catalyst solutions are expected. For example, when spray coating the solvent to dry mass ratio must be optimized to allow for adequate and uniform

coating. This will be discussed further in later chapters of this work. In general, it is clear that overall optimization testing must be performed whenever a new anode catalyst is obtained.

4.2 Anode Catalyst Solution Design

As mentioned in the previous section, each anode catalyst will require optimization in the design of the catalyst solution. While the standard fabrication procedure remains the same, certain parameters such as the solvent to dry mass ratio must be varied to allow for the best dispersion and coating to occur. This is especially important when spray coating is the method chosen for CL fabrication. While there are many techniques for fabrication of the CL, this lab has found spray coating to produce the most uniform layer and desirable porosity. In later sections, blade coating, spray coating, and catalyst coated membranes (CCMs) are investigated in detail. However, the vast majority of GDEs were fabricated using the spray coating method, thus that will be the focus of this section. Due to this reason the solvent to dry mass ratio will be the parameter investigated as once the ionomer to PtRu ratio is optimized, it is rarely changed. The importance of this optimization should be noted though. Ionomers are important both in providing structural integrity within the CL as well as increasing the ionic conductivity of the layer. However, the ratio of ionomer to PtRu plays a crucial role as too much ionomer will result in local resistance increases which will limit the performance of the catalyst [34]. On the other hand too little ionomer will decrease structural integrity and ionic conductivity. Therefore, each time a new catalyst is obtained, this ratio must be optimized to allow for the best performance and strength of the CL.

Figure 4.2 visually illustrates the standard fabrication procedure discussed in section 3.1. The order of catalyst solution fabrication is especially important. This is because PtRu is extremely reactive and will burn on contact with pure IPA. Therefore, it is necessary to first add catalyst to DI water to minimize this contact as it will damage the activity of the catalyst.

Figure 4.2: Fabrication of anode catalyst solution for DMFCs

In this study, the solvent to dry mass ratio of two MEAs is studied. The solvent refers to the total amount of DI water and IPA and the dry mass refers to the amount of Nafion®, and total catalyst including carbon support. Table 4.2 details the construction of each MEA.

Table 4.2: MEAs tested comparing solvent to dry mass ratios

	Cathode	Anode	PEM	Solvent: Dry Mass
MEA 45	JM Pt/C Appx 1.5 mg/cm^2 (HiSPEC 9100)	TKK PtRu 77% Appx 4.5 mg/cm^2 (TEC86E86)	Nafion® 212	25:1
MEA 46				40:1

Figure 4.3 (a-b) shows the results from the standard testing procedure performed on these MEAs. It can be clearly seen that the higher solvent to dry mass ratio results in the power density increasing by nearly twice that of MEA 45 which had a much lower ratio. Some important conclusions can be drawn from these data. First, an adequate amount of solvent must be present to disperse catalyst within the mixture. For catalysts not adequatelydispersed it is also common to see a high degree of cracking and decreased uniformity in the CL especially when spray coating. A study done by Scheepers et al. found that in order to minimize cracking in carbon coating layers the mixture should contain plenty of solvent and maintain a drying point near the azeotropic point [35]. This means that each component of the solvent should maintain the same surface tension throughout the drying process. In addition to having enough solvent, Scheepers et al. found that maintaining a DI water to IPA content between 48% and 63% is ideal [35]. However, they note that very little change occurs between these two concentrations. Therefore, a 1:1 ratio of DI water to IPA was chosen.

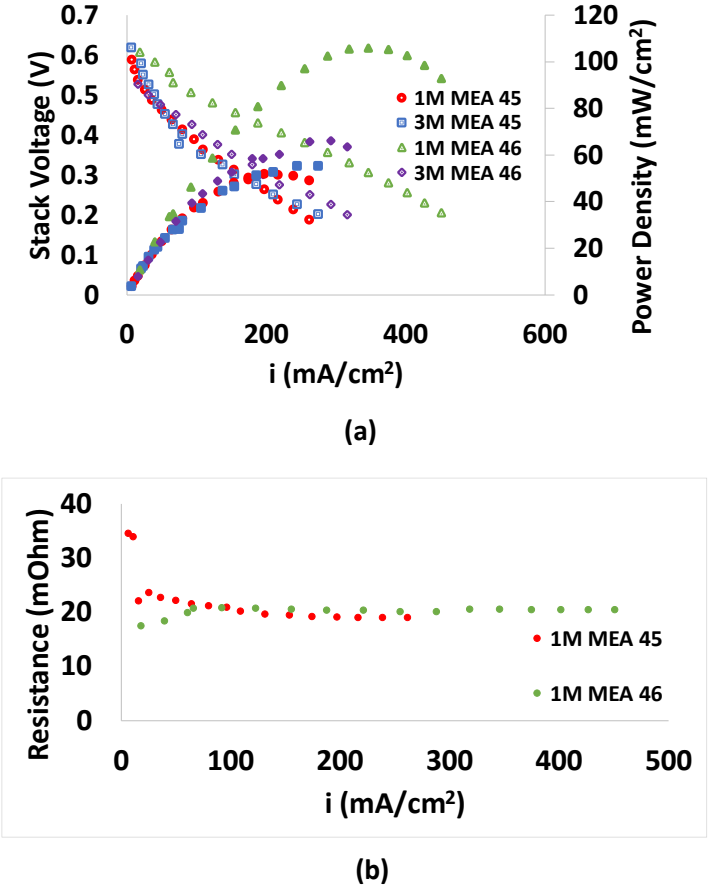

Figure 4.3: Performance results of MEA 45 and MEA 46 (a); Resistance of each MEA at varied concentration (b); 80 °C 1 mL/min fuel (1M), 0.1 L/min air, 50 kPa backpressure

Figure 4.3 (b) shows the slight differences in ohmic resistance by each MEA. It can be seen that at 1M MEA 46 had slightly lower ohmic resistance. As noted before, the resistance measured by the fuel cell tester is a combination of all resistances experienced by the MEA. Since the MEAs were constructed in a similar manner, it is expected the difference in the ohmic resistance is caused by the slight differences in the dispersion of catalyst. Nonuniform dispersions are known to cause increased mass transfer resistances. However, both resistances stabilize at a comparable value, therefore the solvent to dry mass ratio appears to have a negligible effect on overall resistance. Finally, it is important to optimize this solvent to dry mass ratio for each new catalyst. In general, high solvent to dry mass ratios are suggested for catalysts with high PGM content, and lower solvent to dry mass ratios are suggested for lower PGM content catalysts.

4.3 Customized Anode Catalyst

As mentioned previously the slow kinetics of the MOR are a leading barrier for superior DMFC performance. To mitigate this many have studied the use of various anode catalysts such as nickel, iron, and titanium dioxide. Sunitha et al. used a nickel anode catalyst on mesh to improve the speed and activity of the MOR [36]. Consequently, cell costs can also be reduced since the anode is responsible for the highest amount of PGM loading. Titanium dioxide is a popular choice for modification of the anode CL as it can increase the ECSA of the catalyst providing for more active catalyst reaction sites. Malinowski et al. modified PEMFC anode catalyst with both TiO_2 and TiO_2–SiO_2–VTMS and were able to increase peak power density by approximately 72% [37]. Many similar studies have been conducted; however, the primary

principles of anode catalyst optimization remain to increase the ESCA thus improving the speed of the MOR and overall activity of the catalyst.

In this study, the author collaborated with KSU to fabricate and test customized anode catalyst with TiO_2 for DMFC utilization. KSU is responsible for the fabrication of these catalysts and as their work is still in progress, only brief details on catalyst fabrication will be included here. First, TiO_2 was deposited onto Ketjen Black 600JD high surface area carbon support (KB 600JD) via microwave irradiation. Pt and Ru precursors in the amounts of 26.5 mg and 11 mg, respectively, were deposited onto the TiO_2/KB 600JD according to the procedure provided in Sekar et al. using microwave synthesis to form PtRu/TiO_2/KB 600JD-400 [38]. The full procedure for preparation is presented in section 2.2 *Material Synthesis* section of their work. KU is responsible for full cell testing and thus that data is provided to support the need for improved anode catalysts. Three MEAs were fabricated according to the standard fabrication procedure by KU containing customized PtRu/TiO_2 catalysts of varied PGM content. Table 4.3 details the construction of each MEA. A fourth MEA was fabricated using TKK PtRu 77% commercial catalyst as a comparison. Figure 4.4 (a-d) shows the results from the standard activation and testing procedures performed on each MEA.

Table 4.3: MEAs tested comparing customized anode catalysts

	Cathode	**Anode**	**PEM**	**PGM Content**
MEA 48	JM Pt/C Appx 1.5 mg/cm^2	PtRu/TiO_2 KB600JD-400	Nafion® 212	32.6%

MEA 49	(HiSPEC 9100)	$PtRu/TiO_2$ KB600JD-400		47.5%
MEA 53		$PtRu/TiO_2$ KB600JD-4009	Nafion® HP	47.5%
MEA 54		TKK PtRu 77% Appx 4.5 mg/cm^2 (TEC86E86)	Nafion® 212	77%

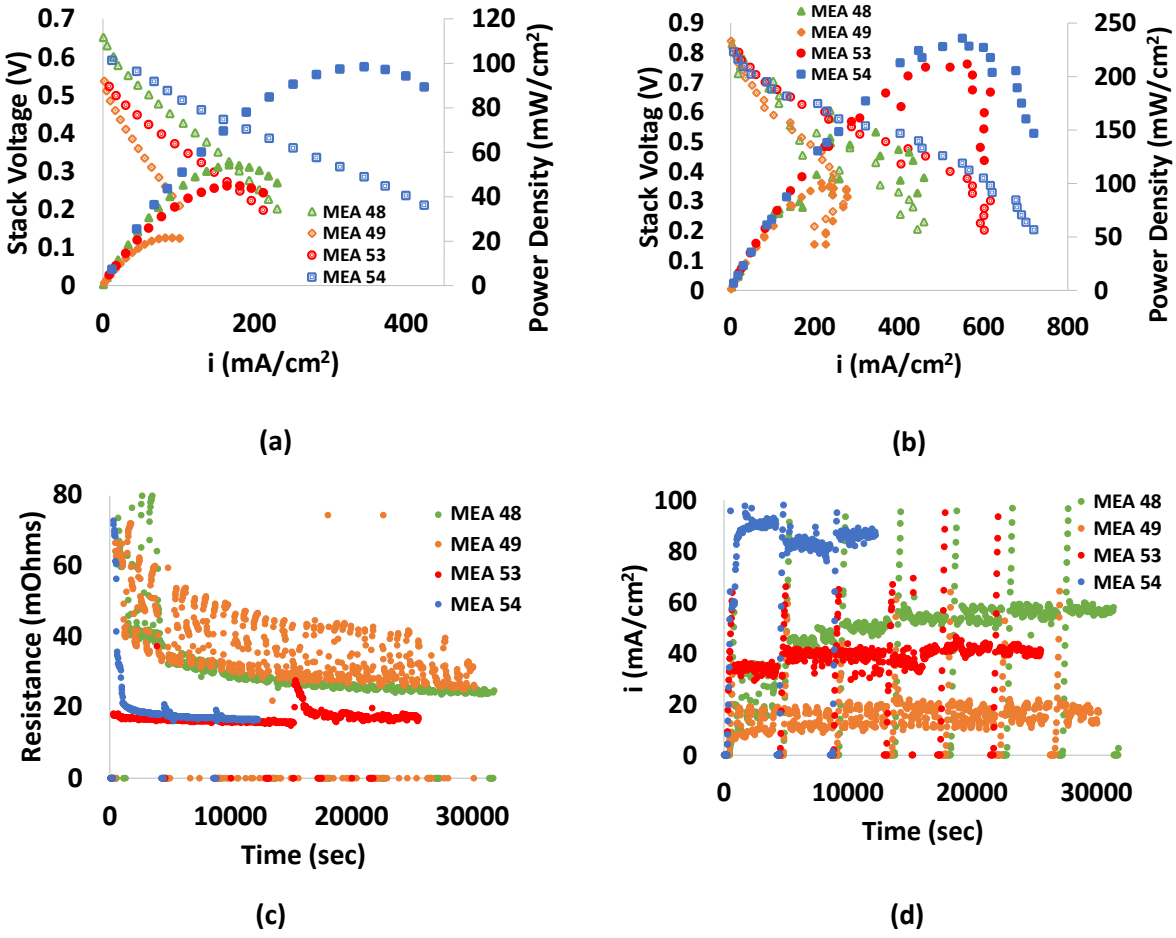

Figure 4.4: Performance results of MEA 48, 49, 53, and 54 at 80°C, 50 kPa backpressure and 1M methanol (a); performance of each MEA using hydrogen at 0.1 L/min H_2, 0.1 L/min air (b); Activation resistance of each MEA (c); and activation current density of each MEA (d)

It can be seen that the customized catalyst did not meet the performance of commercial anode catalyst under full cell conditions. However, KSU has had remarkable results using rotating disk electrode (RDE) tests. While these results are not shown here for confidentiality purposes, RDE tests indicate improved MOR and catalytic activity. It should be noted that PGM loading during RDE testing is very low in comparison to full cell testing. Important conclusions can be drawn from both RDE and full cell tests. First, the customized catalyst requires a much longer activation time to reach full performance. This can be seen in figure 4.4 (c) and (d) in how the three customized MEAs take approximately 8 hours for the resistance and current density to stabilize. Conversely, the commercial component MEA 54 reaches stabilized performance very quickly. Next, the fact that the custom catalyst performs so well in half cell tests with very low loading indicates that the limitations seen in full cells stem from the increased CL thickness. This means mass transfer is different within these catalysts at higher loading levels. An additional conclusion can be drawn from the data seen when the MEAs were tested with hydrogen as seen in figure 4.4 (b). It can be seen the performance in most cases is unstable and does not reach a power density typically seen in MEAs fabricated with commercial components. The exception to this is MEA 53 which contains the Nafion® HP membrane. This suggests the much thinner HP membrane enhances the mass transport and ionic conductivity through the MEA. The activation results also provides an important conclusion in terms of mass transport. In can be seen in figure 4.4 (c) that the resistance experienced by MEA 54, which had a Nafion® 212 membrane, is nearly identical to MEA 53 even though the HP membrane in this MEA is much thinner. Furthermore, MEA 48 and 49 experienced much higher than normal resistance. This indicates that the customized catalysts cause higher resistance, especially from the mass transport perspective.

Finally, it can be seen that customized anode catalysts, particularly with TiO_2, are making significant progress towards reaching the same performance as commercial catalysts. However, figure 4.4 (a) shows peak power with these customized catalysts are still 45-50% lower than that of currently available commercial catalysts. Therefore, it is suggested to further optimize this catalyst, especially in the mass transport region, so that peak power can be matched and eventually exceeded.

Chapter 5

CATHODE CATALYST OPTIMIZATION

5.1 Cathode Catalyst Solution Design

Traditionally, there has not been as many challenges in the design and fabrication of cathodes for DMFCs. However, the basic principles of cathode solution design is important to highlight. In the previous sections, the importance of the solvent to dry mass ratio was discussed. This parameter is especially important in the anode due to the high PGM content of anode catalysts. The same is not necessarily true on the cathode since PGM contents are typically lower. Therefore, it is more beneficial to optimize the ionomer content of the solution to provide for adequate support and oxygen transport. There are three ratios used when discussing the ionomer content of a catalyst solution, namely the ionomer to carbon ratio, the ionomer to catalyst ratio, and the ionomer to total catalyst ratio. As mentioned in the previous chapter, the primary function of the ionomer is to provide binding support for the CL and increase catalyst utilization. Therefore, the ionomer to catalyst content is the ratio chosen to characterize the solution in this work.

In the anode, the ionomer has been shown to influence both the resistance of the CL as well as the MOR. However, on the cathode the ionomer content has been shown to primarily influence the catalyst utilization [34]. Since the cathode is responsible for the ORR, the influence of oxygen and proton transport is also affected by the ionomer content [39]. Since the cathodes of DMFCs generally require less optimization, the authors have not conducted individual studies

on cathode ionomer content and rather based the content off of the work of recent publications. Yakovlev et al. performed a study on the ionomer to carbon content of cathodes in PEMFCs [39]. In this work, the power density, ECSA, and resistance of ionomer in the cathode CL is presented. The authors present many important conclusions. First, they suggest that future studies should be done using a weight percentage of ionomer as opposed to a ratio. This is because PGM contents in catalysts vary, and thus a weight percentage is a more consistent comparison. Next, and perhaps most importantly, it was concluded that the optimum ratio of ionomer is one where sufficient amounts are present for positive gas transport and proton conductivity, but not so much that the ionomer will block active Pt sites [39]. The authors found that conductive proton pathways are established at an ionomer to carbon ratio of 0.3 and that the increased resistance from too much ionomer begins at a ratio of 0.6 [39]. The authors conclude at ratios 0.1-0.3 the low ionomer content results in a reduced ECSA thus limiting the power production of the cell since less Pt sites are available for the ORR to occur. Similarly, at ratios 0.6-1 the thick ionomer layer results in sluggish reaction rates thus limiting the performance [39]. Finally, the authors consider the water generation that occurs at the cathode. While it is important to have some water present for the ORR, too much water will result in cathode flooding which blocks oxygen sites damaging cell performance. They found that at both very high and very low ionomer contents will result in increased water generation additionally contributing to the reduced performance of the cathode [39]. A similar study was conducted by Abdelkareem et al. who came to the same conclusions. The authors of this work also conclude that high ionomer contents results in cathode flooding and low contents results in lower diffusion and proton conductivity

[40]. Similarly, they conclude that an ionomer content of 20% by weight is optimum for increased performance [40].

Based on the results presented in these works the authors has utilized the following catalyst solution design. Since material quantities change for various experiments ratios and weight percentages are presented here. JM Pt/C (HiSPEC 9100) is used as a cathode catalyst and is nominally 60% Pt by weight, and 40% of high surface area carbon support. Nafion® 10% (D1021) in water purchased from the fuel cell store is used as the ionomer. Standard IPA and DI water are used as the solvent. Catalyst solutions are mixed in the following order according to figure 5.1 in a similar manner to anode catalyst solutions. Y.V. Yakovlev et al. reports an ionomer to carbon ratio, however, as mentioned previously designs presented here focus on solutions based on the ionomer to Pt ratio. The recommendations of both works presented in this section are followed and an ionomer to Pt ratio of 0.2 by weight is chosen which corresponds to an ionomer to carbon ratio of 0.3. A high solvent to dry mass ratio of approximately 55:1 is chosen for adequate dispersion of the catalyst. The DI water to IPA ratio is maintained at 1:1 to maintain the azeotropic drying point discussed in chapter 4 so that cracks are minimized during the spray coating process.

Figure 5.1: Fabrication of cathode catalyst solution for DMFCs

These design parameters are summarized in table 5.1 and figure 5.1 illustrates the catalyst solution fabrication process.

Table 5.1: Cathode catalyst solution components

	Ratio	**Material**
DI Water: IPA	1 : 1	Plain DI water; IPA
Solvent: Dry Mass	Appx. 55 : 1	DI Water + IPA; Ionomer + Carbon + Catalyst
Ionomer: Catalyst	0.2	Nafion® 10 % (D1021); Pt
Ionomer: Carbon	0.3	Nafion® 10 % (D1021); High surface area carbon

5.2 PGM Free Catalyst as a Potential Replacement for Pt-based Cathode Catalysts

PGM free catalysts are a recent and very promising area of study that has received much attention. These catalysts work by using cheap precursors, such as Fe, CO, or Mn, to enhance the ORR and water generation at the cathode [41]. These are useful because they address multiple technical barriers that currently plague DMFCs. First, they are capable of producing high current

and power densities. Furthermore, they are naturally resistance to methanol crossover at high concentrations allowing the cell to run optimally even with pure methanol. Finally, they also reduce the overall cell cost by removing the expensive platinum catalyst from the cathode. Of these materials, nitrogen doped iron on carbon (Fe-N-C) support has been a primary candidate in PGM free catalysts. Kosmala et al. performed an extensive study of the fabrication and half-cell testing of hybrid Pt-Fe-N-C catalysts [42]. The authors drew many important conclusions from this study. First, nearly all PGM free catalysts suffer from low durability due to their high ECSA and reaction rates [42]. For that reason, they chose to examine a variety of hybrid versions with varying amounts of Pt per unit Fe. They found that this did help durability, however, some of the tolerance to methanol crossover was reduced seeing reductions from 2M methanol to 5M methanol. Next, they highlighted the importance of pressure, temperature, and flow rates of air and fuel when using these catalysts. Their tests operated between 80 °C and 100 °C as well as pressures between 1 bar and 2 bar. It is shown in this work that increased operating conditions improves the performance of these hybrid catalysts and current densities upwards of 1000 mA/cm^2 were achieved [42]. However, the durability is still a problem that must be addressed in order for wide application of PGM free catalysts. Vecchio et al. carried out the first long term durability test on Fe-N-C catalysts characterizing the performance degradation over 500 h. They found a degradation from 220 mA/cm^2 to 75 mA/cm^2 in the first 100 h, with a much slower degradation from 75 mA/cm^2 to 25 mA/cm^2 over the next 400 hrs [41]. This study also provides useful insight into the possible reasons for this degradation, namely carbon and nitrogen species degradation as well as ruthenium transport from the anode poisoning both the membrane and

cathode CL [41]. For these reasons, the authors of this work chose to investigate the use of pure Fe-N-C cathode catalysts.

This lab has collaborated with the University of Buffalo (UB) to test the use of Fe-N-C customized anode catalysts under full cell conditions. UB is responsible for the fabrication of this catalyst and the cathode GDE. Their development of this catalyst is still in progress thus details of their fabrication procedures are not included here. However, once fabricated the catalyst was spray coated onto Toray 060 CP (190 um) according to the standard fabrication procedure described in this work. KU was responsible for the fabrication of the anode GDE and overall MEA according to the standard fabrication procedure. Three total MEAs were fabricated to test the effectiveness of the PGM free catalyst. Two contained Fe-N-C at varied loadings and PEMs while the third was fabricated entirely by KU using commercial catalysts and a Nafion® 212 membrane to use as a baseline comparison. Table 5.2 details the construction of each MEA used in this study.

Table 5.2: MEAs tested comparing customized cathode catalysts

	Cathode	**Anode**	**PEM**
MEA 50	UB Fe-N-C 4.6 mg/cm^2	TKK 77% Appx. 4.5 mg/cm^2	Nafion® 212
MEA 51	JM Pt/C 60% Appx. 1.5 mg/cm^2 (HiSPEC 9100)	(TEC86E86)	

MEA 52	UB Fe-N-C 5 mg/cm^2	Nafion® HP

Due to the different electrochemical properties of Fe-N based catalysts, the activation and testing parameters of this study varies from the standard procedures defined in this work. MEAs 50 and 52 were activated in the following way. Nitrogen (N_2) was supplied both to the anode and cathode at a rate of approximately 0.5 L/min and was fully humidified by passing the gas through DI water containers boiled at 90°C using a Fischer Scientific Isotherm heated water bath. There was no additional gage pressure applied and this process was continued for one hour. All tests were completed at 80 °C and varied air flow rates and pressures. The varied testing parameters and results are detailed further in figure 5.2 (a-d) . It can be seen in figure 5.2 (a) that the PGM free customized catalyst in MEA 50 is comparable to the performance of MEA 51, even under typical testing conditions. The effect is furthered when pressure and flow rates of air are increased as seen in figure 5.2 (b). This aligns with results seen in other studies presented in that PGM free catalysts require operation at elevated temperatures, pressures, and flow rates. It should be noted here that the UB recommended a pressure of 100-200 kPa and an air flow rate of 1 L/min. However, due to the capabilities of the equipment used only a pressure of 100 kPa and an air flow rate of 0.5 L/min could be achieved.Furthermore, testing under these conditions under a long period of time resulted in the eventual fracture of the PEM. The methanol crossover was negligible as seen in previous studies presented in this section. Figure 5.2 (c) shows that even with pure methanol peak power density was preserved. However, the water management when pure methanol is used must be considered to avoid membrane dehydration. When pure

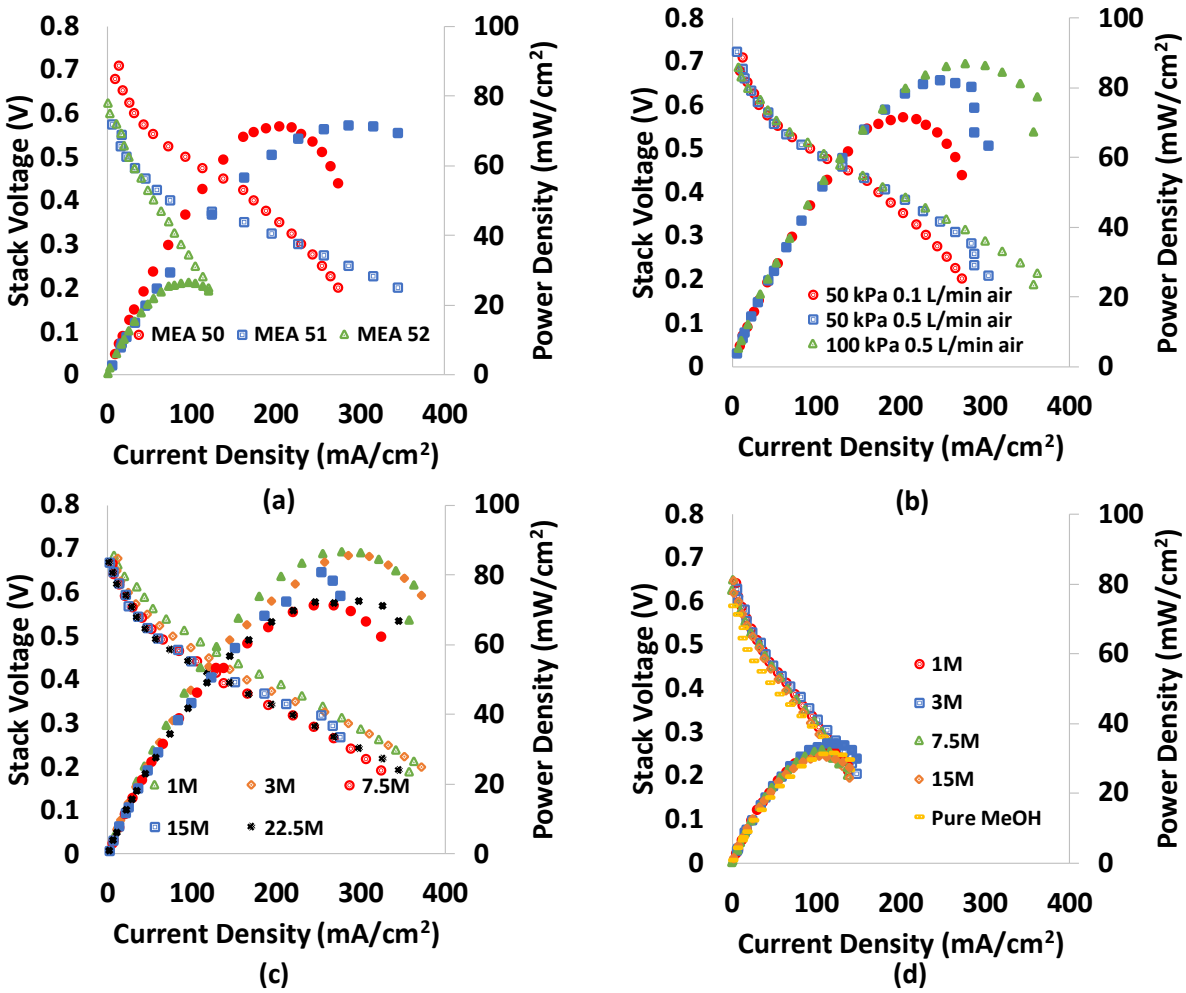

Figure 5.2: Performance results of MEA 50, 51, and 52, at 1M methanol, 0.1 l/min air, 50 kPa (a); performance of MEA 50 at varied pressures and flow rates and 1M (b); Performance of MEA 50 at 100 kPa, 0.5 L/min air and varied concentrations (c); and performance of MEA 52 at 100 kPa and 0.5 L/min air (d); All tests performed at 80 °C, 1 mL/min fuel (1M)

methanol is used the only source of water supply is from the humified air supply. Therefore, it is necessary to ensure adequate insulation along the humidified air inlet line, so the RH remains 100% or to provide water to the cathode through an external pumped water supply. MEA 52 did not have as positive of performance as MEA 50. These results can be seen in figure 5.2 (d). It is believed the decreased performance was because of the HP membrane that was used in this MEA. Vecchio et al.'s insight into the reasons for performance losses support this theory. Since the HP membrane is much thinner, it is likely that poisoning of the cathode CL and degradation

of the Fe-N nanoparticles on the cathode occur much faster. Additionally, the thinner membrane likely results in much quicker membrane dehydration at higher concentrations, however, this does not explain the results at lower concentrations. Figure 5.3 shows that there was no significant difference in the resistances experienced by each MEA when tested under various concentrations. Typical resistance of Nafion® 212 ranges from 20-25 mOhms and Nafion® HP typically stabilizes between 15-20 mOhms. It is important to consider that the PGM free catalyst did not significantly raise the ohmic resistance despite the much thicker catalyst layer.

In order to further improve PGM free catalysts, the following recommendations are made. First, it is clear that the use of PGM free catalyst has numerous benefits and are capable of high power densities. In fact, it is believed the peak power density of MEA 50 was limited by the anode catalyst as a similar peak power density to MEA 51 was produced, which utilized the same anode catalyst. UB has been able to achieve higher peak power densities with Fe-N-C under elevated testing conditions. Next, it is necessary to operate the catalyst at elevated pressures and flow rates. Therefore, it is recommended to highly pressurize the cathode, and have equipment capable of handling at least 1 L/min of air flow. Fracturing of the MEA is also a problem that was encountered by the KU lab. UB uses a self-contained fuel cell testing system capable of higher pressures and flow rates. This also helps to reduce damage to the MEA. It is also recommended to further investigate ways of keeping the membrane hydrated. While acceptable

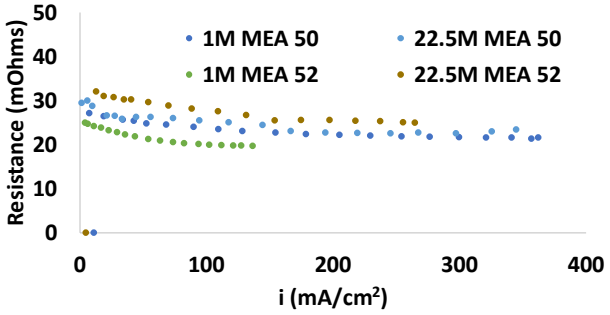

Figure 5.3: Resistance of MEAs 50 and 52 at various concentrations

peak power and resistances were observed when tested with pure methanol, it is expected that the membrane would dehydrate over long-term use. Unfortunately, these MEAs became damaged before duration testing at high concentrations could be performed. Finally, it is recommended to further study methods to improve the durability of these catalyst. Suggestions such as Pt-Fe-N-C alloys can be taken from some of the works presented in this section [41], however, this would partially negate the cost benefit of PGM-free catalysts. In general, it can be seen that PGM free catalysts hold a lot of promise in high power, low cost DMFCs in the future.

CHAPTER 6

MEA DESIGN

6.1 Gas Diffusion Layer Materials and Modifications

The construction of MEAs often vary between different fabricators. Most often, GDLs are comprised of a backing layer, such as CP or CC, with a porous MPL on top. However, in some cases a plain carbon backing can be used as has been done with the cathodes in this lab. The MPL on the GDL helps to improve gas permeability and mass transport through management of the liquid/dry mass interactions through the added layer [43]. Since the primary limiting factors of DMFCs are the slow MOR on the anode and the fuel crossover to the cathode, controlling this layer is especially important on the anode side. On the cathode, the purpose of the GDL is to control the water management in a way that keeps the PEM hydrated without generating so much water that the cathode becomes flooded, and the ORR is reduced. For these reasons, much attention has been devoted in recent years to developing novel GDL designs as well as optimizing existing structures such as commercial CP and CC.

In the 2009 American Institute of Chemical Engineer (AIChE) conference, Virendra Mathur gave a presentation detailing a study of varied GDL designs on both the anode and cathode of DMFCs. In this experiment, he compares the MPL loading and PTFE content of both CP and CC GDLs. He found that for DMFCs, a CP substrate with high PTFE content and a thick moderately hydrophobic MPL for the anode, and a plain CP GDL on the cathode produces the best performance [44]. This has been true in the KU labs findings as well. Others have conducted

studies on modified GDLs with different materials and wettabilities to optimize the performance of these layers. Shu et al. conducted a study on the use of MWCNTs and carbon fibers (CF) as a MPL on the cathode and compared the results to a plain CP GDL (Toray 060H) coated with a strongly hydrophobic MPL. The authors of this work found that by producing the MPL using CNT-CFs a porous hierarchal surface structure was created that improved the porosity, hydrophobicity, and conductivity of the GDL. As a results, they were able to achieve a power density 20-35% higher than that of the Toray 060H (with MPL) CP [43]. Zhang et al. came to a similar conclusion to that reached in chapter 3 of this work regarding hydrophilic gas diffusion layers on the anode. They found that the CO_2 removal at the anode is improved through the use of hydrophilic MPLs as opposed to hydrophobic ones [45].

Since the use of strictly hydrophilic anode GDLs was detailed heavily in Chapter 3 of this work the results will not be presented again here. Furthermore, due to the large amount of studies done previously on various commercial GDLs no direct experiments on these components were performed by the KU lab. However, based on the many works recently published, and the study of custom hydrophilic MPLs on anode GDLs already done, many important conclusions can be made. First, the anode GDL, as well as MPL, make a much larger contribution to cell performance than the cathode GDL. While controlling the water management on the cathode side is important, the primary limiting factors of DMFCs reside mostly on the anode side, such as slow MOR kinetics and fuel crossover. Therefore, more attention should be focused on controlling the anode side. That being said, water management on the cathode side will begin to play a larger role as technology improves and more concentrated methanol solutions are used. When pure methanol is used as a fuel, the lack of water within the cell will begin to contribute to

membrane dehydration and reduction of the ORR. Next, while it is traditional to use GDLs with hydrophobic qualities on the anode, much recent research suggests the use of hydrophilic MPLs helps to reduce fuel crossover in the DMFC. The study presented in Chapter 2 shows that hydrophilic MPLs, or layers of large pores as a FML will increase the gas breakthrough pressure of the layer in the MEA thus reducing crossover [23]. Zhang et al. showed that by using a hydrophilic MPL on the anode GDL, excess CO_2 is more effectively removed leaving more Pt sites available for MOR activity thus improving the kinetics of the reaction [45]. Thus, the use of hydrophilic components should continue to be improved upon to address the primary limiting factors of DMFCs. Finally, while the cathode GDL does not currently play as large of a role in cell performance of the anode, it is certainly important to address. Conventionally, many use a strongly hydrophobic GDL on the cathode to push water away in order to reduce the flooding of Pt sites for the ORR [43]. Others have found that the use of plain CP cathode GDLs results in optimum cell performance [44]. The KU lab has been able to achieve best performance of MEAs using a plain Toray 060 CP GDL on the cathode, that is mildly hydrophobic through the treatment of 5% PTFE.

Based on the recent works and results presented the following recommendations of GDL design is made. For the anode, GDLs (with a hydrophobic MPL) produce superior results at lower concentrations. However, for use of highly concentrated, or even pure methanol, the use of a hydrophilic MPL is suggested, though more research will need to be done on the design of these layers. Furthermore, as shown in Chapter 3, the supplementary use of FMLs with large pores can be employed. On the cathode side, many have found success with GDLs (with a hydrophobic MPL). The KU lab, as well as others presented in this section, has had the best results with plain

CP for use in cathode GDLs. As concentrations increase the water management on the cathode side becomes more important. Therefore, it is recommended to further investigate ways of keeping the PEM and cathode sufficiently hydrated. This means that a strongly hydrophobic GDL or FML may need to be employed for the use of pure methanol as well as the use of an air supplied that is humidified to 100% RH. Additionally, sufficient insulation should be used along the air supply inlet to ensure the RH is preserved as it enters the cathode. The use of an externally pumped water supply can be employed, however, this increases the equipment costs and complicates operating logistics. Therefore, the ideal solution will be one that is internal within the cell.

6.2 Electrode Fabrication Methods

Electrode fabrication has been a widely debated topic since fuel cells were invented. These fabrication methods vary based on the substrate, coating material, and loading required. For DMFCs, high catalyst loadings are required so attention must be paid to how this coating is performed. There are many ways to coat a surface layer, however, three primary methods dominate the DMFC; blade coating, spray coating, and catalyst coated membranes (CCMs). Each method offers its own benefits. For example, blade coating allows for faster coating of the much thicker catalyst layers required for DMFCs [46], however, it is difficult to maintain layer uniformity and reduce cracking in the CL. Spray coating provides a uniform and well dispersed CL by coating many thin layers on top of one another, but for high catalyst loadings such as what is required on the anode, this method can take much longer. CCMs are easily scalable and can produce uniform CLs, however, it can be difficult to adhere the CL to the membrane and increased interfacial

resistance between the CCM and GDL have been reported [47]. In general, the uniformity of the catalyst layer, dispersion of catalyst, and the minimization of cracking in the CL have found to be the most influential parameters in electrode performance. Scheepers et al. found that the two most important factors to control to optimize these is the wet film thickness and ionomer content [35]. In this section, each fabrication method will be individually explained, and experimental results will be provided. When fabricated, the initial intention was not to compare fabrication methods so components such as catalysts and membranes of each MEA vary. Therefore, it is difficult to make a direct comparison. Thus, results will be presented individually, however, important conclusions about the benefits of each fabrication method can still be drawn. Table 6.1 shows the details of each MEA.

Table 6.1: MEAs tested using different methods of fabrication

	Cathode	**Anode**	**PEM**	**Fabrication Method**
MEA 7	JM Pt/C 60%	TKK 50% Appx. 4.5 mg/cm^2 (TEC66E50)	Nafion® 115	Blade Coating
MEA 10	Appx. 1.5 mg/cm^2 (HiSPEC 9100)	Custom Anode Catalyst (KSU) : 2.21 mg/cm^2 PtRu NCNTs + 0.6 mg/cm^2 PtRu	Nafion® 212	CCM

MEA 54	TKK 77% Appx. 4.5 mg/cm^2 (TEC86E86)	Spray Coating

6.2.1 Blade Coating

A common approach to coating GDEs is using blade coating, or sometimes referred to as tape casting. There are a variety of ways to perform this such as the use of a razor blade or another blade like tool to cast a liquid solution in a thin film over the substrate. A common laboratory tool, and one employed at the KU lab, is called a Dr. Blade. This tool allows you to set the blade height at each end of the blade independently to control the film thickness. Figure 6.1 shows the Dr. Blade tool used by the KU team to perform blade coatings.

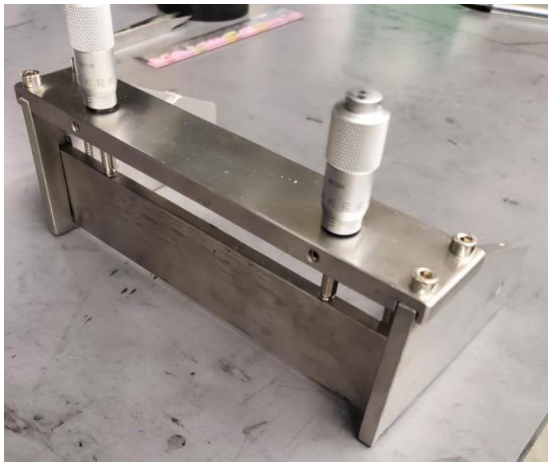

Figure 6.1: Dr. Blade coating tool used by KU team

The fabrication procedure of blade coated GDEs performed by KU is as follows. A catalyst solution for either the anode (TKK 50% PtRu TEC66E50) or the cathode (JM 60% Pt HiSPEC 9100) was fabricated according to the standard catalyst solution fabrication method detailed earlier in this work. The GDL substrate (Toray 060 plain CP 190 um thick) was then taped onto a plain acrylic surface at each of the four corners. Using a standard 5 mL plastic syringe, 2-3 drops of catalyst solution was then placed on one end of the substrate. The Dr. Blade was then adjusted at each

end so the height was approximately 215 um so that a 25 um thick layer of catalyst solution would be applied. The Dr. Blade was then placed at the end of the substrate with the catalyst ink, and with no additional pressure, was dragged across the length of the substrate. The coated layer was allowed to dry for 5-10 minutes in atmospheric conditions. The blade height was then increased by 25 um and the process was repeated until the catalyst loading was approximately 4.5 mg/cm$^2_{PtRu}$. The coated electrode was then allowed to rest in atmospheric conditions for 24 hours to ensure no solvent remained, and the catalyst loading was checked again. A 5 cm^2 electrode was then cut from the sample that had the least number of cracks and best uniformity. The MEA is then fabricated according to the standard fabrication procedure, and then activated and tested according to the standard procedures. Figure 6.2 shows the results of standard testing performed on this MEA.

This fabrication method works well due to its speed and ease of use. The results show that a respectable power density of approximately 49 mW/cm^2 was reached. However, a high level of cracking is evident using blade coating. This helps to explain the instability of the polarization curves seen in figure 6.2. According to Scheeper's, this is because the film thickness was too high and this contributes greatly to cracking in the CL [35]. Additionally, approximately 40% of peak power was lost when increased to 1M. This is also indicative of heavy cracking in the CL as more unreacted methanol can easily pass

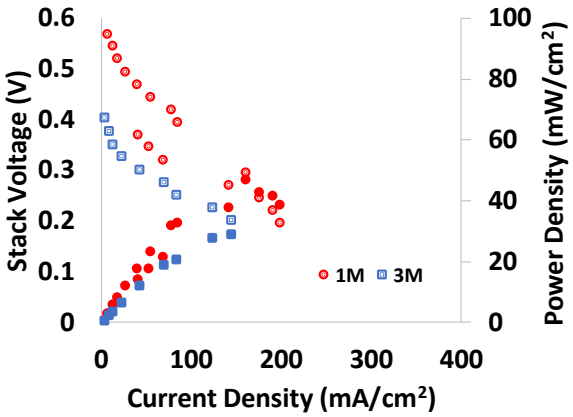

Figure 6.2: Performance results of MEA 7 at 80 °C using 1M (red) and 3M (blue) methanol solution; 1 mL/min fuel (1M), 0.1 L/min air, 50 kPa backpressure

through due to reduced gas breakthrough pressure [23]. It was attempted to reduce the blade height; however, this would result in more solvent being spread and the dry mass of the ink being pushed out by the blade. To mitigate this, it is recommended to use a high solvent to dry mass ratio in future samples.

6.2.2 Spray Coating

Spray coating of electrodes has been widely employed in fuel cells of many kinds. PEMFCs use spray coating dominantly because of the lower catalyst loadings required for hydrogen fuel. This method is beneficial due to the high levels of uniformity and catalyst dispersion seen. This is because much less catalyst ink is deposited in a single layer. Additional layers are then added until the desired loading is achieved. The drawback presents itself at higher catalyst loading scenarios, such as with anode GDEs in DMFCs. At much higher catalyst loadings (4 mg/cm^2_{PtRu} and above) the number of layers required, and thus the time required to coat, increases greatly. It is also known that material losses during this process are higher than similar coating methods. In order to mitigate these issues, automated processes coating may be utilized. Automated spray coating is pracitical for large scale operations in which a large number of identical electrodes must be fabricated. Additionally, the material loss can be reduced through the use of a precise machine that is not subject to human error. Some companies already provide machines that can be programmed for different GDE sizes, or loadings [48].

The KU lab has adopted the spray coating method using an Iwata Ninja Jet spray coater as the standard fabrication for electrodes, and this process has already been detailed in this work. This is due to the high degree of uniformity seen, and consistency in fabrication. MEA 54 was

fabricated using this method and has been used as a baseline comparison for many other studies in this work. However, the results can be individually seen in figure 6.3. It can be seen that the polarization curves are much more stable in comparison to figure 6.2 due to improved uniformity of the CL and catalyst dispersion. The higher peak power density is likely due to an improved commercial catalyst used in this test. However, MEA 54 shows a much higher tolerance to increased methanol concentration with only a 20% loss in peak power density. This is due to minimized cracking in the CL and increased gas breakthrough pressure in the porous layers of the MEA.

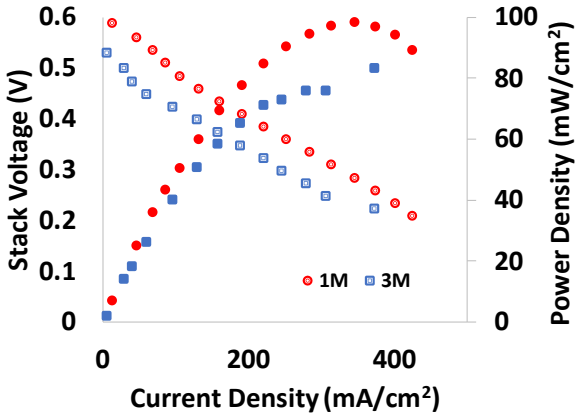

Figure 6.3: Performance results of MEA 54 at 80 °C using 1M and 3M methanol solution; 1 mL/min fuel (1M), 0.1 L/min air, 50 kPa backpressure

Many other studies have demonstrated the benefits of this coating method. Klingele et al. reports an approximate increase of 40% (0.92 W/cm^2 to 1.29 W/cm^2) in the peak power density seen in PEMFCs supplied with hydrogen using a spray coating method versus a CCM method [47]. Rohendi et al. also showed much higher performance, approximately 300%, using spray coating opposed to CCM methods using a novel Pt-Co catalyst [49]. It should be noted that this value appears extremely skewed due to the low peak power density produced (between 0.5 and 4 mW/cm^2). In addition to acceptable catalyst dispersion and uniformity, spray coating has been shown to have the highest range of applicability though the material utilization is known to be quite low due to losses [50]. While many methods of catalyst coatings exist, spray coating is

still considered to be one of the most promising approaches due to its automation capabilities and high performance in DMFC electrodes.

6.2.3 Catalyst Coated Membranes

CCMs refer to the method in which catalyst is applied directly to the membrane as opposed to a GDL. This can be done in a variety of ways, such as spray coating the catalyst directly onto the membrane. It is important to note that in order to use this approach, the membrane must first be treated to allow for adequate adhesion of the CL onto the PEM [50]. Another option is the decal method in which the catalyst is applied to a PTFE substrate and then hot pressed onto the membrane. This removes the need for PEM treatment, but sometimes the addition of a Nafion® topcoat is required for the entirety of the catalyst to transfer to the membrane as was discovered through laboratory experiments at KU.

The CCM fabrication method for KU is as follows. Catalyst was coated onto PTFE substrates with the catalyst dimension being 2.5 cm x 2.5 cm and the substrate dimension being 5 cm x 5 cm. The coating was performed by KSU via spray coating directly onto the PTFE substrate on a 70 °C hotplate to assist in catalyst adhesion. This method was chosen for ease of shipment to KU for final fabrication. Once the coated PTFE substrates were shipped to KU, MEA fabrication was performed in the following way. The first two substrates were attempted to be hot pressed onto a Nafion® 212 membrane using a DulyTek DE10K hot press heated to 135 °C and pressed at 345 kPa for 5 minutes. However, there was inadequate adhesion of the CL to the membrane. Therefore, for the third substrate the CL was coated with a 10% Nafion® solution (D1021) by painting a thin layer on top of the catalyst using a paint brush. The hot press process was

repeated, and the CL was successfully transferred to the Nafion® 212 membrane. The membrane was then removed. A cathode was fabricated according to the standard fabrication procedure on a Toray 060 CP GDL. The MEA was then fabricating by placing the CCM in a PTFE gasket and placing the fabricated cathode on top and pressing the assembly at 135 °C and 345 kPa for 5 minutes. Finally, when the MEA was placed into the fuel cell stack, a 2.5 cm x 2.5 cm Sigracet 29BC (with MPL) was placed between the fuel channels of the anode graphite plate and the CCM. The resulting MEA can be seen in figure 6.4.

Figure 6.4: MEA fabricating via a CCM method; Post hot press procedure

After fabrication MEA 10 was activated and testing according to the standard procedures previously detailed. Figure 6.5 shows the results of these tests. As seen in table 6.1, an experimental custom catalyst using PtRu nitrogen doped carbon nanotubes (NCNTs) was used for this membrane. Additionally, a much lower PGM loading of approximately 3 mg/cm^2 was used. Despite that, figure 6.5 indicates a comparable peak power density to that of commercial catalysts using the blade coating approach. As mentioned, it is difficult to compare the peak power density due to the difference in catalysts. However, the stability of the polarization curves and tolerance to increased

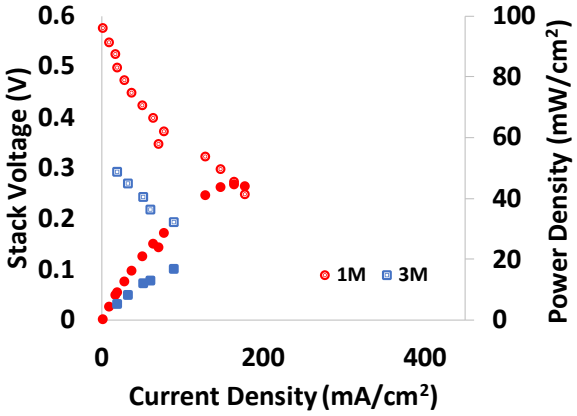

Figure 6.5: Performance results of MEA 10 at 80 °C using 1M (red) and 3M (blue) methanol solution; 1 mL/min fuel (1M), 0.1 L/min air, 50 kPa backpressure

methanol concentrations provides useful information as to the effectiveness of the coatings. MEA 10 results are clearly more stable than MEA 7. This indicates reduced cracking in the CL and improved uniformity and figure 6.5 supports this claim. However, MEA 10 showed much less tolerance to methanol crossover with peak power loss near 60%. This is likely due to interfacial interaction differences between the GDL, CL, and PEM when using the CCM approach.

6.2.4 Fabrication Method Comparisons

While some components of the MEAs tested in the previous three sections vary, clear conclusions can be drawn from the results and fabrication methods used to produce these MEAs. First, the polarization curve stability is heavily dependent upon the presence of cracks, dispersion of catalyst, and interfacial relationships between the porous layers of the MEAs. In terms of polarization stability, it can be seen that blade coating shows the worst performance, CCM shows a median performance, and spray coating shows stability. This supports the evidence published in recent works and seen in experimentation with spray coating consistently giving the most uniform CL with least degree of cracks and best dispersion of catalysts. Next, the methanol crossover is greatly influenced by the presence of cracks in the CL among other factors. MEA 54 showed the greatest tolerance to methanol crossover retaining 80% of its peak power density when the concentration was increased from 1M to 3M. Interestingly, blade coating shows the next best tolerance to methanol crossover retaining 60% of its peak power density. However, blade coating has been shown to have the highest degree of cracks. This can be explained by the interfacial relationship between the GDL and CL when blade coating. Since the blade coating is done on a dry GDLand the CL is applied directly, the methanol is able to better diffuse thus

reducing the crossover [50]. In the CCM method, the GDL is simply placed between the fuel channels and CCM, thus the interfacial relationship is weakened allowing for more crossover due to reduced diffusion. Thus, CCM shows the least tolerance to methanol crossover only retaining 40% of its peak power density. Finally, the ease of coating must be addressed. Blade coating is the best in these terms as it is easily scalable, and high loadings can be achieved much quicker than the other approaches. While spray coating is optimum on a performance level, the process for DMFCs takes very long especially on the anode side. In the KU lab, it takes 4-6 hours to achieve a loading of 4.5 mg/cm^2_{PtRu} on the anode. Finally, the CCM method is considered to be the most time consuming. This is because the catalyst is typically spray coated onto a PTFE substrate, or directly onto the membrane, prior to fabrication. Additionally, treatment of the membrane prior to coating, or to the spray coated CL prior to hot pressing is necessary for adequate CL adhesion. This effectively combines the time for spray coating with additional steps resulting in a longer total fabrication time.

Based on the results presented in the previous sections, the following recommendations are made. For R&D purposes, spray coating will provide the best and most consistent performance. In small scale operations, it is feasible to do this process by hand and necessary equipment to do so is cheap in comparison to large commercial equipment. If large scale operations are necessary, it is recommended to invest in an automated commercial spray coater to allow for consistent loadings and reduced manual labor costs [48]. Next, blade coating has showed promise in other studies, and the scalability and improved interfacial relationship between the GDL and CL is encouraging. However, it is recommended to investigate other tools for tape casting purposes. Many rolling/blade combinations have been proposed and

implemented at a commercial level, and have been shown to both improve speed and reduce cracking in the CL [51]. Finally, the CCM approach have shown promise for high performing DMFCs, however the interfacial relationships between the GDL, MPL, and CL must be improved for viability. Therefore, it is recommended to add an additional step and treat the GDL with an additional layer of Nafion® and then physically hot press it to the CCM prior to testing. This will help to decrease the contact resistance between the GDL and CL and improve the interfacial relationship.

CHAPTER 7

DISUCSSIONS, RECOMMENDATIONS, CONLCUSIONS, AND FUTURE WORK

7.1 Discussion of Results

The results presented in this work are an accumulation of three years of research performed by the author with help from many collaborating Universities, research companies, and colleagues at the University of Kansas. The gas transfer in DMFCs, reduction of fuel crossover, anode catalyst design, cathode catalyst design, and overall MEA design are all studied from an experimental standpoint. In each chapter, key results are presented and discussed individually. However, it is useful to summarize them again here.

The second chapter presents a pore-scale model of the carbon dioxide transfer within DMFCs. The results from this model indicate that controlling the gas pressure in the porous layers of the MEA contributes to how much unreacted fuel crosses the PEM [23]. Since fuel crossover is a leading limiting factor in DMFCs, these results are crucial to better understand how to design these layers so that the crossover is reduced. In this work, it was found that the pore size distribution play a larger role in reducing crossover than the thickness of the layer itself [23]. This provides meaningful direction for designing GDLs, FMLs, and CLs of MEAs. For example, Metzger, Li et al. suggest the use of FMLs with large pores to mitigate the crossover. However, many FMLs add significant thickness to the MEA. Based on the results of this work, it is now known that more focus should be given to the PSD.. This allows for a wider range of usability in FMLs as seen in Chapter 3 with the use of a 3 mm FML. The presented work provides three design proposals

based upon the results of the model, namely the use of an FML, a hydrophilic MPL on the anode GDL, or a layer of large pores between the MPL and CL. In all cases, the function increases the gas breakthrough pressure the methanol must overcome prior to reaching the PEM. Of the three designs proposed, the use of an FML and hydrophilic MPL on the anode GDL are chosen to be studied as they both result in a pressure increase of $1.5x10^5$ Pa, whereas the layer of large pores only results in a pressure increase of $5.1x10^2$ Pa.

Chapter 3 presents the results from testing various fuel crossover reduction methods. Based on the results in Chapter 2, both hydrophilic MPLs and FMLs on the anode are presented. Both studies showed promising results. In the hydrophilic MPL study, peak power density is achieved using 3M methanol solution, reaching comparable levels with the baseline MEA. Furthermore, it is shown that the varied post-fabrication treatment did not play a large role in the effectiveness of the layer, even though the PSD was successfully altered. However, the benefit of the MPL was diminished when the concentration was further increased. The study on FMLs was also promising. In these experiments, power density was maintained up to 3M, and only partially reduced all the way to 15M, or approximately 50% by weight of methanol solution. However, the power density was slightly reduced from the same MEA without an FML. It is shown in this section this is primarily due to the increased ohmic resistance of the MEA. The use of both graphene-enhanced and zwitterionic polymer-coated membranes are also presented in this chapter. Both functions to modify the PEM of the fuel cell and selectively repel methanol based on particle size or a difference in ion-dipole interactions, respectively. Results of these tests show a degree of success at low temperatures. However, in both cases this effect is diminished at elevated temperatures. With graphene, this is primarily because of the delamination of the layers

of Nafion® and graphene coatings as shown by SEM images. In the zwitterionic polymer membranes, both fracturing of the coated layer on the PEM and chemical decomposition of the coating are speculated to be the reason for reduced effectiveness. In general, the results presented in this section show progress in reducing fuel crossover. To the authors' knowledge, no recent literature has shown success with high power densities at increased fuel concentrations. However, more progress must be made in order for pure methanol to be used as a fuel in commercial applications.

The fourth chapter discusses the optimization of the anode catalyst in DMFCs, identified as a leading barrier to market entry for further commercialization. First, a comparative study of commercial anode catalysts was studied. It is shown that there are clear differences in commercial products, including PGM percentages and molar ratios. Of the three catalysts tested, JM 75% PtRu (HiSPEC 12100) is shown to have the best performance. However, it is no longer available for purchase. TKK 77% PtRu (TEC86E86) is shown to have the second-best performance using 1M methanol, and TKK 50% PtRu (TEC66E50) has the worstbest performance. However, at 3M the performance loss is less using the TEC86E86 catalyst showing only a 20% reduction in peak power density. Unfortunately, this catalyst is also unavailable for purchase, though TKK does offer another 77% PGM weight variety with a different molar ratio which this lab has not tested. This section illustrates the difficulty in finding a consistently available commercial catalyst. This chapter also discusses the anode catalyst solution design, in particular, the solvent to dry mass ratio. This makes consistent testing difficult as each time a new catalyst is purchased, optimization testing must be performed to design the ideal solution. Section 4.2 details the study done on the solvent to dry mass ratio. This section shows that when spray coating, catalysts with

high PGM percentages require a high solvent to dry mass ratio of at least 40:1. It was discovered that if this ratio is too low, the solution is not adequately dispersed during the coating process resulting in reduced performance. Finally, the use of customized anode catalysts fabricated by KSU is presented. While complete fabrication details of the catalyst are not provided due to confidentiality purposes, results from KSU RDE tests indicate increased MOR activity and improved ESCA in their novel catalyst, which contributes greatly to overall cell performance [38]. More details on the fabrication and RDE testing of these catalysts can be found in their recently published work, *PtRu Catalysts on Nitrogen-Doped Carbon Nanotubes with Conformal Hydrogenated TiO_2 Shells for Methanol Oxidation*, in the ACS Applied Nanomaterials Journal (January 6th, 2022). Unfortunately, the results were not as promising under full cell conditions. In the results presented, the customized catalyst at various weight percentages did not meet the performance of commercial anode catalysts and was reduced by at least 45%. As mentioned in Chapter 4, RDE tests are performed under extremely low PtRu loading conditions. Thus, the lack of performance under full cell testing conditions can likely be attributed to mass transfer limitations introduced when the catalyst loading is increased. Furthermore, interactions with other components in the MEA may reduce some of this performance. However, the improvement of the MOR on the anode is vital to the performance of the DMFC so the use of customized catalysts in the anode will continue to be a primary focus of research in the field.

Chapter 5 discusses the optimization of the cathode side of the DMFC. As mentioned previously, the cathode does not currently play as large of a role in DMFC performance as the anode. However, the design of the catalyst solution is important to consider in order to allow for proper water retention and ORR at the cathode. In section 5.1, the ionomer to Pt content is

discussed as this is the primary influential factor in water management. A variety of studies is presented and is the basis for the KU lab's design of cathode catalyst solutions. For example, Yakovlev et al. compares the ECSA and resistance of various ionomer contents within the cathode. They conclude that an ionomer to carbon ratio of 0.3-0.6 is optimal for proton conductivity and reduced resistance [39]. Based upon that the KU lab has chosen an ionomer to Pt ratio of 0.2, which corresponds to an ionomer to carbon ratio of approximately 0.32 using JM 60% Pt (HiSPEC 9100). Similarly, Abdelkareem et al. discovered that too high of an ionomer content results in cathode flooding, reduced diffusion and proton conductivity [40]. They also find that an ionomer content of approximately 20% by weight of Pt is optimal. This also supports the KU lab's design as the ionomer content in these cathodes is approximately 13% weight of the total carbon and catalyst content, and exactly 21% by weight of the Pt content. It was decided that the ionomer content related to the Pt content was more relevant than the total carbon+Pt content as the Nafion® acts as a binder between Pt nanoparticles and carbon support. After discussing the baseline catalyst solution design, a detailed study in collaboration with UB on PGM-free catalysts is presented. In these experiments, PGM-free catalysts with varied PEMs are tested with impressive results. First, the peak power density seen is comparable to commercial catalysts under standard testing conditions and slightly improved under elevated flow conditions (0.5 L/min air, 100 kPa backpressure). In fact, it is believed that the anode limited the peak power density as opposed to the PGM-free cathode. This is because peak power density was similar to what we have seen in previous baseline tests using only commercial components. Furthermore, the tolerance to increased methanol concentration, and even pure methanol, allowed the MEA to maintain performance seen at 1M concentrations. This is due to the fact that PGM-free

catalysts are not subject to the same crossover reduction as Pt-based catalysts. MEA 50 was able to retain much of its peak power density up to 22.5M methanol before the membrane fractured. MEA 52 experienced reduced overall performance due to the use of a Nafion® HP membrane, however, performance was entirely retained even with pure methanol. After these tests the PEM in this MEA was also fractured, which points to an important conclusion. The use of PGM-free catalysts, Fe-N-C, requires elevated flow conditions, as mentioned before. This is often not possible in a standard fuel cell set up, such as the one in the KU lab. UB has been able to achieve performance upwards of 250 mW/cm^2 using 1 L/min air and 150-200 kPa backpressure [5]. However, this fuel cell's air supply and inlet could only handle 0.5 L/min air. While that pressure is achievable using the Scribner manual backpressure module, the increased airflow rate and pressure evntuallyresults in PEM fracture within this setup. Therefore, in order for these catalysts to be viable, adjustments in equipment and catalyst design will have to be made. Section 7.2 (Recommendations) of this work will address this further.

Finally, Chapter 6 addresses the overall construction of the MEA and the fabrication of individual components within the MEA. First, the GDL and materials or modifications that can be made is discussed. Recent literature on GDL material and MPLs is discussed. It is typical to see a CC or CP GDL with hydrophobic MPL on both the anode and cathode. The addition of the hydrophobic MPL, especially on the anode, can help to improve gas permeability and mass transport by managing the liquid/dry mass interactions through the porous layer [43]. On the cathode, some have found the addition of a hydrophobic MPL to be useful, while others have found that plain CP moderately treated with PTFE to be more beneficial [44]. This is the case for the KU lab as well, and we have chosen to use a plain CP with hydrophobic MPL on the anode

and plain CP treated with 5% weight PTFE on the cathode, as Mathur concluded in his 2009 conference presentation at the AIChE. However, many studies are being conducted on novel GDLs and MPLs, such as Shu et al.'s use of MWCNTs and CNFs to create a hierarchal microstructure as an MPL on the cathode GDL [43]. These studies will become even more important as fuel crossover reduction technology, as discussed in Chapter 3, and PGM-free catalyst technology, discussed in Chapter 5, continue to improve. As DMFCs continue to advance towards the use of pure fuel, water management on the cathode will become more important to consider. The fabrication of the CL on the GDLs is also discussed in this Chapter. Three common methods of coating the CL are presented; blade coating, spray coating, and CCMs. In this study, it was difficult to compare the peak power density of MEAs 7, 10, and 54 since various anode catalysts were used. This was because the MEAs were tested over a long period of time as fabrication methods continued to develop within the team. However, many observations can be made from the stability of the polarization curves and tolerance to increased methanol concentrations. Since the cathodes are constructed in the same way to similar specifications, inconsistencies in the polarization stability result from the anode and fabrication method chosen. It is shown that spray coating yields the most stable curves, followed by the CCM method, and then the blade coating method. This is because blade coating results in the highest degree of cracking and the least degree of coating uniformity. The presence of these cracks and inconsistent local catalyst loading results in a highly unstable curve due to varied catalyst utilization across the CL. Conversely, spray coating shows the best stability when compared to other fabrication methods. This is because spray coating applies a small amount of catalyst in multiple thin layers, allowing the layer to dry evenly. The CCM approach falls between the

previous two methods with a relatively stable curve. However, figure 6.4 shows a very low degree of cracking. Therefore, the instability in this curve and lack of fuel crossover tolerance likely comes from lack of interaction between the GDL and CCM [49]. Blade coating showed a moderate tolerance to crossover because of the stronger adhesion between the CL and GDL, but the high degree of cracking resulted in performance losses when the concentration was increased due to reduced gas breakthrough pressure through the cracks [23]. Metzger, Li et al. showed that a uniform PSD was one of the largest contributing factors to crossover reduction. Since spray coating has the lowest degree of cracking it provides the strongest interaction between the GDL and CL and showed the highest tolerance to fuel crossover. Finally, from a time and scalability perspective, blade coating is shown to have the shortest time and highest scalability. While spray coating yields the highest performance, the process can be time-consuming and expensive equipment is needed for large-scale operations. The CCM method takes many additional steps and often requires both spray coating and additional treatment of the PEM or CL for adequate adhesion thus resulting in the longest fabrication times.

7.2 Recommendations for High Performing DMFCs

Based on the results discussed in this work, the following recommendations are made for the highest-performing DMFCs as technology continues to advance. The model in Chapter 2 shows that the gas pressure in the anode is critical to control in order to reduce the fuel crossover. One of the most effective ways to do this is through the use of an FML. Section 3.2 shows that AvCarb G300A graphite felt layer was effective in reducing fuel crossover. However, Figure 3.4 (c) shows that the resistance increases by more than two times when the FML is

present. Therefore, it is recommended to design FMLs in a way that reduces this resistance while maintaining a uniform PSD. Plain carbon cloth is one way to do this as the large pore size allows for sufficient diffusion of methanol prior to reaching the CL. Furthermore, the much thinner layer and higher conductivity reduce the resistance greatly. It is also recommended to design multilayer FMLs that aid in diffusion; however, this is still under investigation and process for patent application, thus it is not discussed here. Hydrophilic MPLs on the anode GDLs are also shown to be effective in reducing some degree of crossover. However, the effect is limited past 3M methanol concentration. Therefore, it is recommended to increase the MPL loading to 5 mg/cm^2 of hydrophilic solution. Figure 3.6 (a-d) shows that the carbon fibers are still visible with the coating, so an increased loading will help to fill these pores more completely, further increasing breakthrough pressure. Furthermore, figure 3.6 (d) shows that hot pressing the MPL provides the best PSD, but damage during fabrication did not allow for testing of that design. It is recommended to increase the PTFE gasket thickness to be slightly larger than the GDL and MPL during the hot press process to reduce this damage and allow for hot-pressed GDLs to be used.

The modification of the PEM also shows promise in crossover reduction, especially at low temperatures. However, high performance cannot be achieved below 65 °C, therefore, it is recommended to improve the mechanical and chemical durability of both graphene and zwitterionic-enhanced PEMs. The failure cause of both of the modified membranes is attributed to membrane swelling [30]. The primary recommendation is to further investigate ways to reduce membrane swelling. Rao et al. showed that UV radiation is one promising approach and was able to reduce the swelling by approximately 20% [30]. For zwitterionic polymer-modified PEMs, both increased crosslink density and coating thickness was attempted. Increasing the thickness of the

coating showed moderate improvements at 65 °C, but delamination and decomposition were still an issue. Therefore, it is recommended to explore a sandwiched structure where the coating is placed between two Nafion® membranes. The swelling of the membrane primarily occurs on the in-plane due to clamping pressure on the through-plane so the sandwiching approach will likely reduce damage to the layer. For graphene membranes, delamination of the layers was shown to be the primary problem. Therefore, the mechanical stability must be improved, and it is recommended to explore an approach using a more robust graphene material, such as 3-D graphene, which may be more stable as swelling in the PEM occurs [29]. Additionally, graphene has shown promise within other components of the fuel cell. Further investigation should be done on this due to the low cost and wide application of this material.

Extensive studies on the anode catalyst have yielded the following recommendations. First, a wide variety of commercially available anode catalysts are regularly used by researchers. However, due to a narrow market, the catalysts consistently available for research purposes. However, based on the results presented in this work, the following general recommendations are made. It is recommended to choose an anode catalyst with a high PGM content as that yields higher performance. The data suggests PGM contents near 75% are optimal for performance in excess of 100 mW/cm^2. Furthermore, a 2:1 molar ratio of Pt:Ru yields a higher tolerance to methanol crossover and higher MOR activity. Additionally, it is recommended to perform optimization testing of each new catalyst received. The ionomer content will vary according to the PGM content, and the solvent to dry mass ratio will vary depending on the fabrication method, thus these must be optimized. In general, higher solvent to dry mass ratios will be

needed when spray coating while lower solvent to dry mass ratios are necessary for blade coating approaches.

The following recommendations are made for customized anode catalysts. The performance of these catalysts in RDE tests is better than what is seen with commercial catalysts, however, they tend to underperform in full cell conditions. Therefore, the mass transport qualities of thicker CLs must be investigated to achieve higher power densities. Additionally, the resistance seen in these MEAs are higher than typical. Therefore, a model simulation of this catalyst under full cell conditions may be useful. The use of Nafion® HP membranes is also recommended to further decrease ohmic resistances and improve ion conductivity.

Water management will become more important in the cathode as technology improvements, so the following recommendations are made. The ionomer content in the cathode should remain low to allow for Pt sites to be available for the ORR. In this work an ionomer to Pt ratio of 0.2 is shown to be optimal. Additionally, too high ionomer contents will result in cathode flooding which sources state becomes prevalent at ionomer contents of 30% weight and above [40]. An ionomer to Pt ratio of 0.2 is recommended for commercial catalysts. For custom PGM-free catalysts, this ratio will need to be reoptimized based on the electrochemical properties of that particular catalyst. Additionally, a plain CP GDL treated moderately with PTFE is recommended to make the cathode slightly hydrophobic [44]. As concentrations increase past 75% by weight of methanol, a strongly hydrophobic MPL on the cathode GDL, or hydrophobic water management layer (WML) between the cathode GDL and serpentine air channels as shown in figure 3.3 (a).

For the use of PGM-free catalysts on the cathode the following recommendations are made. The performance of these catalysts exceed what is seen with commercil catalysts; however, the catalytic activity must be improved so that standard operating conditions can be used. Furthermore, the durability of these catalysts must be improved. Therefore, hybrid catalysts are recommended by doping the PGM-free catalyst with a PGM such as Pt for long-term use of these catalysts. Previous research has shown success with a Pt catalyst doped with Fe to improve the durability [42]. The degradation of the carbon and nitrogen species must also be addressed in order for these catalysts to be commercially viable [41]. It is also recommended to improve the cathode hardware to reduce membrane dehydration when pure methanol is used. Primarily, the air inlet from the humidifying mechanism to the air inlet of the cathode should be as short as possible and well insulated so that the RH remains near 100% within the cathode. In this work this is achieved by maintaining the shortest possible path, of around 18 inches, between the humidifier and the air inlet, as well as placing a foam insulation material along the tube. This will help to provide the water necessary for the ORR and keep the membrane hydrated. Additionally, externally pumped water supplies can be explored to mitigate this problem.

Finally, the following recommendations regarding MEA fabrication are made. As mentioned before, a CP (with hydrophobic MPL) is recommended for the anode, and a plain CP GDL moderately treated with PTFE is recommended for the cathode at lower concentrations (< 75% by weight). For R&D purposes, spray coating is recommended for the best performance of the CL. If it is necessary to perform spray coating on a larger scale, automatic spray coaters are recommended for consistency and manhour reduction [48]. Blade coating may be used for large-scale commercial operations, but improved tooling such as a roller-blade combination is

recommended [51]. The CCM approach has promise. However, the GDL and CCM interface must be improved. It is recommended to apply a thin Nafion® layer to the GDL and physically hot press it to the CCM prior to testing to improve this interaction. Furthermore, spray coating of this Nafion® layer is recommended to keep the applied layer thin and avoid adding local resistance increases to the CCM.

In general, these recommendations are given in reference to specific components of the DMFC. However, the overall optimized DMFC will be a combination of some or all of the methods presented in this work. For example, a DMFC with low resistance FML and an improved customized anode catalyst on a GDL (with hydrophilic MPL) could yield improved MOR activity with highly reduced fuel crossover. Similarly, a PGM-free catalyst with a hydrophobic WML may yield a DMFC with extremely high power density using pure methanol. In any case, the technology of each of these aspects of the DMFC continues to improve each year, and it continues to be a promising candidate for stationary power applications.

7.3 Conclusions

Concerns about sustainability and environmental effects of traditional means of power production continue to grow. This is only furthered as countless energy crisis that have struck simultaneously in recent years. Recent shifts towards renewable energies have left a gap in the market that DMFCs can help to fill. However, as shown in this work, there is a long list of technical limitations that are preventing the widespread use of DMFCs as a reliable means of power production, namely the slow MOR, large fuel crossover, and elevated installation costs. One of these limitations continues to be the lower peak power densities seen in DMFCs as opposed to

PEMFCs. In 2020, the goal for the project sponsored by the Department of Energy (DoE) that funded this research required a peak power density of 250 mW/cm^2 using 4 mg/cm^2_{PGM} loading or less [5]. This goal was increased to 300 mW/cm^2 using 3 mg/cm^2_{PGM} loading or less in 2021. It can be seen in this work that using commercial components, peak power densities of only 100-140 mW/cm^2 are achievable with total PGM loadings of 6 mg/cm^2_{PGM}. It is clear the target is still a long way off. As shown, this is primarily due to the slow reaction kinetics of the MOR in the anode, and the crossing over of unreacted methanol from the anode to the cathode which results in voltage instabilities reducing cell performance. However, other teams have gotten much closer to this target using PGM-free catalysts though the operating conditions were outside of those defined by the DoE. For example, UB was able to achieve 256 mW/cm^2 with a PGM loading of 3.5 mg/cm^2_{PtRu} using the Fe-N-C catalyst at a pressure of 2.5 bar and 1 L/min air [5]. Additionally, the high cost of DMFCs relative to their low power density makes them unattractive to many commercial markets. Currently, PEMFCs cost approximately 1,868 $/kW whereas DMFCs cost 3,772 $/kW [5]. The installation cost of the DMFC heavily dominates this price due to the much higher catalyst loadings required. Once installed, the fuel costs of DMFCs are much cheaper than that of PEMFCs, with methanol costing only 0.43 $/GGE, whereas hydrogen costs approximately 8 $/GGE [5]. Even when the hydrogen costs are reduced to 4 $/GGE, DMFCs are a much cheaper option from a fuel perspective.

Despite setbacks seen in the cost and performance of DMFCs, large advancements have been made in DMFCs throughout this research. Highly concentrated methanol has been able to achieve power density higher than that seen in recent literature, to the author's best knowledge, using a variety of customized GDLs and FMLs. Both graphene and zwitterionic polymers have

been employed to reduce fuel crossover near room temperature. This is particularly applicable in small portable power applications such as communications equipment, which require relatively low power and temperatures. Furthermore, customized anode catalysts have shown improved MOR activity and ECSA during RDE tests [38]. Significant improvements in PGM-free cathode catalysts have also exhibited improved power densities and tolerance to increased methanol concentrations. Furthermore, catalyst solutions for both the anode and cathode have been investigated and optimized. Finally, the fabrication process for MEAs, particularly CLs and GDLs, has been optimized. This work has been able to identify the best approaches for MEA design in the R&D environment and provide recommendations for scalability in commercial applications. While there is much research left to do, this work has made significant progress in the optimization of the overall DMFC.

7.4 Future Work

As mentioned, there is still significant progress to be made in this field. Fuel crossover should continue to be reduced, and MOR activity on the anode will need to be improved. Methods of PEM modification need to be improved upon, and the mechanical durability of the PEM and coatings need to be increased. PGM-free catalysts still require improved durability and performance under typical operating conditions in order to be commercially viable. As DMFCs become more widely available, fabrication methods will need to be improved upon to allow for large-scale production on a consistent basis. The cost of DMFCs also needs to be greatly reduced in order to make them a realistic power supply choice in the future. This will need to be done at the same time performance is improved, which provides unique challenges. In order to clearly

articulate this future work, specific action items on future tasks related to this research are listed below.

1. Continue development on FMLs, particularly on FMLs that exhibit low ohmic resistance and high conductivity.
2. Increase MPL loading of hydrophilic MPLs to 5 mg/cm^2 and improve hot press procedure to improve PSD.
3. Improve mechanical and chemical durability and temperature sensitivity of graphene and zwitterionic modified PEMs.
4. Reduce swelling of Nafion® membranes by exploring the possibility of UV irradiation or coating of on an already swelled membrane.
5. Investigate the mass transfer properties of customized PtRu/TiO_2 KB600JD-400 anode catalyst under full-cell conditions. Determine causes for performance differences between full-cell and half-cell tests.
6. Improve the durability of PGM-free catalysts and ability to run under normal operating conditions as defined by the DoE (0.1 L/min air, 1 mL/min fuel).
7. Improve water management on the cathode side for highly concentrated fuel conditions.
8. Reduce cracking in the blade coating approach and improve interfacial GDL and CCM relationship in the CCM approach to make them more viable for commercial fabrication applications.
9. Reduce cost by reducing overall PGM loading to 3 mg/cm$^2_{PGM}$ required in DMFCs.

APPENDICES

Appendix A – Procedures

Appendix A-1: GDE and MEA Fabrication Procedure

GDE and MEA Fabrication Procedure

Author: Nathaniel Metzger

PI: Dr. Xianglin Li

University of Kansas: Department of Mechanical Engineering

Standard Anode Solution Fabrication Procedure

Steps

1. Gather DI water, IPA, anode catalyst, and Nafion® 10% ionomer.
2. Obtain opaque glass container with a lid and a scale.

Note: Amounts will vary depending on sample size, so the ratios are the most important to control

3. Mix appropriate amounts of DI water, catalyst, IPA, and ionomer so that the ionomer to PtRu ratio is 0.4 and the solvent to dry mass ratio is 40:1. Add materials in the following order.

4. Seal glass container with a lid.
5. Place in Branson 1800 sonicator and sonicate on high for two hours

Standard Cathode Fabrication Procedure

Steps

1. Gather DI water, IPA, anode catalyst, and Nafion® 10% ionomer.

2. Obtain opaque glass container with a lid and a scale.

Note: Amounts will vary depending on sample size, so the ratios are the most important to control

3. Mix appropriate amounts of DI water, catalyst, IPA, and ionomer so that the ionomer to Pt ratio is 0.2 and the solvent to dry mass ratio is 55:1. Add materials in the following order.

4. Seal glass container with a lid.
5. Place in Branson 1800 sonicator and sonicate on high for two hours.

Standard electrode fabrication procedure

Steps (Same for both anode and cathode solution)

1. Gather catalyst solution fabricated in previous steps, a 5 mL plastic syringe, Sigracet 29BC (with hydrophobic MPL) (anode) or Toray 060 (without an MPL) (cathode) GDLs, aluminum foil, tape, and Iwata Ninja Jet Airbrush with a compressed air supply.
2. Cut approximately a 30 cm x 30 cm piece of aluminum foil.
3. Cut an appropriate size of GDL depending on desired sample size.
    a. Most commonly 2.5 cm x 2.5 cm or 5 cm x 5 cm for one or four samples, respectively
4. Record the initial weight of the GDL
5. Using the tape, secure the four corners of the GDL to the center of the aluminum foil.
    a. Try to cover as little of the GDL as possible
6. Using the syringe, place 1-2 mL of catalyst solution in the airbrush.
7. Turn on the compressed air supply.
8. Using the airbrush, depress the trigger and pull all the way back to allow for air and catalyst flow.
9. Move the air brush back and forth in an even motion across the whole GDL until a thin coating of catalyst and solvent is deposited.
10. Allow to dry in ambient conditions.
11. Repeat steps 7-9 approximately 10 times.
12. Place the foil and GDL in the Magic Mill food dehydrator.
13. Remove the taped corners and measure the weight of the GDL and applied catalyst.
14. Calculate the catalyst percentage by the following equation.

$$Catalyst\ \% = \frac{Total\ Catalyst * PGM\ \%}{Total\ Catalyst + Ionomer} \quad (1)$$

15. Calculate the PGM loading by the following equation.

$$PGM\ Loading = \frac{Final\ GDL\ weight - Initial\ GDL\ weight}{GDL\ Area} * Catalyst\ \% \quad (2)$$

16. Repeat steps 7-15 until a loading of 4.5 mg/cm$^2_{PtRu}$ or 1.5 mg/cm$^2_{Pt}$ is reached for either the anode or cathode, respectively.

Standard MEA Fabrication Procedure

Steps

1. Gather the following materials
    a. PTFE Sheet
    b. Anode and cathode (Previously fabricated)
    c. Tweezers
    d. Aluminum foil
    e. DulyTek DE10K Hot press
    f. Nafion® membrane of desired thickness

2. Prepare a Teflon template with an approximately 2.5 cm x 2.5 cm square cutout (slightly larger than the anode and cathode) that is two layers thick. Also prepare a two-layer folded sheet of aluminum foil to protect the MEA during pressing.

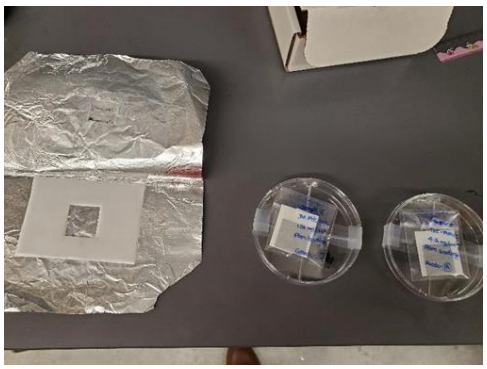

3. Place the anode with the catalyst layer facing up on the bottom of the Teflon template.

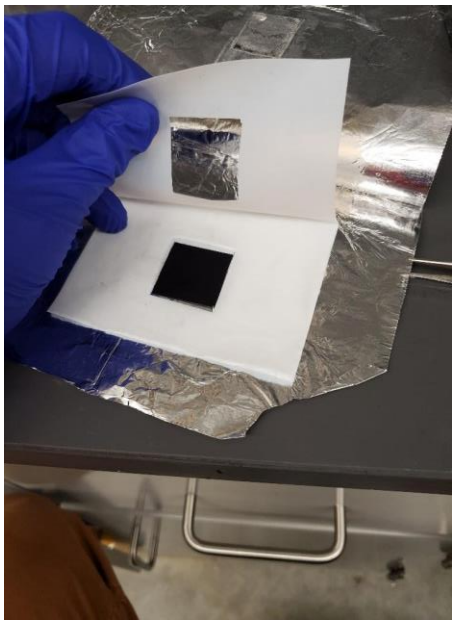

4. Place a Nafion® membrane in the middle layer of the Teflon sheet over the anode. Be sure to label the top side as cathode for future reference.

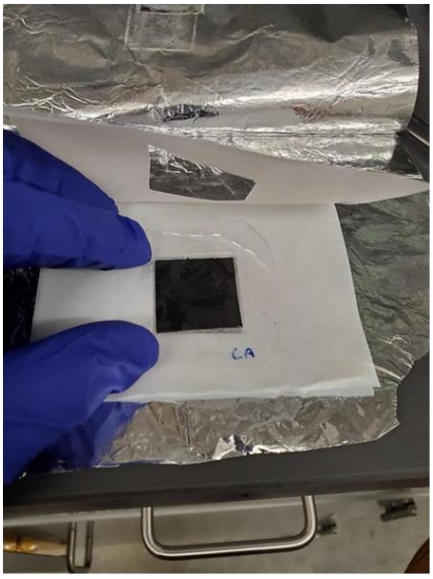

5. Close the second layer of the Teflon template over the membrane and anode and place the cathode with the catalyst layer facing the Nafion® membrane.

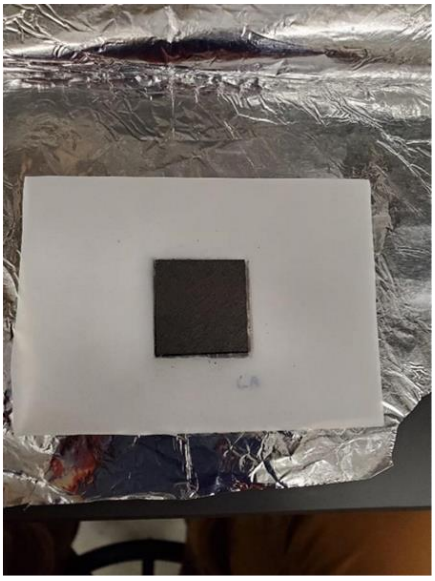

6. Close the second layer of aluminum foil firmly to hold the template and MEA together. Be cautious of the anode and cathode moving out of alignment with each other.

7. Turn on the hot press using the power button and press the “heat” button to begin to heat the plates to 275 F. This should be the default, however, if the temperature needs to be changed use the “set” button followed by the arrow buttons to adjust temperature as needed.
   Note: Some pressure discrepancy is normal

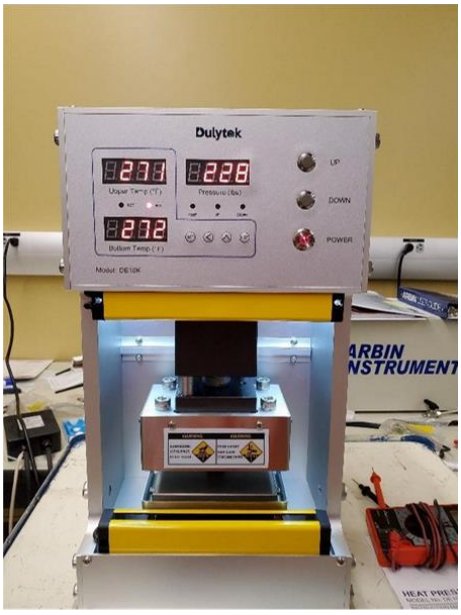

8. Place the MEA between the plates and press the down button until the top plate makes contact with the MEA and begins to read pressure. Quickly toggle the down button as the pressure increases (this happens very quickly)

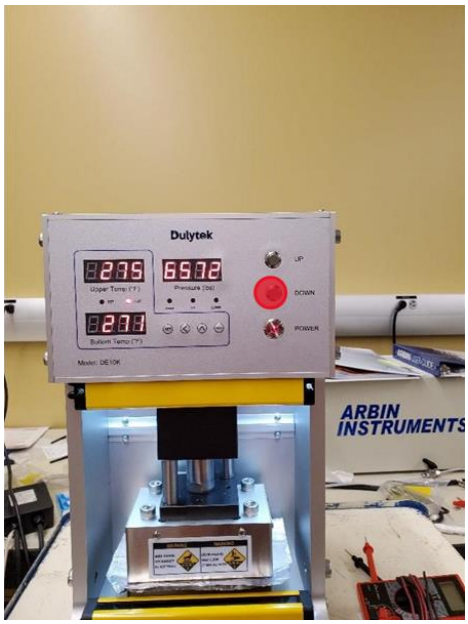

9. Hot press the MEA for five minutes, then use the "up" button to release the pressure

10. Remove the MEA from the hot press, open the template, and carefully remove the MEA using tweezers. Be sure to check the alignment of the anode and cathode and to be care removing it as the membrane sometimes sticks to the Teflon

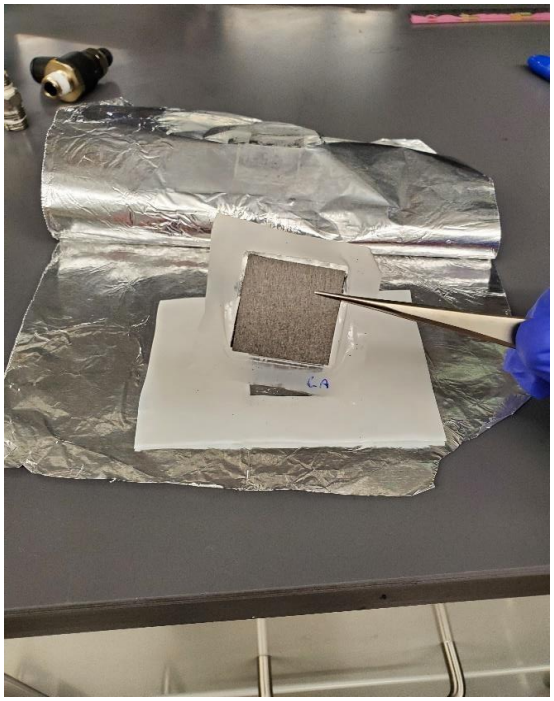

General Notes

- Catalyst ink preparation and cathode/anode coating precede this procedure. Please refer to those procedures before continuing to these steps.
- Employ proper safety precautions including but not limited to
  - Potential pinch points
  - Dangerously hot surfaces

Appendix A-2: Fuel Cell Set Up, Activation, and Testing Procedures

Fuel Cell Set Up, Activation, and Testing Procedure

Author: Nathaniel Metzger

PI: Dr. Xianglin Li

University of Kansas: Department of Mechanical Engineering

Fuel Cell Setup Procedure

Steps

1. Gather basic tools including a pair of tweezers and a torque wrench set to 20 ft-lbs.
    a. The torque wrench will "click" when the desired torque has been reached

2. Use the torque wrench to remove the bolts on the cathode plate (blue). Once loose the bolts can be loosened by hand.

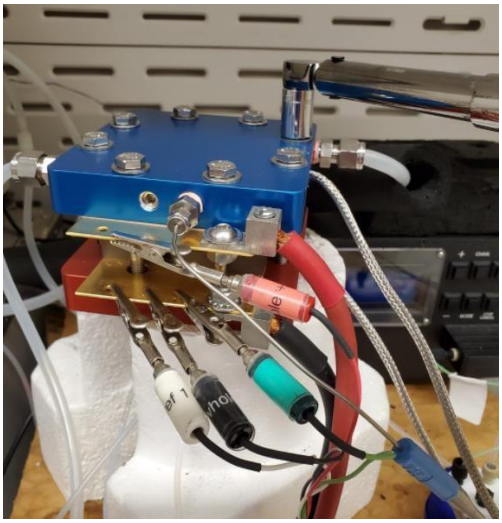

3. Remove the blue cathode plate and set aside being careful of the tubes and wires attached.

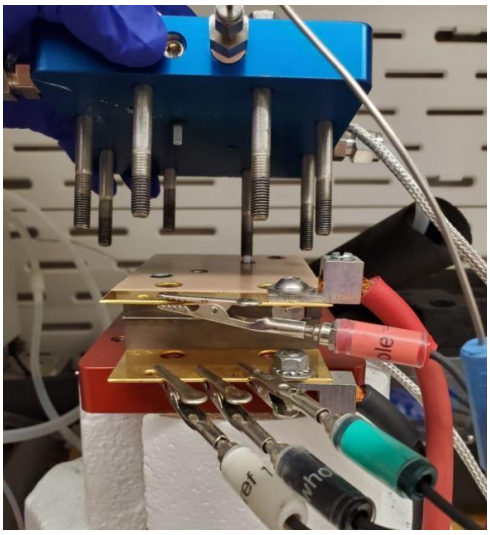

4. Remove the top current collector and graphite plate and set aside in the same manner. Be especially cautious of the small inlet and exit tubing with rubber gaskets as they easily fall out.

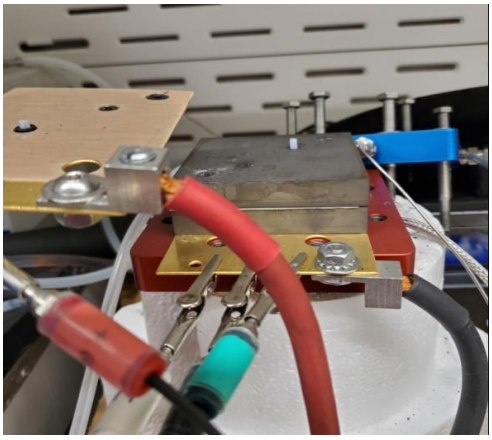

5. Using the tweezers lift the top layer of the white Teflon gasket and remove the previous MEA carefully.

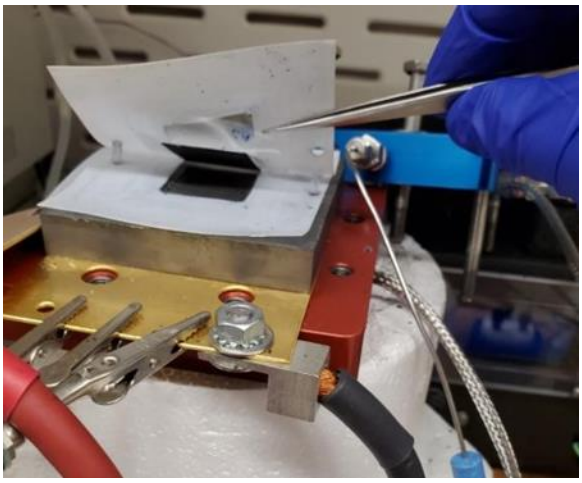

6. Place the previous sample in a bag and label it with the sample name, components, loading, and date. Put a 3-5 ml of DI water in the bag to keep the membrane from drying out and store safely.

7. Use tweezers to place the new MEA between the two Teflon gasket layers. **Make sure the cathode is on the top side – the membrane should be labeled with "CA" on the cathode side.**

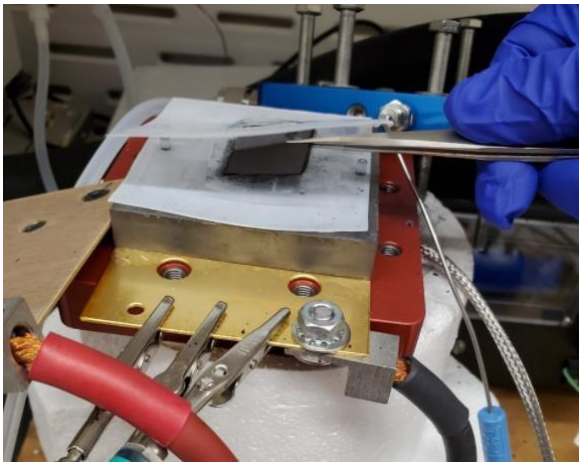

8. Close the gasket layer over the MEA so that it is centered over the fuel channels of the graphite plates.

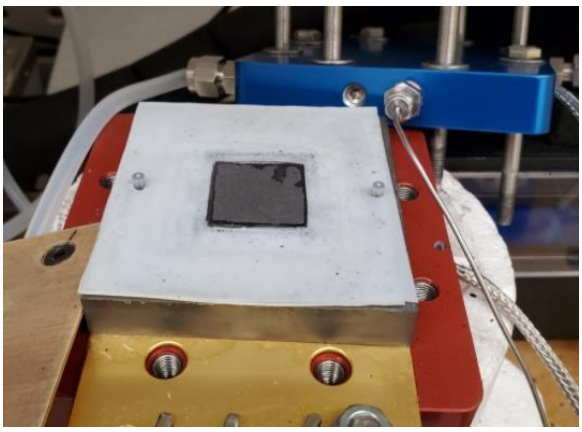

9. Replace the top graphite plate.

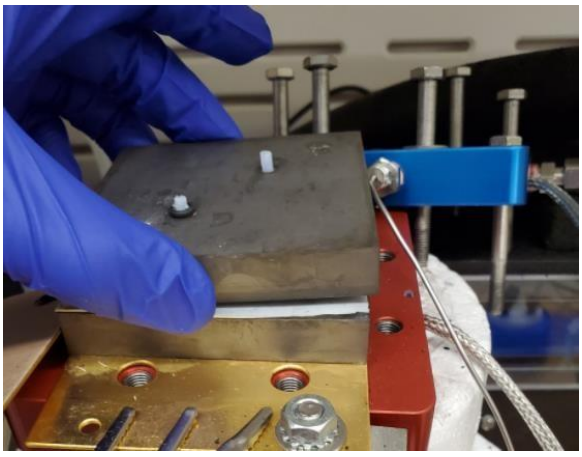

10. Replace the top current collector ensuring that all tubes and gaskets are in place. (There should be two tubes and four gaskets as seen in the picture to the right)

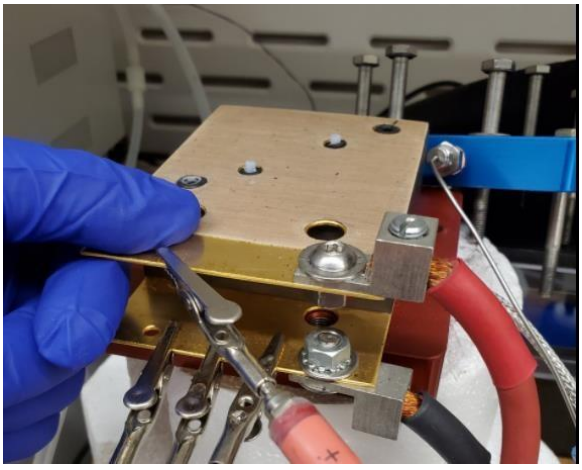

11. Replace the cathode plate and use the torque wrench to tighten each bolt to 20 ft-lbs.

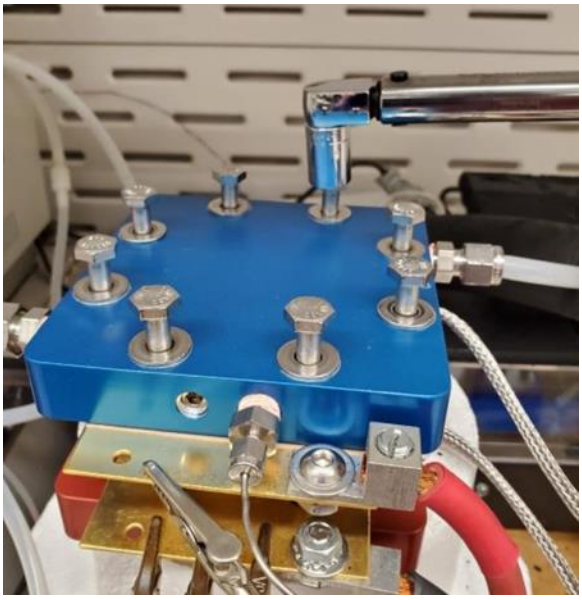

12. Make sure the surge protector is turned on and power on the testing station and attach the DI water bottle to the blue cap and flow controller.

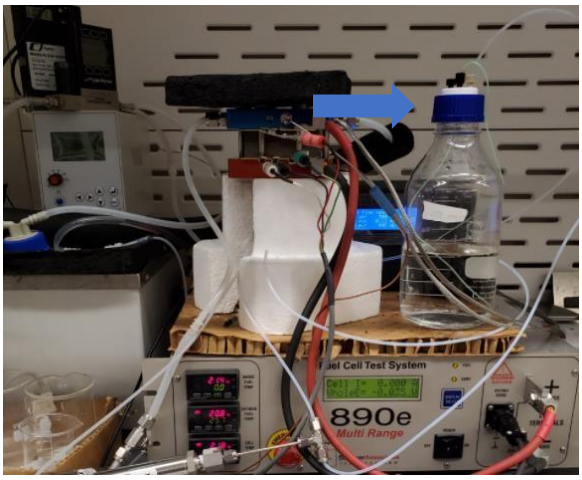

13. Power on the flow controller and click “mode” twice to set the flow to microliters. Set the flow to 500 ul, or 0.5 mL/min.

14. Power on the water bath and press enter to set the temperature to 90 C. This will provide fully humidified air to the cathode side of the fuel cell.

15. Use the orange knob on the left of the flume hood to provide dry air to the water bath. Turn the knob until the flow meter reads approximately 0.1 L/min.

16. Go to the computer and select the Fuel Cell program in the left-hand column second from the bottom. Make sure the cell temperature is set to 80 °C and press “OK”.

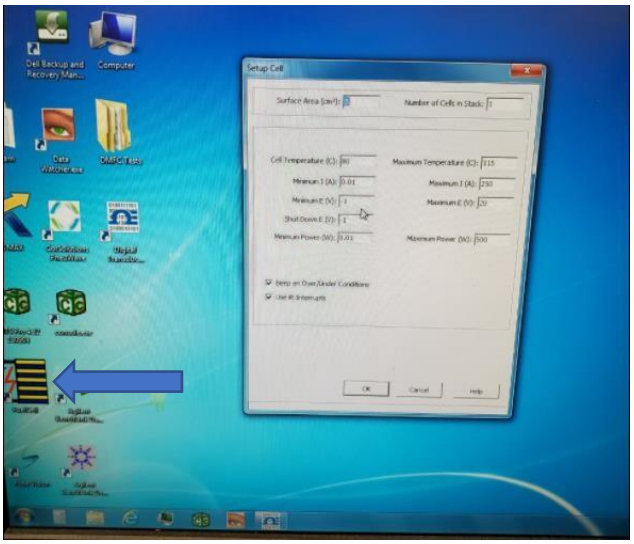

17. Once the Fuel Cell program opens click “Apply All Temp” in the top left.

18. Once the fuel cell reaches 80 °C it is ready for activation or testing and the DI water may be replaced with the desired fuel. See below list for some typical test conditions.

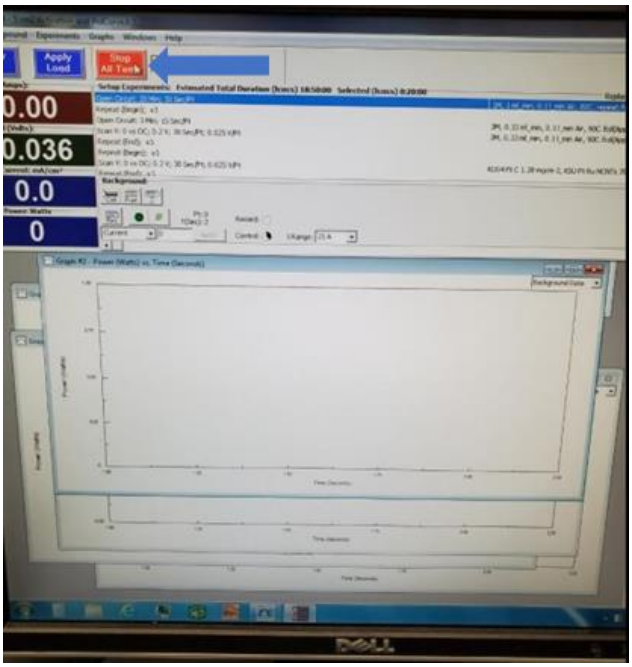

Standard Activation Procedure

Steps

1. Complete fuel cell set up procedure above.
2. Supply the anode with 0.25M methanol at 0.5 mL/min.
3. Supply the cathode with air at 0.1 L/min and 100% RH.
4. Using the fuel cell program, perform the following tests.
    a. Rest at OCV for 3 minutes.
    b. Perform a polarization scan from OCV to 0.2V.

    c. Hold at a constant 0.4V for one hour
5. Repeat step 4 until the performance of the MEA stabilizes.
    a. The fuel cell program will allow you to define a number of times to repeat the experiment.

Standard Testing Procedure

Steps

1. Complete fuel cell set up and activation procedure above.
2. Supply the anode with 1M methanol at 1 mL/min.
3. Supply the cathode with air at 0.1 L/min and 100% RH.
4. Apply 50 kPa of backpressure to the cathode using the Scribner manual backpressure module.
5. Using the fuel cell program, perform the following test.
    a. Rest at OCV for 3 minutes.
    b. Perform a polarization scan from OCV to 0.2V.
    c. Repeat 3x.
        i. This ensures the performance is stable across polarization scans
        ii. The best scan will be chosen unless an outlier is identified
6. Increase concentration as desired and repeat steps 2-5.
    a. Keep fuel flow rates at stoichometric ratios as concentration increases.
        i. i.e. 3M methanol would yield 0.33 mL/min fuel etc.
    b. Keep air flow rates, RH, and backpressure the same.
7. Retrieve data from computer and export to excel for analysis.

Appendix A-3: Fuel Cell Set Up, Activation, and Testing Procedures

Commercial Catalyst Specifications

Table A-3: Commercial catalyst specificantions

Catalyst	Pt Content (%)	Ru Content (%)	Metal Surface Area (m^2/g)	Maximum Crystalline Size (nm)
JM Pt/C 60% (HiSPEC 9100)	60	N/A	85	2.8
JM PtRu/C 75% (HiSPEC 12100)	50	25	Not available	3
TKK PtRu/C 77% (TEC86E86)	51	26	89.9	Not available
TKK PtRu/C 50% (TEC66E50)	32.4	16.8	137.9	Not available

Appendix A-4: Understanding Carbon Dioxide Transfer Using a Pore-Scale Model

RE: Inquiry on requesting permission for use of publication - Case # 00112162

Permissions <Permissions@asme.org>
Tue 3/29/2022 8:00 AM

To: Metzger, Nathaniel <nathanhmetzger@ku.edu>

Dear Mr. Metzger,
This permissions letter has been updated. It is our pleasure to grant you permission to use **all or any part of** the following ASME paper "Understanding Carbon Dioxide Transfer in Direct Methanol Fuel Cells Using a Pore-Scale Model," by Nathaniel Metzger, Archana Sekar, Jun Li, Xianglin Li, J. Electrochem. En. Conv. Stor. February 2022, 19(1), cited in your letter for inclusion in a thesis entitled Optimization of Direct Methanol Fuel Cells to be published by University of Kansas.

Permission is granted for the specific use as stated herein and does not permit further use of the materials without proper authorization. Proper attribution must be made to the author(s) of the materials. **Please note**: if any or all of the figures and/or Tables are of another source, permission should be granted from that outside source or include the reference of the original source. ASME does not grant permission for outside source material that may be referenced in the ASME works.

As is customary, we request that you ensure full acknowledgment of this material, the author(s), source and ASME as original publisher.

Many thanks for your interest in ASME publications.

Sincerely,

Beth Darchi
Publishing Administrator
ASME
2 Park Avenue
New York, NY 10016-5990

Understanding Carbon Dioxide Transfer in Direct Methanol Fuel Cells Using a Pore-Scale Model

Nathaniel Metzger[a], Archana Sekar[b], Jun Li[b], Xianglin Li[a*]

[a] *Department of Mechanical Engineering, University of Kansas, Lawrence, KS 66046, USA*

[b] *Department of Chemistry, Kansas State University, Manhattan, KS 66506, USA*

Abstract

The gas flow of carbon dioxide from the catalyst layer (CL) through the micro porous layer (MPL) and gas diffusion layer (GDL) has great impacts on the water and fuel management in direct methanol fuel cells (DMFCs). This work has developed a liquid-vapor two-phase model considering the counter flow of carbon dioxide gas, methanol, and water liquid solution in porous electrodes of DMFC. The model simulation includes the capillary pressure as well as the pressure drop due to flow resistance through the fuel cell components. The pressure drop of carbon dioxide flow is found to be about 2-3 orders of magnitude higher than the pressure drop of the liquid flow. The big difference between liquid and gas pressure drops can be explained by two reasons: volume flow rate of gas is three orders of magnitude higher than that of liquid; only a small fraction of pores (<5%) in hydrophilic fuel cell components are available for gas flow. Model results indicate that the gas pressure and the mass transfer resistance of liquid and gas are more sensitive to the pore size distribution than the thickness of porous components. To build up high gas pressure and high mass transfer resistance of liquid, the MPL and CL should avoid micro cracks during manufacture. Distributions of pore size and wettability of the GDL and MPL have been designed to reduce the methanol crossover and improve fuel efficiency. The model results provide design guidance to obtain superior DMFC performance using highly concentrated methanol solutions or even pure methanol.

Keywords*:* Direct Methanol Fuel Cell; Liquid-Vapor Two-Phase Model; Pore Size Distribution;

* Corresponding author. Tel.: +1 (785) 864 8165; E-mail address: xianglinli@ku.edu

CO_2 Flow; Water Management; Methanol Crossover.

1 Introduction

The mass transfer of carbon dioxide within a direct methanol fuel cell (DMFC) is critical to regulate the mass transfer of fuel (methanol) and water[1–3]. This study focuses on the liquid-vapor two-phase flow of carbon dioxide, methanol, and water within porous electrodes of DMFCs to propose design criteria for DMFCs using concentrated methanol solutions. In DMFCs fed with dilute liquid methanol solutions, the anode methanol oxidation reaction (MOR) oxidizes methanol and water and generates carbon dioxide, while the cathode oxygen reduction reaction (ORR) reduces oxygen and generates water:

$$\text{Anode (MOR): } CH_3OH + H_2O \rightarrow CO_2\,(g) + 6H^+ + 6e^- \quad (1)$$

$$\text{Cathode (ORR): } 6H^+ + 6e^- + 1.5\,O_2 \rightarrow 3H_2O \quad (2)$$

$$\text{Overall: } CH_3OH + 1.5\,O_2 \rightarrow CO_2\uparrow + 2H_2O \quad (3)$$

The liquid fuel (methanol-water solution) transfer from the fuel channel through the gas diffusion layer (GDL) to the anode catalyst layer (CL) while the generated carbon dioxide gas moves in the opposite direction from the anode CL through the GDL to the fuel channel. Carbon dioxide, methanol, and water have the same molar flux in the anode catalyst layer, determined by the anode MOR reaction Eq. (1). Because carbon dioxide is generated as gas while methanol and water react in the MOR as liquid, the densities of carbon dioxide gas and methanol solution are different by about 1,000 times. As a result, the volume flow rate of carbon dioxide away from the anode catalyst layer is about three orders of magnitude higher than the volume flow rate of the methanol solution into the anode catalyst layer. The counter flow of carbon dioxide and liquid fuel supply has imperative impact on the fuel supply and crossover rates[4]. Therefore, understanding the pressure change and flow rate of carbon dioxide in fuel cell electrodes (especially in the anode) is critical and will be the focus of this study.

There have been studies to visualize carbon dioxide bubble flow within the fuel channel and to design the anode channels to quickly remove carbon dioxide, especially at high current densities. Yang et al.[5] conducted a detailed study to visualize carbon dioxide bubble flow in a serpentine

channel at three different cell orientations: horizontal with the anode facing up, vertical, and horizontal with the anode facing down. The 4-cm^2 DMFC was tested with 1 M methanol solution at 60^oC with a flow rate of 1 ml/min. In addition, carbon dioxide bubble behavior when the methanol flow rates varied from 0.25 to 8.0 ml/min using 1M methanol was studied and visualized. This study identified the transition from discrete bubbles to gas slugs when the operating current increased. The orientation of the fuel cell was found to have impact on the performance, especially at low methanol flow rates. Li et al. has designed the anode flow channels of a micro DMFC with a non-equipotent serpentine flow field[6]. The new flow channel design had a gradient cross-section area along the flow direction, while keeping the same hydraulic diameter, open ratio, and channel length with the traditional design that uses a uniform cross-section area. The micro DMFC reduced the anode pressure drop by half (from 3.21 kPa to 1.65 kPa) at 0.1 A current and less fluctuation of pressure caused by carbon dioxide bubble clogging was seen using the new channel. Previous studies focusing on DMFCs using dilute methanol solutions have indicated that current density has insignificant impact on the overall mass-transfer of methanol and water in the anode of DMFCs and hence relative low impact on fuel cell performance[7]. Therefore, early model studies focusing on the kinetics of DMFCs made the assumption that carbon dioxide was dissolved in liquid[8,9] or neglected the convection of methanol solution and carbon dioxide[10]. Most liquid-gas two-phase models of DMFCs neglected the impact of carbon dioxide[11] or indirectly calculated the mass fraction of carbon dioxide from the mass fractions of other species so that the summary of the total mass fractions equals unity[12–15]. Only very small number of models have simulated the CO_2 bubble flow within flow channels[16] and counter flow of carbon dioxide gas and liquid fuel during operation[17]. He et al. [17] considered the counter flow of gas and liquid in the fuel cell GDL using a volume average model. The model quantitatively studied the magnitude of fuel convection and diffusion. The pressure distributions of liquid and gas, which drive gas and liquid flow within the GDL, were calculated in the model. Convection was found to be relatively small, compared with diffusion, in transport fuel to the catalyst layer. We are not aware of a model study that simulates liquid-gas two-phase counter flow in a DMFC taking the pore size effect on capillary pressure into

consideration. Therefore, this study can fill the knowledge gap to understand the impact of pore-scale capillary pressure on liquid fuel and carbon dioxide gas transfer. Designs of fuel cell structures have also been proposed based on the model to enable DMFCs using highly concentrated methanol solution or pure methanol.

2 Model Description

2.1 Computational Domain

Figure 1 shows the one-dimensional physical domains of a typical membrane electrode assembly (MEA), which consists of a pair of GDLs, microporous layers (MPLs), and CLs on both sides of a polymer electrolyte membrane. The MEA is sandwiched between two parallel flow fields. A liquid-vapor two-phase mass transport model was developed to investigate the multi-physics phenomena in the MEA. The pore size distribution of the GDL and MPL were derived from literature. The geometric dimensions and some model parameters of the DMFC are listed in Table 1.

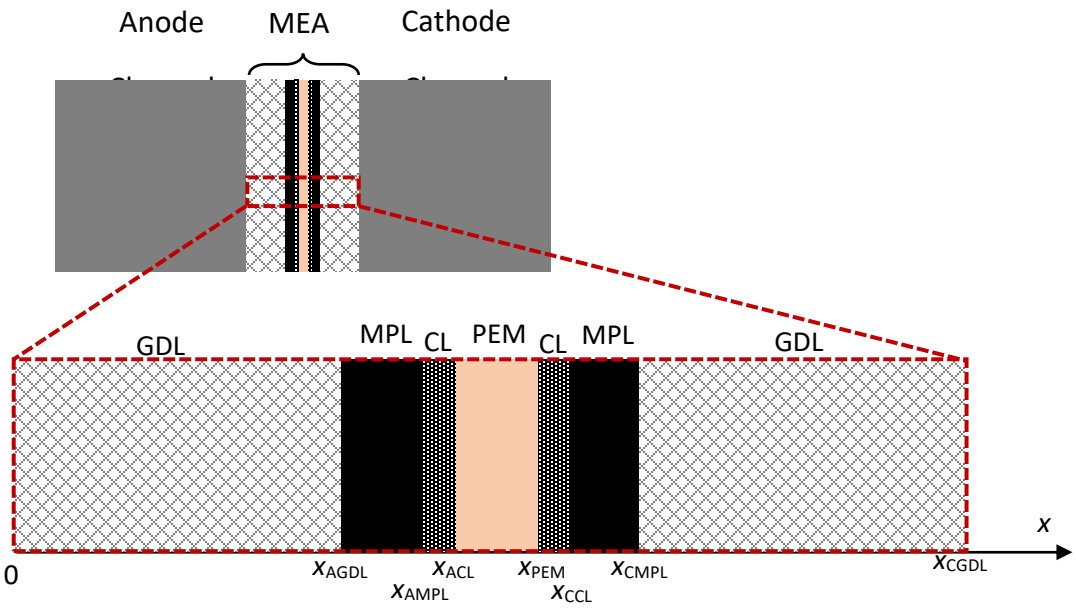

Figure 1. Schematic of the computational domain (1D model).

2.2 Model Assumptions

- The anode fuel channel is supplied with only liquid methanol solutions.
- The gas escape from the MEA to the fuel channel is only carbon dioxide, the partial pressure of

water vapor and methanol vapor are negligible compared with the total gas pressure.

- The fuel cell has a uniform temperature of 80°C everywhere.
- Porous media can be simplified as a bundle of micro cylinders with the same contact angle but different diameters.
- The gravity force is negligible. The Bond number, defined as the ratio between the gravitational force over the surface tension force ($\frac{\rho g d^2}{\sigma}$), in porous structures with pore size of 10 μm is on the order of 10^{-3}. This extremely low Bo number indicates that the gravitational force is negligible in such small length scale and can be neglected.
- The catalyst layer is thin and the generated carbon dioxide uniformly fills the CL. The pressure difference within the CL is negligible.

2.3 Pore Size Distribution

This study assumes that the pore size distributions in porous fuel cell electrodes following lognormal distributions with different mean pore sizes and shape factors[18]. The probability of pore size of x in a fuel cell component follows the following probability distribution function (PDF):

$$\mathrm{PDF}(x) = \exp\left[\frac{-(\ln x - d_{\mathrm{mean}})^2}{2\sigma^2}\right] \Big/ \left(\sqrt{2\pi}\cdot\sigma x\right) \text{ for } x > 0. \quad (4)$$

where the mean pore size d_{mean} and the shape factor σ can be estimated from experimental data reported in literature[19]. Then the fraction of pores with diameter of x or smaller can be calculated using the following cumulative distribution function:

$$\mathrm{CDF}(x) = \frac{1}{2} + \frac{1}{2}\mathrm{erf}\left(\frac{\ln x - d_{\mathrm{mean}}}{\sqrt{2}\sigma}\right) \text{ for } x > 0. \quad (5)$$

The mean pore size, the shape factor, and other properties of fuel cell components are summarized in Table 1.

Table 1. Properties of MEA components in this model[20].

	Thickness δ (μm)	Mean pore size d_{mean} (μm)	Shape Factor σ (/)	Porosity ε (/)	Contact angle θ (°)	Permeability K (m^2)
GDL	200	10	1.0	0.8	50[21]	3×10^{-12}
MPL	50	0.1	1.0	0.3	70	7×10^{-13}

CL	20	0.1	1.0	0.2	30	3×10^{-14}
PEM	50	0.01	1.0	0.2	25[22]	7.13×10^{-20} [23]

2.4 Governing Equations

2.4.1 Gas Pressure Drop

The surface tension of methanol-water mixture varies significantly with temperature and methanol concentration[24]. The mass fraction of methanol is 3.3% and 10.9% when the methanol concentration is 1 and 3M, respectively. The surface tension of the 1M methanol solution at 80°C is estimated to be 50 mN/m. Assuming the liquid can wet all MEA components, including the MPL, the gas (carbon dioxide) pressure that breaks through cylindrical pores filled with liquid is determined by the capillary pressure:

$$p_{\mathrm{C}} = p_{\mathrm{g}} - p_{\mathrm{l}} = \frac{4\cdot\gamma\cdot\cos\theta}{d}. \tag{6}$$

Assume the liquid pressure is the atmospheric pressure, p_0, the gas pressure that is required to break through pores with diameter d is:

$$p_{\mathrm{g}} = p_0 + \frac{4\cdot\gamma\cdot\cos\theta}{d}. \tag{7}$$

where γ is the surface tension of liquid, 50 mN/m, and θ is the contact angle between the liquid and gas on the solid surface. Once the gas bubble breaks through the pore, the pressure drop of the gas flow through the MPL and GDL can be determined by the permeability and volume flow rate following the Kozeny–Carman equation:

$$\frac{\Delta p_{\mathrm{g}}}{\delta} = -\frac{150\mu}{d_{\mathrm{avg,g}}^2}\frac{(1-\varepsilon)^2}{\varepsilon^3}v_S. \tag{8}$$

Where $d_{\mathrm{avg,g}}$ is the average diameter of pores larger than d (which are filled with gas) and μ is the dynamic viscosity of carbon dioxide gas, 1.755×10^{-5} Pa·s, and ε is the porosity. It should be noted that the sphericity is assumed to be unity in this study. The superficial velocity $v_{s,g}$ is calculated by the volumetric gas flow rate, Q_g, and the cross-sectional area that have gas flow:

$$v_{s,g} = \frac{Q_g}{A\times(1-\mathrm{CDF}(d))}. \tag{9}$$

Since gas can only go through pores with size larger than d, the area of the gas flow is calculated by $A\times$(1-CDF(d)), where CDF(d) is the cumulative distribution function at pore size d. The volume

flow rate of carbon dioxide per projected area of the MEA is proportional to the operating current density i:

$$\frac{Q_g}{A} = \frac{i}{6F} \times \frac{R_u T}{p_g} \tag{10}$$

where F is the Faraday constant, 96485 C/mol, R_u is the universal gas constant, 8.314 J/mol/K, and p_g is the gas pressure. Therefore, the pressure drop through the thickness direction (δ is the thickness) of the fuel cell component, Δp_g, can be calculated by:

$$\frac{\Delta p_g}{\delta} = -\frac{150\mu}{d_{avg,g}^2} \frac{(1-\varepsilon)^2}{\varepsilon^3} \times \frac{i}{6F} \times \frac{R_u T}{p_g} \times \frac{1}{(1-\mathrm{CDF}(d))}. \tag{11}$$

The total gauge pressure of carbon dioxide in the catalyst layer includes the breakthrough pressure of the bubbles (Eq. 7) and the pressure drop of the gas flow (Eq. 11):

$$\Delta p_{g,tot} = \frac{4 \cdot \gamma \cdot \cos\theta}{d} + \frac{150\mu}{d_{avg,g}^2} \frac{(1-\varepsilon)^2}{\varepsilon^3} \times \frac{i}{6F} \times \frac{R_u T}{p_g} \times \frac{\delta}{(1-\mathrm{CDF}(d))}. \tag{12}$$

Applying Eq. 12 to different porous fuel cell components, which have different pore size distribution and wettability, can result in a balanced pressure with the operating current density.

2.4.2 Liquid Pressure Drop

The flow pressure drop of liquid flow through porous media, Δp_g, can be calculated by:

$$\frac{\Delta p_l}{\delta} = \frac{150\mu}{d_{avg,l}^2} \frac{(1-\varepsilon)^2}{\varepsilon^3} v_{s,l}. \tag{13}$$

where $d_{avg,l}$ is the average diameter of pores smaller than d (which are filled with liquid). The superficial velocity is calculated by the volumetric liquid flow rate, Q_l, and the cross-sectional area that have gas flow:

$$v_{s,l} = \frac{Q_l}{A \times \mathrm{CDF}(d)}. \tag{14}$$

The volumetric flow rate of liquid (methanol and water) per projected area of the MEA is proportional to the operating current density i:

$$\frac{Q_l}{A} = \frac{i \times (M_{H2O} + M_{MeOH})}{6F} / \rho_l. \tag{15}$$

Therefore, the liquid pressure drop through the thickness direction of the fuel cell component can be calculated by:

$$\Delta p_l = \frac{150\mu}{d_{avg}^2} \frac{(1-\varepsilon)^2}{\varepsilon^3} \times \frac{i \times (M_{H2O} + M_{MeOH})}{6F\rho_l} \times \frac{\delta}{\mathrm{CDF}(d)}. \tag{16}$$

2.5 Experiments to Validate the Model

This study has also conducted experiments to measure the pressure change during fuel cell operation to validate the model. The anode gas diffusion electrode (GDE) was fabricated by airbrush spraying PtRu/C (32.8:16.9:50.3) catalysts (TEC 66E50 – Tanaka Kikinzoku Kogyo K.K.) dispersed in ionomer-containing ethanol (at about 2 mg catalyst per milliliter of ethanol) on Toray TGP-H-60 carbon paper at 70 °C on a hotplate and the cathode GDE was made by spraying Pt/C(60:40) (HiSPEC® 9100 – Johnson Matthey) catalysts on TGP-H-60 carbon paper in the similar way. The anode catalyst loading was 4.4 mg_{PtRu}/cm^2 and the cathode catalyst loading was 1.2 mg_{Pt}/cm^2. The ionomer to total catalyst ratio was 0.2 in the anode GDE and the ionomer to carbon ratio was 1 in the cathode GDE. The anode and cathode GDEs were then hot-pressed with a pre-treated Nafion 212 membrane at 135ºC (275 F) and 0.345 MPa (50 psi) for 5 min to make the MEA. After activation using 0.25 M methanol and air, polarization curves of activated MEAs were tested at 80ºC with 1M (0.1 mL/min) methanol solutions and fully hydrated air (0.1 L/min with 50 kPa back pressure) using a Scribner Associates 890e 500W 50/125/250A Fuel Cell Test System. The methanol and air supply rates were controlled by a PeriWave Milliþ5 pump (CorSolutions) with 10 µl/min accuracy and a Cole-Parmer mass flow controller with 2.5 ml/min accuracy. Air from a compressed air cylinder was fully humidified at 80ºC before being supplied to the fuel cell. In addition to the performance test, this study has also applied two pressure transducers (PX409-050GUSBH – Omega) with ±0.5% full scale accuracy both near the exit of flow channels to measure the pressure variations in the anode and cathode when the fuel cell operated at different current densities. Details of the experimental setup can be found from our recent publication[25].

3 Model Comparisons

3.1 Model with Constant Pore Size and Wettability

In the model that assumes a constant pore size and wettability in each component, the pressure drop at a given current density (Eq. 12) will be reduced to:

$$\Delta p_{\mathrm{g,tot}} = \frac{4\cdot\gamma\cdot\cos\theta}{d} + \frac{150\mu}{d_{\mathrm{avg}}^2}\frac{(1-\varepsilon)^2}{\varepsilon^3} \times \frac{i}{6F} \times \frac{R_u T}{p_g} \times \delta. \quad (17)$$

The capillary pressure for the bubble to break through the hydrophilic pores and pressure drop due to the volume flow rates at 0.1 A/cm^2 are compared in Table 2. It could be seen that the pressure drop due to flow resistance is negligible (more than two orders of magnitude smaller) compared with the capillary pressures in GDL, MPL, and CL. While the flow resistance is higher than the capillary pressure in the PEM. Because the flow resistance changes faster (proportional to d^{-2}) than the capillary pressure (proportional to d^{-1}) with the pore size (d), the flow resistance is significant in components with extremely small pore size such as the PEM. The constant-pore-size model under-estimates the pressure drop due to gas flow because of the assumption that all pores are available for gas transfer. Meanwhile, the constant-pore-size model over-estimates the capillary pressure for the gas to break through pores without considering the fact that gas prefers to go through large pores with lower capillary pressure.

Table 2. Pressure Drop Across Various Fuel Cell Components with Constant Pore Size

	Total (Pa)	**Capillary Pressure (Pa)**	**Flow Pressure (Pa)**
GDL	1.3×10^{4}	1.3×10^{4}	1.7×10^{-2}
MPL	6.9×10^{5}	6.8×10^{5}	1.0×10^{4}
CL	1.7×10^{6}	1.7×10^{6}	1.8×10^{4}
PEM	6.3×10^{7}	1.8×10^{7}	4.5×10^{7}

Figure 2 shows a sketch of liquid-gas two-phase flow through porous fuel cell components. The porous structure of the MPL has been simplified into bundles of microtubes with various diameters. Since the MPL is hydrophilic to methanol-water solution, with a contact angle of 70^{o}, liquid is the wetting phase that can invade the MPL by capillary pressure. The pressure of the gas phase, which is the non-wetting phase, must be higher than the local capillary pressure in order to break through the liquid-filled pores (Eq. 6). Even though the mean pore size of the MPL is estimated to be 0.1 μm, which has the capillary pressure of 6.8×10^{5} Pa, larger pores and cracks in the MPL have lower capillary pressure. Therefore, carbon dioxide gas will first burst through large pores and cracks in the MPL, demonstrated in Figure 2. The breakthrough pressure of carbon dioxide gas is much lower than the capillary pressure estimated by the mean pore size. But this phenomenon cannot be captured by models assuming a constant pore size. In order to have

continuous gas flow, the gas pressure must be higher than the summary of the capillary pressure and pressure drop due to flow resistance (Eq. 12). The following pore-scale model can consider these factors and generate more accurate results.

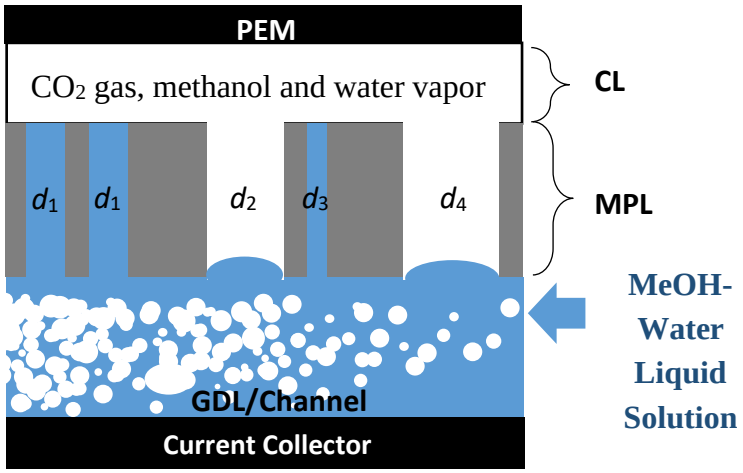

Figure 2. Schematic of liquid-gas two-phase flow through the anode fuel cell components.

3.2 Model with Distributions of Pore Size

The pore-scale model considers the pore size distribution within porous components (Figure 3a). Both the capillary pressure and the pressure caused by flow resistance are highly dependent on the pore size distribution. Figure 3b shows an example of the capillary pressure and the flow pressure drop through a MPL with log-normal pore size distribution when the operating current density is 0.1 A/cm^2. The capillary pressure decreases with the increase of the cut-off pore size (pores larger than the cut-off pores are available for gas flow) following Eq. 6. Meanwhile, the pressure drop introduced by flow resistance increases with the increase of the cut-off pore size. Larger cut-off pore size results in higher cumulative distribution function in Eq. 11 and fewer pores available for gas flow. Even though the flow resistance is smaller in each large pore, there are a much smaller number of large pores available for the gas flow. As a result, the flow pressure increases with the increase of cut-off pore size. The resulting total pressure, which is the sum of the capillary pressure and pressure drop, reaches a minimum of 2.6×10^5 Pa at the cut-off pore size of about 0.33 μm in the MPL at the current density of 0.1 A/cm^2. Based on the log-normal distribution of pore size, only a small fraction of pores (12%) are filled by gas while the rest of

pores with diameter of 0.33 μm or smaller are filled by liquid solution. Similar trends of the total pressure are obtained in other components (GDL, CL, and PEM) with different minimum pressures and cut-off pore sizes to obtain the minimum pressure.

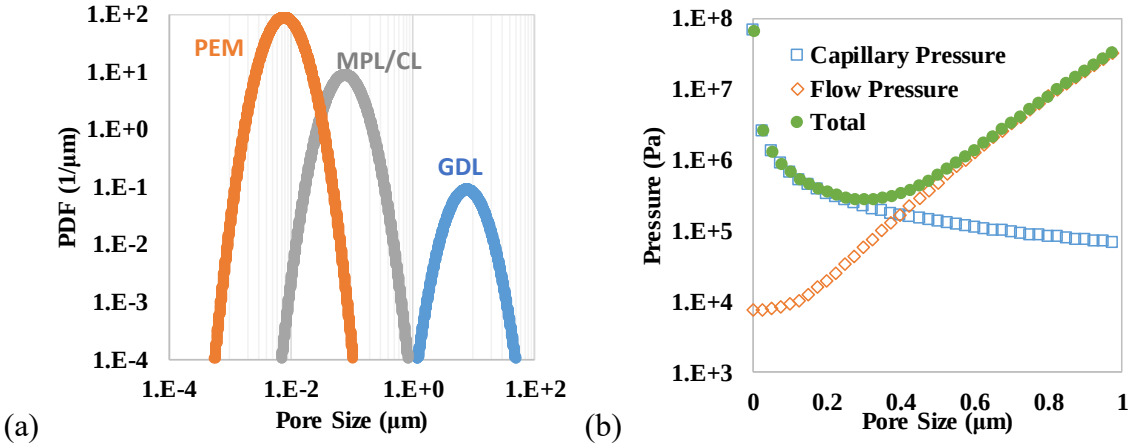

Figure 3. (a) Pore size distributions of different fuel cell components and (b) the capillary pressure and pressure drop through the MPL with average pore size of 0.1μm, thickness of 50 μm, porosity of 0.3, and contact angle of 70°, the operating current density is 0.1 A/cm^2.

The total pressure drops at different current densities are compared in Figure 4. Values of pressure change by capillary pressure and flow pressure drop are also compared in Table 3. Please note that the pressure drop in Figure 4 and Table 3 are the minimum total pressure drop balancing the capillary pressure and pressure drop by flow resistance. The pressure increases with the increase of current density in all components since the gas generation rate increases linearly with the increase of current density. The pressure drop is very high through the polymer electrolyte membrane (PEM) because of its extremely small pore size and low contact angle. The pressure drop through the GDL is negligible comparing with the pressure drop across the MPL and CL since the pore size in the GDL is roughly two orders of magnitude larger than the pore size in the MPL and CL. In order to regulate the gas flow, and the flow of liquid methanol and water, efforts should be focused on engineering the MPL.

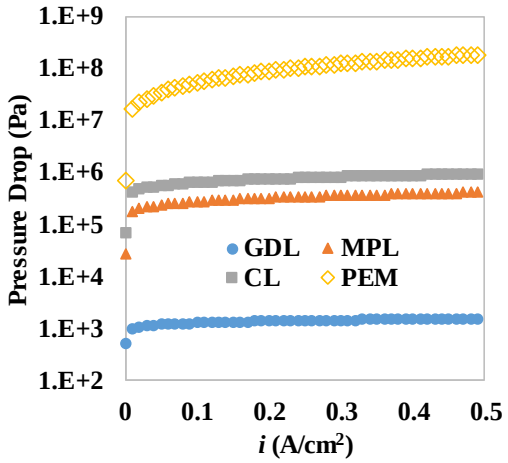

Figure 4. Total pressure drops across each component at different operating current densities.

Table 3. Pressure breakdowns of the pore size distribution model at 0.1 A/cm^2.

	Total Gas Pressure (Pa)	Capillary Pressure (Pa)	Gas Flow Pressure (Pa)
GDL	5.1×10^{2}	5.1×10^{2}	5.1×10^{-2}
MPL	5.2×10^{4}	3.5×10^{4}	1.7×10^{4}
CL	1.2×10^{5}	8.1×10^{4}	3.7×10^{4}
PEM	1.9×10^{7}	4.6×10^{6}	1.4×10^{7}

3.3 Model Validations

According to the previous discussions, the pressure increases with the operating current density because of the higher generation rate of carbon dioxide gas. When the liquid and gas are in equilibrium in porous fuel cell components, Figure 2, the experimentally measured pressure changes using the pressure transducer indicates the pressure drop required to drive gas through the fuel cell components (mainly the GDL and MPL). Although the total gas pressure in the CL is high, the pressure measured in the flow channel has been significantly reduced by the high capillary pressure through the MPL and GDL. The gas pressure at various current densities measured by the pressure transducer and model predictions are shown in Figure 5. Error bars in Figure 5 were calculated from four set of experimental data. The prediction using the liquid-vapor pore-scale model matches with experimental measurements with average error of 23%. The discrepancy between simulation and data is partially caused by the simplification of porous structure to bundles of straight tubes in the model. Nevertheless, the trend and magnitude of

pressure change predicted by the mode have a good agreement with experimental data. The following results and discussions are derived based on the model with pore size distributions in each fuel cell components.

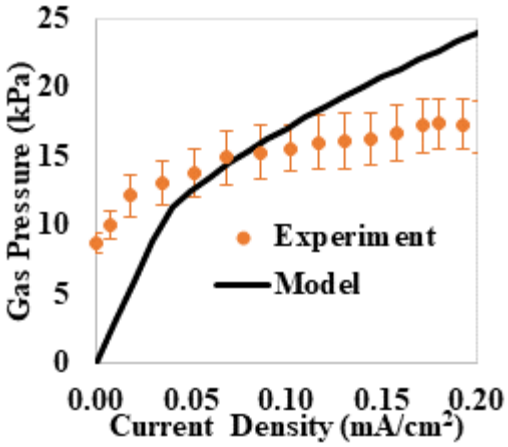

Figure 5. Variations of gas pressure with operating current density.

4 Results and Discussions

4.1 Gas and Liquid Pressure Distributions in MEA

The pressure drops of gas flow across different components when the current density is 0.1 A/cm^2 are illustrated in Figure 6. Distributions at other current densities follow a similar trend. Due to the high flow resistance, the generated carbon dioxide in the anode CL cannot cross-over the PEM and must move across the MPL and GDL to the anode fuel channel. Most fuel cell components and the majority of pores are hydrophilic to methanol solutions. As a result, liquid fuel can be automatically delivered to the CL through capillary force. The mass transfer of liquid to the catalyst is sufficiently quick to provide enough fuel and water to reaction sites. The un-reacted methanol and water will cross-over from the anode CL through the strongly hydrophilic PEM and reach the cathode CL.

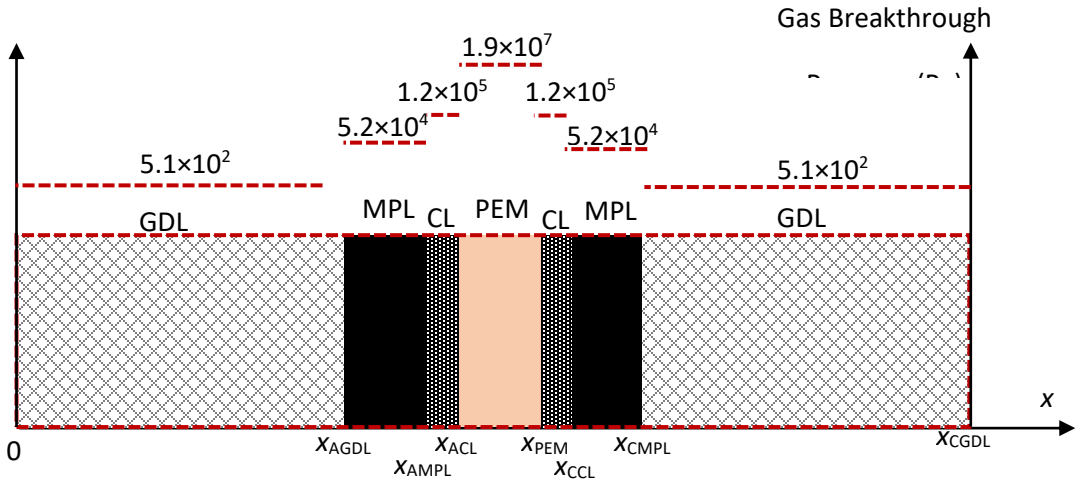

Figure 6. Pressure drop of gas flow through different fuel cell components at the current density of 0.1 A/cm^2.

4.2 Impact of the Shape Factor of Pore Size Distribution

The shape factor has significant impact on the pore size distribution and hence the mass transfer properties of fuel cell components. This section quantitatively compares the gas pressure drop across fuel cell components when the shape factor changes between 1 and 0.25. Reducing the shape factor will lead to a narrower range of pore sizes. When the shape factor approaches 0, the log-normal distribution approaches a constant pore size.

Results in 7a show that the gas pressure drops are lower when the pore size has a wider distribution (larger shape factor). Capillary pressure and the flow pressure drop are both lower in larger pores. Gas as the non-wetting phase tends to flow through larger pores and the model results show that gas only fill less than 1% of pores (larger) in the GDL, MPL, and CL at 0.1 A/cm^2. As a result, the porous components with wider distributions of pore size have lower resistance for gas flow and hence lower pressure drop. Comparisons between experimental data and model results using different shape factors in 7b indicate that pressure drops simulated using a shape factor of 1 result in better agreements with experimental results. The pressure drop of gas flow is over-estimated based on pore size distributions with smaller shape factor. On the contrary, the model using constant pore size under-estimated the pressure drop since this model assumes that all pores are available for gas flow. Shape factors of fuel cell components can be engineered during the

fabrication of the MEA components using raw materials with different sizes, amounts of binding material, compression pressures etc. In addition, results also indicate that the amount and size of microcracks in MPLs and CL can dramatically change the shape factor and overall mass transfer properties.

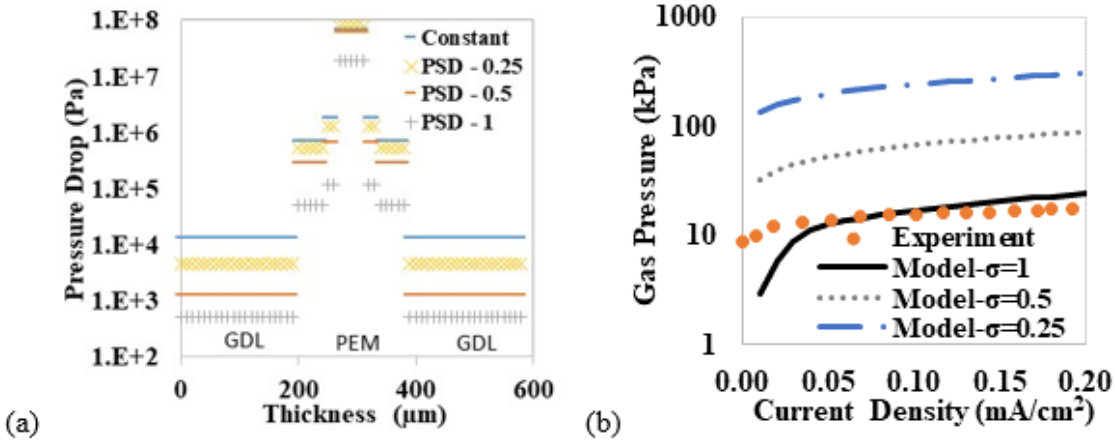

Figure 7. (a) Total gas pressure drop (capillary pressure + flow pressure drop) through different parts of the fuel cell at the current density of 0.1 A/cm^2. (b) Simulated and experimentally measured gas pressure change with the operating current density.

4.3 Impact of Component Thickness

Another important designing parameter is the thickness of fuel cell components. This study simulated the pressure drop of gas flow through the MPL with different thicknesses in Figure . The total pressure drops through the MPL only changes between 42 kPa and 86 kPa at 0.1 A/cm^2 and between 60 kPa and 140 kPa at 0.3 A/cm^2 when the MPL thickness increases from 25 to 200 μm (Figure a). As a comparison, the total pressure drops changes between 52 kPa to 293 kPa and then 537 kPa when the shape factor of the MPL changes from 1 to 0.5 and then 0.25(Figure b) at 0.1 A/cm^2. These results show that changing the pore size distribution and minimizing the micro cracks is more effective than changing the thickness in order to regulate the liquid and gas flow in MEAs.

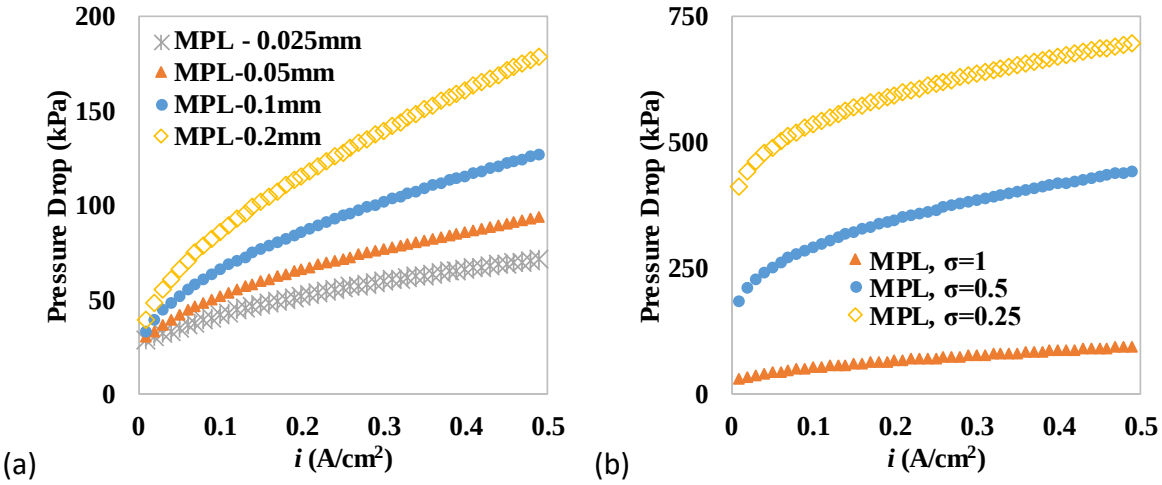

Figure 8. Total gas pressure drops through MPLs with (a) different thicknesses at the shape factor of 1.0 and (b) different shape factors at the thickness of 50 µm.

4.4 Designs of MEA Structures to Reduce Fuel Crossover

In order to reduce the methanol crossover when highly concentrated methanol solutions are used, the MEA design needs to consider the impact of capillary pressure to increase the gas pressure escaping the CL or reduce the capillary pressure of liquid flow into the CL. The following designs are proposed and compared by the model to quantify the gas and liquid flow resistance within MEA. The capillary pressure of micro-meter-size pores are much higher than the liquid flow resistance and the time scale for contact angle dynamics is on the order of 1~10 ms[26]. Therefore, the design principle is to reduce the liquid connection between the CL and the fuel channel.

The first design includes a strongly hydrophilic layer between the MPL and the GDL (Figure a). The hydrophilic layer has similar wettability and pore size with the catalyst layer and can build a pressure gradient to trap the liquid fuel between the CL and the channel using capillary pressure. This layer serves as a sink for methanol fuel to reduce the methanol crossover across the PEM. The second design includes an electric-conductive porous structure with very large pores (~mm) between the MPL and the CL. The pore size in this structure (labelled as large pores in Figure b) is much larger than those in the MPL and CL so it has negligible capillary

pressure and can easily be filled by carbon dioxide gas. As a result, this structure (gap) can serve as a gas trap and reduce the methanol crossover. The third design in Figure c uses a strongly hydrophilic MPL instead of the traditional hydrophobic MPL. This hydrophilic MPL can be made from mixtures of carbon and Nafion to have contact angle similar to that of the PEM (25° in this study). The strongly hydrophilic MPL has extremely high capillary pressure so the breakthrough pressure of the carbon dioxide gas generated in the CL is high. The high gas pressure in the CL will increase the liquid flow resistance and can reduce the methanol crossover rate. The following discussions will quantitatively analyze the mass transfer in these different designs of MEAs.

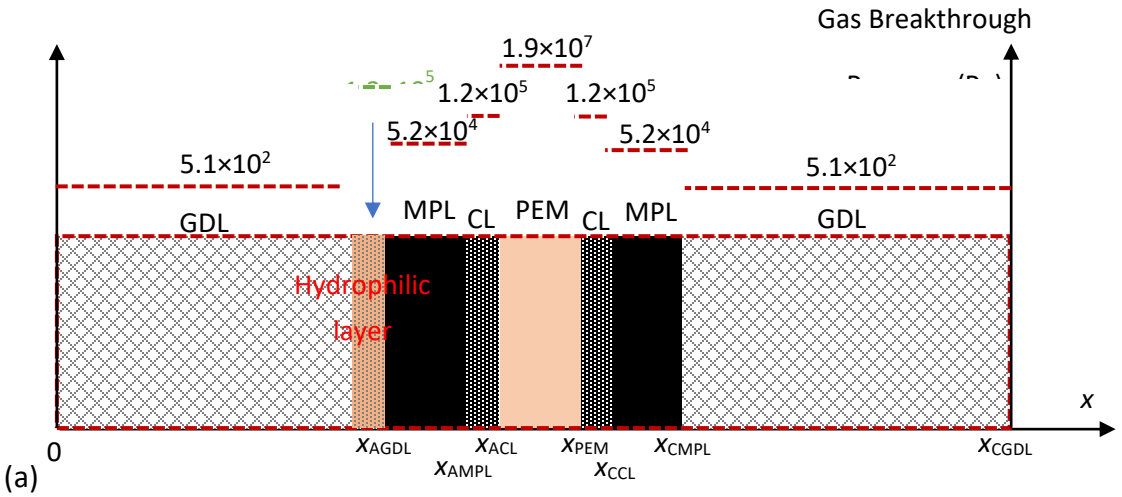

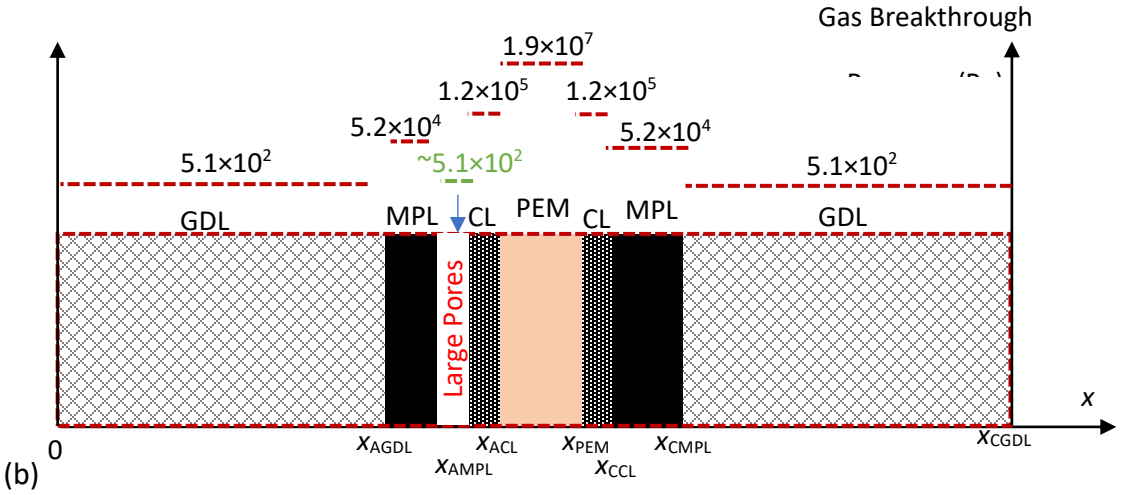

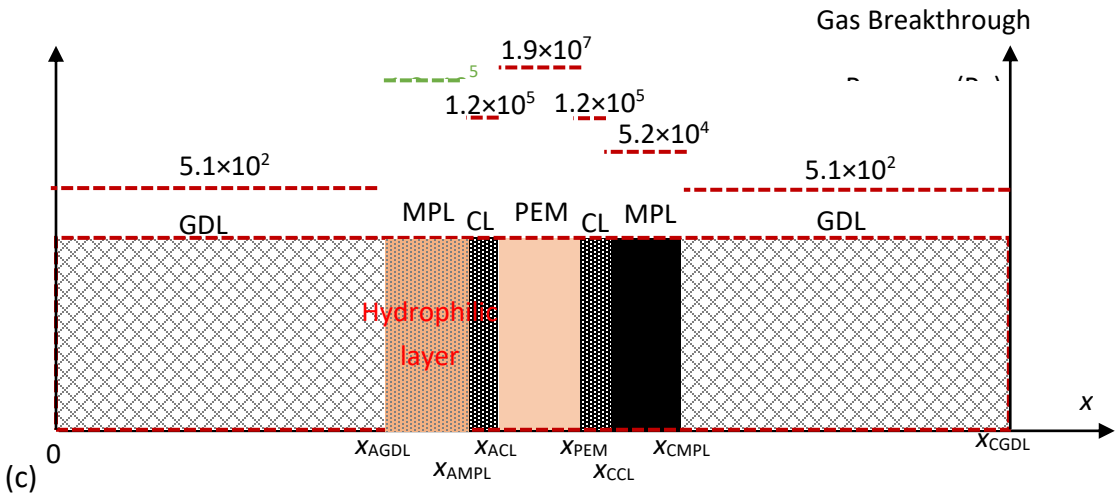

Figure 9. Pressure drop of gas flow through two new fuel cell structures with (a) a hydrophilic layer between GDL and MPL, (b) a gap or porous structure with large pore size between MPL and CL, and (c) a hydrophilic MPL at the current density of 0.1 A/cm^2.

In the first design in Figure a, if the hydrophilic layer has similar properties with the CL, carbon dioxide gas needs to build up a pressure of at least 1.2×10^5 Pa at 0.1 A/cm^2 to go across this hydrophilic layer. When the gas pressure is 1.2×10^5 Pa in the MPL, 4.1% of pores (with pore size larger than 0.57 µm) in MPL are filled by gas where the rest of pores (smaller than 0.57 µm) are filled by liquid solution. As a result, the resistance of liquid transfer is increased, and the fuel and water crossover could be reduced. Comparing with the baseline case without this hydrophilic layer, the liquid pressure drop to go through the MPL is increased from 1.8×10^2 Pa to 7.0×10^2 Pa. In this case, most pores connected with CL are still filled by liquid. If the hydrophilic membrane has an even lower contact angle or pore size, carbon dioxide gas needs to build up even higher pressure to transfer through the MPL. For instance, when the gas pressure is 2.5×10^6 Pa in the MPL, more than 90 % of pores (with pore size larger than 0.027 µm) in MPL are filled by gas where the rest of pores (smaller than 0.027 µm) are filled by liquid solution. Since very limited pores (less than 10%) are available for liquid flow, the liquid mass transfer resistance is extremely high so that the fuel and water crossover is significantly

reduced. The liquid pressure drop to go through the pores smaller than 0.027 μm in MPL is calculated to be 3.7×10^5 Pa.

In the second design in Figure b, carbon dioxide gas can easily fill up the whole gap between the MPL and CL. As a result, the mass transfer resistance of the liquid transfer is much larger due to the lack of capillary pressure. The liquid must evaporate to go through the gap and then condense within the CL for the reaction to occur. This design is similar to the concept of passive DMFCs applying a Nafion membrane between the fuel channel (or tank) and the GDL to evaporate methanol when highly concentrated methanol solutions are used as the fuel[27]. Methanol solutions cannot transfer through the evaporation (Nafion) membrane due to the extremely high capillary pressure of liquid. As a result, methanol solution must evaporate in order to go through the GDL and reach the CL. The first and second designs may result in similar fuel and water reduction results, but the mechanisms are different. The first design increases the gas pressure to reduce the number of pores filled by liquid that connect to the CL. The second design has much lower gas pressure in the CL and reduces the liquid flow by significantly decreasing the capillary pressure that connect the GDL with the CL.

In the third design in Figure c, the MPL is strongly hydrophilic. The contact angle of the MPL is similar to the PEM (25^o). Because the MPL is more hydrophilic, the capillary pressure of gas flow is higher. The calculated pressure drop across the MPL at 0.1 A/cm^2 is 1.26×10^6 Pa (similar to the pressure across the CL) or higher. The pressure drop due to liquid flow across the MPL at 0.1 A/cm^2 is increased to 7.2×10^2 Pa. If the MPL is further pressed to have smaller pore size (mean pore size of 0.05 μm), the pressure drop of the gas flow is further increased to 2.7×10^6 Pa at 0.1 A/cm^2. The calculated liquid pressure drop across the MPL at 0.1 A/cm^2 is further increased to 3.0×10^3 Pa.

4.6 Impact of Current Density (0.3 A/cm^2)

In the first design in Figure (a), if the hydrophilic layer has similar properties with the CL, carbon dioxide gas needs to build up a 1.7×10^5 Pa pressure at 0.3 A/cm^2 to go across this

hydrophilic layer. When the gas pressure drop is 1.7×10^5 Pa in the MPL, 8.2% of pores (with pore size larger than 0.4 μm) in the MPL are filled by gas where the rest of the pores (smaller than 0.4 μm) are filled by liquid solution. As a result, the resistance of liquid transfer is increased, and the fuel and water crossover could be reduced. Comparing with the baseline case without this hydrophilic layer, the liquid pressure drop to go through the MPL is increased from 5.2×10^2 Pa to 9.3×10^2 Pa.

In the third design in Figure c, the MPL is strongly hydrophilic. The contact angle of the MPL is similar to the PEM (25^o). Because the MPL is more hydrophilic, the capillary pressure of gas flow is higher. The calculated pressure drop across the MPL at 0.3 A/cm^2 is 1.4×10^6 Pa (similar to the pressure across the CL) or higher. The calculated liquid drop across the MPL at 0.3 A/cm^2 is increased from the base case of 5.2×10^2 to 2.15×10^3 Pa. If the MPL is further pressed to have smaller pore size (mean pore size of 0.05 μm), the pressure drop of the gas flow is further increased to 3.2×10^6 Pa at 0.3 A/cm^2. The calculated liquid pressure drop across the MPL at 0.3 A/cm^2 is increased to 9.15×10^3 Pa.

5 Conclusion

The mass transfer of carbon dioxide is critical to understand and regulate the fuel and water crossover in DMFCs. We developed a simple liquid-vapor two-phase model to simulate the counter flow of carbon dioxide gas and liquid methanol solution during fuel cell operation. Even though this study did not consider the non-isotropic properties of the porous fuel cell component[28] and the tortuosity of the porous media, the clear understanding of multi-phase flow in straight tubes derived from this work is necessary to understand mass transfer in more complicated geometries. Results and conclusions developed by this study can be easily applied to tortuous porous media with corrections of tortuosity. Several MEA designs have been proposed and analyzed based on this model to enable DMFCs driven by highly concentrated methanol solutions or even pure methanol. The main conclusions from this study include:

(1) The pressure drop of carbon dioxide is highly dependent on the wettability and pore size

distribution of the MPL and GDL. The high carbon dioxide pressure can be utilized to repel liquid and reduce liquid fuel and water crossover through the PEM.

(2) The high capillary pressure within the porous components of MEAs facilitates the transfer of liquid from channel to the CL. In order to reduce the fuel and water crossover through the PEM, liquid connections between the fuel channel and CL should be reduced.

(3) The pore size distribution and wettability have much more significant impact on mass transfer of liquid and vapor than the thickness of components.

(4) DMFCs fed with highly concentrated fuel prefers highly hydrophilic MPLs or a gap between the GDL and CL to reduce liquid transfer from the fuel channel to the CL. Both approaches will build a high-pressure gas layer between the CL and the channel and add liquid flow resistance.

(5) Model results are sensitive to the pore size distribution. The breakthrough pressure and the pressure drop due to gas flow through hydrophilic components with narrow range of pore size could be very high. It also indicates the importance to minimize the number and size of micro cracks within the MPL and CL to build up carbon dioxide gas flow resistance.

Acknowledgment

The authors highly appreciate the support by the U.S. Department of Energy's Office of Energy Efficiency and Renewable Energy (EERE) under the Fuel Cell Technologies Office Award Number DE-0008440.

Nomenclature

Abbreviation

CL Catalyst Layer

DMFC Direct Methanol Fuel Cell

GDL Gas Diffusion Layer

MEA Membrane Electrode Assembly

MPL Micro Porous Layer

PEM Proton Exchange Membrane

List of symbols

A	Projected area of MEA (m^2)
F	Faraday constant, (96,485 C/mol)
i	Current Density (A/cm^2)
K	Absolute permeability of porous media (m^2)
M	Molecular weight (kg/mol)
p	Pressure (Pa)
p_C	Capillary pressure (Pa)
R_u	Universal gas constant ($\mathrm{J/(mol \cdot K)}$)
T	Temperature (K)
Q	Volumetric flow rate of gas (m^3/s)
v_s	Superficial velocity (m/s)

Greek

ε	Porosity of the porous media (/)
μ	Kinetic viscosity (Pa·s)
ϑ	Contact angle (^{o})

ρ	Density (kg/m^3)
σ	Surface tension (N/m)

Subscripts

g	Gas phase
H2O	Water
l	Liquid phase
MeOH	Methanol

Reference

[1] Joghee, P., Malik, J. N., Pylypenko, S. & O'Hayre, R. A review on direct methanol fuel cells – In the perspective of energy and sustainability. *MRS Energy Sustain.* **2,** (2015).

[2] Li, X. & Faghri, A. Review and Advances of Direct Methanol Fuel Cells (DMFCs) Part I: Design, Fabrication, and Testing with High Concentration Methanol Solutions. *J. Power Sources* **226**(15), pp. 223–240.

[3] Alias, M. S., Kamarudin, S. K., Zainoodin, A. M. & Masdar, M. S. Active direct methanol fuel cell: An overview. *Int. J. Hydrog. Energy* **45,** 19620–19641 (2020).

[4] Shrivastava, N. K., Thombre, S. B. & Chadge, R. B. Liquid feed passive direct methanol fuel cell: challenges and recent advances. *Ionics* **22,** 1–23 (2016).

[5] Yang, H., Zhao, T. S. & Ye, Q. In situ visualization study of CO2 gas bubble behavior in DMFC anode flow fields. *J. Power Sources* **139,** 79–90 (2005).

[6] Li, M., Liang, J., Liu, C., Sun, G. & Zhao, G. Effects of Anode Flow Field Design on CO2 Bubble Behavior in μDMFC. *Sensors* **9,** 3314–3324 (2009).

[7] Xu, C., He, Y. L., Zhao, T. S., Chen, R. & Ye, Q. Analysis of Mass Transport of Methanol at the Anode of a Direct Methanol Fuel Cell. *J. Electrochem. Soc.* **153,** A1358 (2006).

[8] Meyers, J. P. & Newman, J. Simulation of the Direct Methanol Fuel Cell : II. Modeling and Data Analysis of Transport and Kinetic Phenomena. *J. Electrochem. Soc.* **149,** A718 (2002).

[9] García, B. L., Sethuraman, V. A., Weidner, J. W., White, R. E. & Dougal, R. Mathematical Model of a Direct Methanol Fuel Cell. *J. Fuel Cell Sci. Technol.* **1,** 43–48 (2004).

[10] Kulikovsky, A. A. Analytical model of the anode side of DMFC: the effect of non-Tafel kinetics on cell performance. *Electrochem. Commun.* **5,** 530–538 (2003).

[11] Wang, Y. & Sauer, D. U. Optimization of DMFC regulation based on spatial modeling. *Int. J. Hydrog. Energy* **40,** 12023–12033 (2015).

[12] Miao, Z., Xu, J.-L. & He, Y.-L. Modeling of the Transport Phenomena in Passive Direct Methanol Fuel Cells Using a Two-Phase Anisotropic Model. *Adv. Mech. Eng.* **6,** 812706 (2014).

[13] García-Salaberri, P. A. & Vera, M. On the effect of operating conditions in liquid-feed direct methanol fuel cells: A multiphysics modeling approach. *Energy* **113,** 1265–1287 (2016).

[14] Jiang, J., Li, Y., Liang, J., Yang, W. & Li, X. Modeling of high-efficient direct methanol fuel cells with order-structured catalyst layer. *Appl. Energy* **252,** 113431 (2019).

[15] Wang, Z. H. & Wang, C. Y. Mathematical Modeling of Liquid-Feed Direct Methanol Fuel Cells. *J. Electrochem. Soc.* **150,** A508 (2003).

[16] Su, X., Yuan, W., Lu, B., Zheng, T., Ke, Y., Zhuang, Z., Zhao, Y., Tang, Y. & Zhang, S. CO2 bubble behaviors and two-phase flow characteristics in single-serpentine sinusoidal corrugated channels of direct methanol fuel cell. *J. Power Sources* **450,** 227621 (2020).

[17] He, Y.-L., Li, X.-L., Miao, Z. & Liu, Y.-W. Two-phase modeling of mass transfer characteristics of a direct methanol fuel cell. *Appl. Therm. Eng.* **29,** 1998–2008 (2009).

[18] Li, X. A Modeling Study of the Pore Size Evolution in Lithium-Oxygen Battery Electrodes. *J. Electrochem. Soc.* **162,** A1636–A1645 (2015).

[19] Inoue, G., Yokoyama, K., Ooyama, J., Terao, T., Tokunaga, T., Kubo, N. & Kawase, M.

Theoretical examination of effective oxygen diffusion coefficient and electrical conductivity of polymer electrolyte fuel cell porous components. *J. Power Sources* **327,** 610–621 (2016).
[20] Miao, Z., Zihang, L., Yaling, H., Jinliang, X. & Xianglin, L. A Liquid-Vapor Two-Phase Model of Direct Methanol Fuel Cells with PGM-Free Cathode Catalyst. *Energy* **Under Review,**
[21] Kozbial, A., Trouba, C., Liu, H. & Li, L. Characterization of the Intrinsic Water Wettability of Graphite Using Contact Angle Measurements: Effect of Defects on Static and Dynamic Contact Angles. *Langmuir* **33,** 959–967 (2017).
[22] Goswami, S., Klaus, S. & Benziger, J. Wetting and Absorption of Water Drops on Nafion Films. *Langmuir* **24,** 8627–8633 (2008).
[23] Duan, Q., Wang, H. & Benziger, J. Transport of liquid water through Nafion membranes. *J. Membr. Sci.* **392–393,** 88–94 (2012).
[24] Vazquez, G., Alvarez, E. & Navaza, J. M. Surface Tension of Alcohol Water + Water from 20 to 50 .degree.C. *J. Chem. Eng. Data* **40,** 611–614 (1995).
[25] Li, X., Miao, Z., Marten, L. & Blankenau, I. Experimental measurements of fuel and water crossover in an active DMFC. *Int. J. Hydrog. Energy* **46,** 4437-4446 (2020).
[26] Kim, H., Lim, J.-H., Lee, K. & Choi, S. Q. Direct Measurement of Contact Angle Change in Capillary Rise. *Langmuir* **36,** 14597–14606 (2020).
[27] Xu, C., Faghri, A. & Li, X. Development of a High Performance Passive Vapor-Feed DMFC Fed with Neat Methanol. *J. Electrochem. Soc.* **157,** B1109–B1117 (2010).
[28] Sun, J., Zhang, G., Guo, T., Che, G., Jiao, K. & Huang, X. Effect of anisotropy in cathode diffusion layers on direct methanol fuel cell. *Appl. Therm. Eng.* **165,** 114589 (2020).

References

[1] Elesia Fasching and Suparna Ray, “Solar power will account for nearly half of new U.S. electric generating capacity in 2022 - Today in Energy - U.S. Energy Information Administration (EIA),” *eia.gov*, Jan. 10, 2022. https://www.eia.gov/todayinenergy/detail.php?id=50818 (accessed Jan. 10, 2022).

[2] Perry Lindstrom, “Carbon intensity of energy use is lowest in U.S. industrial and electric power sectors - Today in Energy - U.S. Energy Information Administration (EIA),” *eia.gov*, May 01, 2017. https://www.eia.gov/todayinenergy/detail.php?id=31012 (accessed Jan. 10, 2022).

[3] J. Milliken, R. Nowak, and P. Zelenay, “Direct Methanol Fuel Cell,” p. 2.

[4] Dr. Sunita Satyapal, “DOE Hydrogen and Fuel Cell Remarks.” The California Energy Comission, Jul. 28, 2021. Accessed: Jan. 10, 2022. [Online]. Available: https://efiling.energy.ca.gov/getdocument.aspx?tn=239019

[5] X. Li, “Stationary Direct Methanol Fuel Cells Using Pure Methanol,” May 30, 2020. [Online]. Available: https://www.hydrogen.energy.gov/pdfs/review20/fc317_li_2020_o.pdf

[6] M. S. Alias, S. K. Kamarudin, A. M. Zainoodin, and M. S. Masdar, “Active direct methanol fuel cell: An overview,” *Int. J. Hydrog. Energy*, vol. 45, no. 38, pp. 19620–19641, Jul. 2020, doi: 10.1016/j.ijhydene.2020.04.202.

[7] T. Ramsden, “An Evaluation of the Total Cost of Ownership of Fuel Cell-Powered Material Handling Equipment,” *Renew. Energy*, p. 37, 2013.

[8] “Hydrogen Production Cost Analysis.” https://www.nrel.gov/hydrogen/production-cost-analysis.html (accessed May 23, 2022).

[9] P. P. Edwards, V. L. Kuznetsov, W. I. F. David, and N. P. Brandon, “Hydrogen and fuel cells: Towards a sustainable energy future,” *Energy Policy*, vol. 36, no. 12, pp. 4356–4362, Dec. 2008, doi: 10.1016/j.enpol.2008.09.036.

[10] U. B. Demirci, “Direct liquid-feed fuel cells: Thermodynamic and environmental concerns,” *J. Power Sources*, vol. 169, no. 2, pp. 239–246, Jun. 2007, doi: 10.1016/j.jpowsour.2007.03.050.

[11] S. Hikita, K. Yamane, and Y. Nakajima, “Measurement of methanol crossover in direct methanol fuel cell,” *JSAE Rev.*, vol. 22, no. 2, pp. 151–156, Apr. 2001, doi: 10.1016/S0389-4304(01)00086-8.

[12] M. F. Sgroi *et al.*, “Cost Analysis of Direct Methanol Fuel Cell Stacks for Mass Production,” *Energies*, vol. 9, no. 12, Art. no. 12, Dec. 2016, doi: 10.3390/en9121008.

[13] “Manufacturing Cost Analysis of 100 and 250 kW Fuel Cell Systems for Primary Power and Combined Heat and Power Applications,” p. 289, 2016.

[14] J. A.J, A. Abdulkareem, A. Jimoh, and A. Afolabi, “Theoretical Energy and Exergy Analyses of Direct Methanol Fuel Cell,” *Adv. Mater. Sci. Appl.*, vol. 4, pp. 63–75, Sep. 2015, doi: 10.5963/AMSA0403001.

[15] J. Liu, T.-S. Zhao, R. Chen, and C. Wai Wong, “Effect of methanol concentration on passive DMFC performance,” *Fuel Cells Bull.*, vol. 2005, no. 2, pp. 12–17, Feb. 2005, doi: 10.1016/S1464-2859(05)00521-3.

[16] R. H. Henne and K. A. Friedrich, “APPLICATIONS – TRANSPORTATION | Auxiliary Power Units: Fuel Cells,” in *Encyclopedia of Electrochemical Power Sources*, J. Garche, Ed. Amsterdam: Elsevier, 2009, pp. 157–173. doi: 10.1016/B978-044452745-5.00369-5.
[17] W. Li, A. Manthiram, M. Guiver, and B. Liu, “High performance direct methanol fuel cells based on acid–base blend membranes containing benzotriazole,” *Electrochem. Commun.*, vol. 12, pp. 607–610, Apr. 2010, doi: 10.1016/j.elecom.2010.02.011.
[18] M. Albani, J. Llorca, and D. Borello, “Escola Tècnica Superior d’Enginyeria Industrial de Barcelona,” p. 77.
[19] D. Santiago, H. Tawfik, Y. Ryu, K. El-Khatib, and D. Mahajan, “Performance Optimization Of Direct Methanol Fuel Cell,” Jun. 2010, p. 15.950.1-15.950.8. Accessed: May 24, 2022. [Online]. Available: https://strategy.asee.org/performance-optimization-of-direct-methanol-fuel-cell
[20] S. Huria, A. Pundir, T. K. Raj, A. Jain, and A. Academy, “Optimisation of Direct Methanol Fuel Cell,” p. 5.
[21] V. Baglio *et al.*, “Influence of TiO 2 Nanometric Filler on the Behaviour of a Composite Membrane for Applications in Direct Methanol Fuel Cells,” *J. New Mater. Electrochem. Syst.*, vol. 7, Oct. 2004.
[22] Z. Miao, B. Hu, Y.-L. He, J. Xu, and X. Li, “A Liquid–Vapor Two-Phase Model of Direct Methanol Fuel Cells With Platinum Group Metal-Free Cathode Catalyst,” *J. Electrochem. Energy Convers. Storage*, vol. 18, no. 4, Jun. 2021, doi: 10.1115/1.4051209.
[23] N. Metzger, A. Sekar, J. Li, and X. Li, “Understanding Carbon Dioxide Transfer in Direct Methanol Fuel Cells Using a Pore-Scale Model,” *J. Electrochem. Energy Convers. Storage*, vol. 19, no. 1, Mar. 2021, doi: 10.1115/1.4050369.
[24] “Scribner Product Catalog 2016.pdf.” Accessed: May 24, 2022. [Online]. Available: https://www.scribner.com/files/distributor/Scribner%20Product%20Catalog%202016.pdf
[25] M. Chatenet, J. Benziger, M. Inaba, S. Kjelstrup, T. Zawodzinski, and R. Raccichini, “Good practice guide for papers on fuel cells and electrolysis cells for the Journal of Power Sources,” *J. Power Sources*, vol. 451, p. 227635, Mar. 2020, doi: 10.1016/j.jpowsour.2019.227635.
[26] F. Liu, G. Lu, and C.-Y. Wang, “Low Crossover of Methanol and Water Through Thin Membranes in Direct Methanol Fuel Cells,” *J. Electrochem. Soc.*, vol. 153, pp. A543–A553, Mar. 2006, doi: 10.1149/1.2161636.
[27] J. Li, D. Ye, X. Zhu, Q. Liao, Y. Ding, and X. Tian, “Effect of wettability of anode microporous layer on performance and operation duration of passive air-breathing direct methanol fuel cells,” *J. Appl. Electrochem.*, vol. 39, pp. 1771–1778, Oct. 2009, doi: 10.1007/s10800-009-9876-4.
[28] F. Aydın Ünal, V. Erduran, C. Timuralp, and F. Şen, “15 - Fabrication and properties of polymer electrolyte membranes (PEM) for direct methanol fuel cell application,” in *Nanomaterials for Direct Alcohol Fuel Cells*, F. Şen, Ed. Elsevier, 2021, pp. 283–302. doi: 10.1016/B978-0-12-821713-9.00015-9.
[29] H. Su and Y. H. Hu, “Recent advances in graphene-based materials for fuel cell applications,” *Energy Sci. Eng.*, vol. 9, no. 7, pp. 958–983, 2021, doi: 10.1002/ese3.833.

[30] A. Rao, R. K. R., D. V. Manjunatha, J. A., S. Prabhu, and R. Pinto, “Pore size tuning of Nafion membranes by UV irradiation for enhanced proton conductivity for fuel cell applications,” *Int. J. Hydrog. Energy*, vol. 44, Aug. 2019, doi: 10.1016/j.ijhydene.2019.07.084.
[31] B. P. Tripathi and V. K. Shahi, “3-[[3-(Triethoxysilyl)propyl]amino]propane-1-sulfonic Acid−Poly(vinyl alcohol) Cross-Linked Zwitterionic Polymer Electrolyte Membranes for Direct Methanol Fuel Cell Applications,” *ACS Appl. Mater. Interfaces*, vol. 1, no. 5, pp. 1002–1012, May 2009, doi: 10.1021/am800228s.
[32] S. Basri, S. K. Kamarudin, W. R. W. Daud, Z. Yaakob, and A. a. H. Kadhum, “Novel Anode Catalyst for Direct Methanol Fuel Cells,” *Sci. World J.*, vol. 2014, p. e547604, Apr. 2014, doi: 10.1155/2014/547604.
[33] M. Mansor, S. N. Timmiati, K. L. Lim, W. Y. Wong, S. K. Kamarudin, and N. H. Nazirah Kamarudin, “Recent progress of anode catalysts and their support materials for methanol electrooxidation reaction,” *Int. J. Hydrog. Energy*, vol. 44, no. 29, pp. 14744–14769, Jun. 2019, doi: 10.1016/j.ijhydene.2019.04.100.
[34] B. Krishnamurthy, S. Deepalochani, and K. S. Dhathathreyan, “Effect of Ionomer Content in Anode and Cathode Catalyst Layers on Direct Methanol Fuel Cell Performance,” *Fuel Cells*, vol. 8, pp. 404–409, Dec. 2008, doi: 10.1002/fuce.200800055.
[35] F. Scheepers, A. Stähler, M. Stähler, M. Carmo, W. Lehnert, and D. Stolten, “Layer Formation from Polymer Carbon-Black Dispersions,” *Coatings*, vol. 8, p. 450, Dec. 2018, doi: 10.3390/coatings8120450.
[36] M. Sunitha, N. Durgadevi, A. Sathish, and T. Ramachandran, “Performance evaluation of nickel as anode catalyst for DMFC in acidic and alkaline medium,” *J. Fuel Chem. Technol.*, vol. 46, no. 5, pp. 592–599, May 2018, doi: 10.1016/S1872-5813(18)30026-4.
[37] M. Malinowski, A. Iwan, A. Hreniak, and I. Tazbir, “An anode catalyst support for polymer electrolyte membrane fuel cells: application of organically modified titanium and silicon dioxide,” *RSC Adv.*, vol. 9, no. 42, pp. 24428–24439, 2019, doi: 10.1039/C9RA04862F.
[38] A. Sekar *et al.*, “PtRu Catalysts on Nitrogen-Doped Carbon Nanotubes with Conformal Hydrogenated TiO 2 Shells for Methanol Oxidation,” *ACS Appl. Nano Mater.*, Jan. 2022, doi: 10.1021/acsanm.1c03742.
[39] Y. V. Yakovlev *et al.*, “Ionomer content effect on charge and gas transport in the cathode catalyst layer of proton-exchange membrane fuel cells,” *J. Power Sources*, vol. 490, p. 229531, Apr. 2021, doi: 10.1016/j.jpowsour.2021.229531.
[40] M. Abdelkareem, T. Tsujiguchi, and N. Nakagawa, “Effect of black catalyst ionomer content on the performance of passive DMFC,” *J. Power Sources - J POWER SOURCES*, vol. 195, pp. 6287–6293, Oct. 2010, doi: 10.1016/j.jpowsour.2010.04.070.
[41] C. Lo Vecchio, A. Serov, M. Dicome, B. Zulevi, A. S. Aricò, and V. Baglio, “Investigating the durability of a direct methanol fuel cell equipped with commercial Platinum Group Metal-free cathodic electro-catalysts,” *Electrochimica Acta*, vol. 394, p. 139108, Oct. 2021, doi: 10.1016/j.electacta.2021.139108.
[42] T. Kosmala *et al.*, “Stable, Active, and Methanol-Tolerant PGM-Free Surfaces in an Acidic Medium: Electron Tunneling at Play in Pt/FeNC Hybrid Catalysts for Direct Methanol Fuel Cell Cathodes,” *ACS Catal.*, vol. 10, no. 14, pp. 7475–7485, Jul. 2020, doi: 10.1021/acscatal.0c01288.

[43] Q. Shu *et al.*, “A novel gas diffusion layer and its application to direct methanol fuel cells,” *New Carbon Mater.*, vol. 36, no. 2, pp. 409–419, Apr. 2021, doi: 10.1016/S1872-5805(21)60017-3.
[44] V. Mathur, “Gas Diffusion Layers in Direct Methanol Fuel Cells (DMFC).” https://aiche.confex.com/aiche/s09/techprogram/P143435.HTM (accessed Mar. 21, 2022).
[45] J. Zhang, G.-P. Yin, Q. Lai, Z. Wang, K.-D. Cai, and P. Liu, “The influence of anode gas diffusion layer on the performance of low-temperature DMFC,” *J. Power Sources*, vol. 168, pp. 453–458, Jun. 2007, doi: 10.1016/j.jpowsour.2007.03.027.
[46] A. Glüsen, M. Müller, N. Kimiaie, I. Konradi, J. Mergel, and D. Stolten, “Manufacturing Technologies for Direct Methanol Fuel Cells (DMFCs),” Dec. 2010.
[47] M. Klingele *et al.*, “A Completely Spray-Coated Membrane Electrode Assembly,” *Electrochem. Commun.*, vol. 70, Jul. 2016, doi: 10.1016/j.elecom.2016.06.017.
[48] cheersonic, “Ultrasonic Spraying Fuel Cell GDL - Coating Gas Diffusion Layer,” *Cheersonic*, Nov. 23, 2020. https://www.cheersonic.com/ultrasonic-spraying-fuel-cell-gdl/ (accessed Mar. 22, 2022).
[49] D. Rohendi, N. Syarif, M. Said, M. T. Utami, and Y. Marcelina, “Utilization of catalyst-coated membrane (CCM) and spraying methods in fabrication membrane electrode assembly (MEA) for direct methanol fuel Cell (DMFC) using Pt-Co / C catalyst,” *J. Phys. Conf. Ser.*, vol. 1282, no. 1, p. 012065, Jul. 2019, doi: 10.1088/1742-6596/1282/1/012065.
[50] W. Zheng, A. Suominen, and A. Tuominen, “Discussion on the Challenges of DMFC Catalyst Loading Process for Mass Production,” *Energy Procedia*, vol. 28, pp. 78–87, Jan. 2012, doi: 10.1016/j.egypro.2012.08.042.
[51] S. Mauger, K. Neyerlin, A. Yang-Neyerlin, K. More, and M. Ulsh, “Gravure Coating for Roll-to-Roll Manufacturing of Proton-Exchange-Membrane Fuel Cell Catalyst Layers,” *J. Electrochem. Soc.*, vol. 165, pp. F1012–F1018, Jan. 2018, doi: 10.1149/2.0091813jes.